**Université catholique de Louvain (UCLouvain)**

**Cliniques Universitaires Saint-Luc**

**Department of Ophthalmology**

# Defining Normative OCTA Vascular Density Values and AI-Based Vascular Ageing Models for Glaucoma Risk Assessment

**Sayeh Pourjavan, MD**

**Ophthalmologist – Glaucoma Specialist**

**PhD Candidate in Medical Sciences**

**PhD Thesis Manuscript**

**10 June 2025**

***“Now that you have attention... all you need is empathy and love….in layers.”***

Adapted from **“Attention Is All You Need”**

(Vaswani et al., 2017)

**“All You Need Is Love”** (The Beatles, 1967)

# Dedication

To my children, Kiana and Kiarmin,

Luci dei miei occhi,

Those who see my passion and dedication to my profession every day,

and who remind me to leave behind places and people who don't.

To my sweet father and my beautiful mother,

who passed away just as I began this PhD, taken too early,

but who never stopped believing I would one day earn my doctorate.

ممنونم برای مهاجرتتان، برای اینکه همه چیز را در ایران عزیزتان پشت سر گذاشتید تا من بتوانم درس بخوانم

Your strength gave me mine.

To my brother and sister,

for listening, standing by me, always.

Jullie zijn mijn anker, ’t Is een eer om jullie zus te zijn

This is for all of you

for your unconditional love, for your presence,

and because we are, in every way, DNA-bound

Merci

# Acknowledgment

Thank you from the bottom of my heart.

I am profoundly grateful to my children, **Kiana** and **Kiarmin**, for their unconditional love. I feel lucky every day to be their mum. Thanks also to my sweet dad, my beautiful mum (who is gone but always with me), and my lovely brother and sister for their unwavering support.

I would like to express my deep gratitude to **Mr. Adil El Maftouhi** for inspiring the idea of this PhD from our very first discussions during the ESCRS congress and for encouraging me to see my career from a new perspective.

I am deeply grateful to **Professor Benoît Macq** for granting me the opportunity to work alongside such brilliant minds and for his unwavering support throughout this project. I look forward to continuing future collaborations with his team, particularly in realising an operational, commercial-grade algorithm as part of my postdoctoral journey.

I sincerely thank **Thomas Van Drooghenbroeck**, **François Gouverneur**, **Tom Vaucourt**, and **Niki Nazaran**, who generously and with extraordinary patience taught me the fundamentals of artificial intelligence and machine learning, literally pushing this new knowledge into my medically trained neurons. Their brilliance, kindness, and encouragement made this learning experience truly transformative.

I would also like to thank **Professor Patrick De Potter** and **Dr. Antonella Boschi**, who helped me realise one of my dreams. Their support made it administratively possible for me to begin this doctoral journey, even during the final years of their careers.

My gratitude extends to the **Clinical Trial Centre** at Cliniques Universitaires Saint-Luc, whose guidance was invaluable in preparing my studies for ethical committee submissions, and to the Ethical Committee for considering and supporting my research projects.

I am thankful to **Professor Jean-Louis Vanoverschelde**, former Medical Director of Cliniques Universitaires Saint-Luc, whose decision enabled me to become the principal investigator of my clinical studies.

I warmly thank Madame **Sandrine Wollanders**, Gestionnaire administrative des doctorats & Support à la Recherche at UCLouvain, for her unfailingly prompt help and kindness in answering all my administrative questions with patience and without judgment.

My heart goes out to my (former) residents for their understanding, support, and scientific discussions, as well as for helping me with outpatient administration and

presenting our studies at congresses. I am deeply proud of you and grateful to have been part of your journey toward becoming brilliant ophthalmologists. Thank you, **Amira, Nasim, Thomas C, Thomas H, Kyou, Sami W, Sami Z, Grégoire, Saad, Ibrahim, Anna, Zoé, Roxane, Serdal, Gabriel, Victorine, Meriem** and **Antony N**.

My heartfelt thanks also go to **Sarah Koudad** and **Yasemin Akar**, my secretaries, and to **Cristina, Carine, and Nathalie** from the **Planification des Opérations** team, whose flexibility and dedication allowed me to adapt my outpatient clinics and surgical schedules to meet the needs of my studies.

I am deeply grateful to all the **anaesthetists** and **nurses** and **administrators** of the **Hospiday** at **CUSL**, who often witnessed my quiet escapes between surgical cases to study for a few precious minutes and helped make my operating theatre time a true moment of zenitude. I will truly miss you all.

Thanks to my **co-promotors**, **accompanying group**, **jury members**, and the **president** for reading my work and guiding me through this process.

Thanks also to **my friends**, who accepted my many absences, especially during these last two intense years.

I thank you all for opening doors for me....

Finally, I wish to thank all my **PATIENTS**, who continue to inspire my ongoing commitment to advancing glaucoma care. Without them, there would be no reason to seek progress.

And last but not least
Thank you, **Sayeh**, for your grit, lots of grit
Even when everything was against you, you pushed through...

## Résumé

Cette thèse se concentre sur l’établissement de valeurs normatives de densité vasculaire en angiographie OCT (OCTA) chez des sujets sains, en analysant leur pertinence pour la détection précoce et le suivi de la progression du glaucome. Grâce à une évaluation systématique des paramètres vasculaires péripapillaires et maculaires, l'étude fournit des références solides permettant d'interpréter les variations physiologiques liées à l’âge, au sexe et à d’autres facteurs de risque.

Ce travail met en évidence l'importance de la vascularisation rétinienne dans le développement et la progression du glaucome, une pathologie neurodégénérative majeure et silencieuse, encore difficile à diagnostiquer à ses premiers stades. L'analyse fine de ces biomarqueurs structurels et vasculaires ouvre de nouvelles perspectives pour une prise en charge plus personnalisée des patients à risque.

En s’appuyant sur ces bases scientifiques, la thèse propose un cadre conceptuel pour le développement de futurs modèles d'intelligence artificielle (IA), notamment GlauOCTA et GlauOCTA-AI, actuellement en phase de conception. Ces modèles ont pour ambition de détecter des schémas subtils de progression glaucomateuse, invisibles cliniquement, bien avant que les altérations fonctionnelles ne soient mesurables.

L’étude explore également les défis éthiques liés à l’intégration de l’IA en ophtalmologie, notamment les questions de biais algorithmique, de transparence, de responsabilité médicale, et de maintien du jugement humain dans les décisions cliniques. L’IA est envisagée comme un outil complémentaire, destiné à soutenir et renforcer l'expertise du clinicien, sans jamais s'y substituer.

En conclusion, cette recherche établit les bases pour le futur développement d’outils d’aide au diagnostic du glaucome basés sur des biomarqueurs vasculaires enrichis par l'IA, tout en posant les jalons d'une médecine de précision plus éthique, proactive et individualisée.

## Abstract

This thesis focuses on establishing normative vascular density values using optical coherence tomography angiography (OCTA) in healthy subjects, evaluating their clinical relevance in the early detection and monitoring of glaucoma progression. Through a systematic assessment of peripapillary and macular vascular parameters, the study provides robust reference values essential for interpreting physiological variations associated with age, sex, and other risk factors.

The work highlights the critical role of retinal vascularisation in the development and progression of glaucoma, a major neurodegenerative disease that remains challenging to diagnose at its earliest stages. By offering a detailed analysis of structural and vascular biomarkers, this thesis lays the foundation for a more personalized approach to risk stratification and patient care in glaucoma.

Building upon these scientific foundations, the thesis proposes a conceptual framework for the future development of artificial intelligence (AI) models such as GlauOCTA and GlauOCTA-AI, currently in the design phase. These models aim to predict glaucoma progression by detecting subtle vascular patterns that remain clinically invisible during the early disease stages, potentially allowing earlier intervention.

The study further addresses the ethical challenges associated with the integration of AI in ophthalmology, including concerns about algorithmic bias, transparency, medical accountability, and the essential preservation of human clinical judgment. AI is positioned as a complementary tool intended to enhance, not replace, the expertise of clinicians.

In conclusion, this research establishes the groundwork for the future development of AI-assisted glaucoma diagnostic tools based on vascular biomarkers, while advocating for a more ethical, proactive, and patient-centred approach to precision medicine in ophthalmology.

# Contents

## Objectives

1. To investigate the causes of variability in optic disc evaluations and determine which artificial intelligence (AI) models provide the most reliable and reproducible support for clinical glaucoma diagnosis.

2. To define normative OCTA vascular density values in a healthy population, stratified by age, using a high-resolution OCTA device.

3. To identify novel imaging biomarkers for glaucoma diagnosis with AI support, through comparative analysis of OCT and OCTA imaging, demonstrating the added diagnostic value of combining macular and disc OCTA and OCTA parameters.

4. To develop and validate a multimodal AI model that integrates OCT, OCTA, and relevant clinical data to estimate vascular and structural ageing of the eye, with the aim of detecting early deviation from healthy ageing and predicting glaucoma progression risk.

## Abbreviations

ACG: Angle Closure Glaucoma

AI: Artificial Intelligence

ANN Artificial neural network

Asta: Acuity Standard Text for Adults

AUC: Area under the curve

AUROC: Area Under the Receiver Operating Characteristic curve

BMO: Bruch Membrane Opening

CCT: Central Corneal Thickness

CNN: Convolutional neural network

CRA: Central Retinal Artery

CT: Computed Tomography

C/D: Cup-to-disc ratio

dB: Decibel

DL: Deep learning

DRP: Diabetic Retinopathy

ECG: Electrocardiogram

En face: Face-on visualization of OCT data between defined boundaries

FA: Fluoangiography

FAZ: Foveal Avascular Zone

FD: Foveal Vessel Density

FVL: Focal Volume Loss

GCC: Ganglion cell complex

GCL: Ganglion cell layer

GPA: Glaucoma Progression Analysis

GVL: Global Volume Loss

HFA: Humphrey Field Analyzer

ILM: internal limiting membrane

IOP: Intraocular pressure

IPL: Inner Plexiform Layer

LE: Left Eye

LLM: Large Language Model

LSTM: Long Short-Term Memory

MD: Mean Deviation

ML: Machine learning

MRI: Magnetic Resonance Imaging

NNT: Number Needed to Treat

NTG Normal-tension glaucoma

OAG: Open Angle Glaucoma

OCT: Ocular coherence tomography

OCTA: Ocular Coherence Tomography Angiography

ONH: Optic nerve head

PCA: Principal Component Analysis

PCA': Posterior Capillary Arteries

PPG: PrePerimetric Glaucoma

RBC: Red Blood Cell

RDB: Reference Data Base

RE: Right Eye

RGC: Retinal Ganglion Cell

RMSE: Root Mean Squared Error

RNFL: Retinal Nerve Fibre Layer

RoP: Rate of Progression

RPC: Radial Peripapillary Capillary

RPE: Retinal Pigment Epithelium

SAP: Standard Automated Perimetry

SITA Swedish interactive testing algorithm

SD-OCT: Spectral Ocular Coherence Tomography Angiography

SL: Supervised Learning

SLT: Selective Laser Trabeculoplasty

SSL: Semi Supervised Learning

SS-OCT: Swept-Source Ocular Coherence Tomography Angiography

SSI: Signal strength index

SVR: Support Vector Regression

TD-OCT: Time-domain Ocular Coherence Tomography Angiography

VA: Visual Acuity

VD: Vascular Density

VF: Visual field

VFI: Visual Field Index

QoL: Quality of Life

# Chapter 0. Prologue: Framing the Challenge of Glaucoma Diagnosis

Glaucoma remains a leading cause of irreversible blindness, yet its diagnosis, particularly in the early stages, remains complex and imprecise and often results in late diagnosis [1-3]. As highlighted by multiple large-scale studies, including the Early Manifest Glaucoma Trial and the Ocular Hypertension Treatment Study, early detection and treatment can delay disease progression [4,5].

However, the absence of a single, reliable biomarker hinders timely intervention, elevating the risk of vision loss. This thesis emerges from both the limitations encountered in daily clinical practice and the promise of advanced imaging recognition by artificial intelligence (AI) to bridge critical diagnostic gaps.

## 0.1 The Limitations of the Current Diagnostic Tools

The traditional glaucoma work-up includes measurement of intraocular pressure (IOP), examination of the optic nerve head, structural imaging (e.g., optical coherence tomography, OCT), and visual field testing [6]. However, these modalities are variably sensitive, highly dependent on technician skill and patient cooperation [7]. Furthermore, physiological interindividual variability, such as optic disc size, nerve fibre distribution, vascular density, and IOP tolerance, limits the accuracy of population-based diagnostic thresholds.

According to the European Glaucoma Society (EGS) guidelines, intraocular pressure (IOP) is not a diagnostic criterion, but it remains essential for classification and treatment decisions [8]. IOP exhibits diurnal variability and is influenced by factors such as central corneal thickness (CCT), body position, and measurement technique [9,10]. Its role in glaucoma pathogenesis is well acknowledged, but normal-tension glaucoma and ocular hypertension further complicate the clinical picture [11]. Moreover, functional testing, such as perimetry, often lags behind structural degeneration by several years [12]. This diagnostic ambiguity hinders timely intervention and increases the risk of late-stage detection, particularly in individuals with rapid disease progression.

Standard automated perimetry (SAP), though widely used, detects functional loss only after significant retinal ganglion cell damage has occurred [13]. Moreover, SAP has high test–retest variability and is susceptible to learning effects and fatigue [14]. Optical coherence tomography (OCT) provides high-resolution imaging of the retinal nerve fibre layer (RNFL) and macula; however, its interpretability is sometimes compromised by artefacts, segmentation errors, or poor signal quality [15].

## 0.2 Why Imaging Needs a New Framework?

OCTA (Optical Coherence Tomography Angiography) has recently emerged as a non-invasive technique for visualising retinal and choroidal vasculature, revealing vessel density (VD) reductions that may signal early glaucomatous changes [16].

However, image quality is heavily dependent on patient cooperation, ocular media clarity, and scan acquisition protocols [17]. Projection artefacts, especially in the deep vascular plexus, further hinder accurate quantification. Manufacturers have implemented Projection Artefact Removal (PAR) algorithms to address this issue [18]. What is currently missing is a way to interpret imaging data, both structural and vascular, against the backdrop of healthy ageing. Without such context, distinguishing early glaucomatous change from normal senescence becomes an exercise in uncertainty.

## 0.3 The Role of Artificial Intelligence

Over the last decade, AI has shown promise in ophthalmology, particularly in the analysis of OCT and OCTA. AI models can integrate large amounts of multimodal data, reducing human subjectivity and improving diagnostic performance [19]. Recent studies have demonstrated that AI models trained on well-labelled datasets can achieve human-level performance in specific image classification tasks, such as detecting referable glaucoma [20,21].

However, challenges persist regarding model generalisability, interpretability, and data bias. Moreover, the reliance on binary classification limits AI's ability to capture the full spectrum of disease severity or distinguish subtle ageing-related changes from pathology [22].

To ensure accessibility for a mixed audience, key AI terms are precisely defined:

- Artificial Intelligence (AI): refers broadly to computational systems capable of performing tasks that usually require human intelligence. In this work, AI encompasses both machine learning and deep learning methods.
- Machine Learning (ML): refers to algorithms that learn relationships from data. Here, we apply support vector regression (SVR) to predict ocular age from quantitative vascular and structural imaging features.
- Deep Learning (DL): It is a subdomain of ML based on neural networks. We utilise convolutional neural networks (CNNs) trained on OCT and OCTA images to estimate biological age and identify structural–vascular mismatches.
- Convolutional Neural Networks (CNNs): DL architectures with convolutional layers for feature extraction from imaging data.

- Support Vector Regression (SVR): An ML method predicting continuous outcomes by mapping data into high-dimensional spaces [23].

All models used in this thesis are supervised learning algorithms, trained on explicitly labelled data from rigorously screened healthy participants. No unsupervised, reinforcement, generative, or foundation models are explored. The focus is on clinically interpretable, task-specific prediction models designed for structured imaging data.

## 0.4 A New Approach: Modelling Ocular Ageing with AI

This thesis proposes an alternative paradigm: to define normative vascular and structural ageing trajectories and use them as a biological benchmark to detect deviations that may signal early disease. The approach builds on evidence that vascular changes may contribute to disease onset, complementing traditional structural and functional metrics [23].

By training AI models on healthy OCT/OCTA scans, we aim to estimate a person's ocular age (Predicted Ocular Age). Deviations from the predicted ocular age (Δ age), particularly when structural and vascular markers are mismatched, may indicate pathological changes that precede clinical detection.

We introduce a novel multimodal AI system, GlauOCTA, designed to leverage high-dimensional normative data to enhance early diagnosis and personalised risk stratification. By modelling what is "normal for age," GlauOCTA moves beyond binary classification toward a nuanced, biologically anchored risk model.

## 0.5 Research Questions

This work addresses the following key questions:

1. Can normative vascular density values from OCTA be established across age groups as a benchmark for healthy ocular ageing?
2. How accurately can machine learning models predict ocular age using structural and vascular imaging data?
3. Do deviations from predicted ocular age (Δ age) correlate with early glaucomatous damage?
4. What are the ethical and clinical implications of integrating AI-based risk models into glaucoma care?

## 0.6 Research Objectives

This work seeks to:

- Establish normative, decade-stratified OCTA vascular density reference values from a rigorously screened healthy population.

- Develop vascular and structural ageing models using ML to predict ocular age.
- Identify deviation patterns (Δ age) that may serve as early biomarkers of glaucomatous damage.
- Explore the implications of such models for individualised glaucoma monitoring and future AI-guided screening protocols.

## 0.7 Key contribution

- A normative OCTA dataset for vascular ageing across decades.
- An SVR-based model for ocular age prediction.
- GlauOCTA-AI, a multimodal CNN for glaucoma risk assessment.
- Ethical guidelines for AI-driven diagnostics in ophthalmology.

## 0.8 Structure of the Thesis

- Chapter 1 provides a detailed clinical and anatomical foundation for understanding the neurovascular nature of glaucoma.
- Chapter 2 reviews the fundamentals of AI in medicine and ophthalmology.
- Chapter 3 describes our imaging dataset and pre-processing pipeline.
- Chapter 4 presents the development, training, and internal validation of the AI model.
- Chapter 5 focuses on the normative vascular ageing study.
- Chapter 6 explores clinical integration, ethical considerations, and future directions.

By redefining the diagnostic approach through the lens of ageing, imaging, and AI, this thesis aims to provide a more personalised and timely method of glaucoma detection, ultimately improving outcomes for the many patients who remain undiagnosed until their vision is already compromised.

## References


1. Tham YC, Li X, Wong TY, Quigley HA, Aung T, Cheng CY. Global prevalence of glaucoma and projections of glaucoma burden through 2040: a systematic review and meta-analysis. Ophthalmology. 2014 Nov;121(11):2081-90. doi: 10.1016/j.ophtha.2014.05.013. Epub 2014 Jun 26. PMID: 24974815.
2. Quigley HA, Broman AT. The number of people with glaucoma worldwide in 2010 and 2020. Br J Ophthalmol. 2006 Mar;90(3):262-7. doi: 10.1136/bjo.2005.081224. PMID: 16488940; PMCID: PMC1856963.
3. Weinreb RN, Aung T, Medeiros FA. The pathophysiology and treatment of glaucoma: a review. JAMA. 2014 May 14;311(18):1901-11. doi: 10.1001/jama.2014.3192. PMID: 24825645; PMCID: PMC4523637.
4. Heijl A, Peters D, Bengtsson B. Long-term Impact of Immediate Versus Delayed Treatment of Early Glaucoma: Results From the Early Manifest Glaucoma Trial. Am J Ophthalmol. 2023 Aug;252:286-294. doi: 10.1016/j.ajo.2023.04.010. Epub 2023 May 2. PMID: 37142174.
5. Kass MA, Heuer DK, Higginbotham EJ, Johnson CA, Keltner JL, Miller JP, Parrish RK 2nd, Wilson MR, Gordon MO. The Ocular Hypertension Treatment Study: a randomized trial determines that topical ocular hypotensive medication delays or prevents the onset of primary open-angle glaucoma. Arch Ophthalmol. 2002 Jun;120(6):701-13; discussion 829-30. doi: 10.1001/archopht.120.6.701. PMID: 12049574.
6. European Glaucoma Society. Terminology and Guidelines for Glaucoma, 5th Edition.
7. Glen FC, Baker H, Crabb DP. A qualitative investigation into patients' views on visual field testing for glaucoma monitoring. BMJ Open. 2014 Jan 10;4(1):e003996. doi: 10.1136/bmjopen-2013-003996. PMID: 24413347; PMCID: PMC3902333.
8. Heijl A, Leske MC, Bengtsson B, Hyman L, Bengtsson B, Hussein M; Early Manifest Glaucoma Trial Group. Reduction of intraocular pressure and glaucoma progression: results from the Early Manifest Glaucoma Trial. Arch Ophthalmol. 2002 Oct;120(10):1268-79. doi: 10.1001/archopht.120.10.1268. PMID: 12365904.
9. Grippo TM, Liu JH, Zebardast N, Arnold TB, Moore GH, Weinreb RN. Twenty-four-hour pattern of intraocular pressure in untreated patients with ocular hypertension. Invest Ophthalmol Vis Sci. 2013 Jan 17;54(1):512-7. doi: 10.1167/iovs.12-10709. PMID: 23211815; PMCID: PMC3558295.
10. Brandt JD, Beiser JA, Kass MA, Gordon MO. Central corneal thickness in the Ocular Hypertension Treatment Study (OHTS). Ophthalmology. 2001 Oct;108(10):1779-88. doi: 10.1016/s0161-6420(01)00760-6. PMID: 11581049.
11. Leske MC, Heijl A, Hussein M, Bengtsson B, Hyman L, Komaroff E; Early Manifest Glaucoma Trial Group. Factors for glaucoma progression and the effect of treatment: the early manifest glaucoma trial. Arch Ophthalmol. 2003 Jan;121(1):48-56. doi: 10.1001/archopht.121.1.48. PMID: 12523884.
12. Johnson CA, Cioffi GA, Liebmann JR, Sample PA, Zangwill LM, Weinreb RN. The relationship between structural and functional alterations in

glaucoma: a review. Semin Ophthalmol. 2000; 15 (4): 221-233. Doi: 10.3109/08820530009037873.
13. Miki A, Medeiros FA, Weinreb RN, Jain S, He F, Sharpsten L, Khachatryan N, Hammel N, Liebmann JM, Girkin CA, Sample PA, Zangwill LM. Rates of retinal nerve fiber layer thinning in glaucoma suspect eyes. Ophthalmology. 2014 Jul;121(7):1350-8. doi: 10.1016/j.ophtha.2014.01.017. Epub 2014 Mar 13. PMID: 24629619; PMCID: PMC4310561.
14. Bengtsson B, Heijl A. False-negative responses in glaucoma perimetry: indicators of patient performance or test reliability? Invest Ophthalmol Vis Sci. 2000 Jul;41(8):2201-4. PMID: 10892863.
15. Leung CK, Chan WM, Yung WH, Ng AC, Woo J, Tsang MK, Tse RK. Comparison of macular and peripapillary measurements for the detection of glaucoma: an optical coherence tomography study. Ophthalmology. 2005 Mar;112(3):391-400. doi: 10.1016/j.ophtha.2004.10.020. PMID: 15745764.
16. Moghimi S, Zangwill LM, Penteado RC, Hasenstab K, Ghahari E, Hou H, Christopher M, Yarmohammadi A, Manalastas PIC, Shoji T, Bowd C, Weinreb RN. Macular and Optic Nerve Head Vessel Density and Progressive Retinal Nerve Fiber Layer Loss in Glaucoma. Ophthalmology. 2018 Nov;125(11):1720-1728. doi: 10.1016/j.ophtha.2018.05.006. Epub 2018 Jun 12. PMID: 29907322.
17. Spaide RF, Fujimoto JG, Waheed NK, Sadda SR, Staurenghi G. Optical coherence tomography angiography. Prog Retin Eye Res. 2018 May;64:1-55. doi: 10.1016/j.preteyeres.2017.11.003. Epub 2017 Dec 8. PMID: 29229445; PMCID: PMC6404988.
18. Zhang A, Zhang Q, Wang RK. Minimizing projection artifacts for accurate presentation of choroidal neovascularization in OCT micro-angiography. Biomed Opt Express. 2015 Sep 28;6(10):4130-43. doi: 10.1364/BOE.6.004130. PMID: 26504660; PMCID: PMC4605069.
19. Ting DSW, Pasquale LR, Peng L, Campbell JP, Lee AY, Raman R, Tan GSW, Schmetterer L, Keane PA, Wong TY. Artificial intelligence and deep learning in ophthalmology. Br J Ophthalmol. 2019 Feb;103(2):167-175. doi: 10.1136/bjophthalmol-2018-313173. Epub 2018 Oct 25. PMID: 30361278; PMCID: PMC6362807.
20. Nguyen V, Iyengar S, Rasheed H, Apolo G, Li Z, Kumar A, Nguyen H, Bohner A, Bolo K, Dhodapkar R, Do J, Duong AT, Gluckstein J, Hong K, Humayun LL, James A, Lee J, Nguyen K, Wong BJ, Ambite JL, Kesselman C, Daskivich LP, Pazzani M, Xu BY. Comparison of Deep Learning and Clinician Performance for Detecting Referable Glaucoma from Fundus Photographs in a Safety Net Population. Ophthalmol Sci. 2025 Feb 25;5(4):100751. doi: 10.1016/j.xops.2025.100751. PMID: 40235827; PMCID: PMC11999268.
21. Ran AR, Tham CC, Chan PP, Cheng CY, Tham YC, Rim TH, Cheung CY. Deep learning in glaucoma with optical coherence tomography: a review. Eye (Lond). 2021 Jan;35(1):188-201. doi: 10.1038/s41433-020-01191-5. Epub 2020 Oct 7. Erratum in: Eye (Lond). 2021 Jan;35(1):357. doi: 10.1038/s41433-020-01244-9. PMID: 33028972; PMCID: PMC7852526.
22. Ting DSW, Cheung CY, Lim G, Tan GSW, Quang ND, Gan A, Hamzah H, Garcia-Franco R, San Yeo IY, Lee SY, Wong EYM, Sabanayagam C,

Baskaran M, Ibrahim F, Tan NC, Finkelstein EA, Lamoureux EL, Wong IY, Bressler NM, Sivaprasad S, Varma R, Jonas JB, He MG, Cheng CY, Cheung GCM, Aung T, Hsu W, Lee ML, Wong TY. Development and Validation of a Deep Learning System for Diabetic Retinopathy and Related Eye Diseases Using Retinal Images From Multiethnic Populations With Diabetes. JAMA. 2017 Dec 12;318(22):2211-2223. doi: 10.1001/jama.2017.18152. PMID: 29234807; PMCID: PMC5820739.

23. Donkor R, Jammal AA, Greenfield DS. Relationship between Blood Pressure and Rates of Glaucomatous Visual Field Progression: The Vascular Imaging in Glaucoma Study. Ophthalmology. 2025 Jan;132(1):30-38. doi: 10.1016/j.ophtha.2024.07.026. Epub 2024 Aug 6. PMID: 39111669.

# Chapter 1. Rethinking Glaucoma: A Neurovascular Disease Revealed Through Imaging Innovation

This chapter provides the clinical and imaging context necessary to understand the evolving nature of glaucoma as a neurovascular disease. It introduces the rationale for vascular biomarkers and highlights the limitations of current diagnostic modalities, setting the stage for the AI-focused exploration in the following chapters.

## 1.1 Clinical and Anatomical Foundations of Glaucoma

Glaucoma is a heterogeneous group of optic neuropathies characterised by chronic degeneration of retinal ganglion cells (RGCs) and their axons, leading to structural damage at the optic nerve head and corresponding functional loss [1-2].

The disease encompasses a spectrum of presentations and progression rates, often independent of intraocular pressure (IOP) values [3]. This observation has fuelled growing recognition of glaucoma as a multifactorial disease with neurovascular and neurodegenerative components [4]. It remains one of the leading causes of irreversible blindness worldwide, posing a substantial burden on healthcare systems [5,6].

Structural damage in glaucoma is anatomically localised to the lamina cribrosa, peripapillary retina, and macular ganglion cell complex. These regions are particularly vulnerable to mechanical and vascular stress. The lamina cribrosa, a collagenous structure traversed by retinal ganglion cell (RGC) axons, is a critical site where intraocular pressure (IOP)- induced strain and impaired perfusion may initiate axonal degeneration [7]. Advancements in imaging, particularly spectral-domain optical coherence tomography (SD-OCT) and optical coherence tomography angiography (OCTA), now allow detailed evaluation of these anatomical substrates.

Open-angle glaucoma (OAG) is the most prevalent among the different subtypes, affecting around 3.5% of individuals over 40 years of age [8]. In contrast, angle-closure glaucoma (ACG) is less common, at roughly 0.5%, but is associated with a higher risk of blindness. Both conditions exhibit an age-related increase in incidence [9,10].

A 2021 meta-analysis reported a cumulative risk ratio of 2.39, indicating that ACG patients have more than twice the risk of blindness compared to those with OAG [11]. Overall, the cumulative incidences of blindness in at least one eye and bilateral blindness from glaucoma were 26.5% and 5.5%, respectively, after 10 years, and 38.1% and 13.5% at 20 years [12].

The incidence and probability of blindness due to glaucoma have decreased over the last 45 years, as described in the previously mentioned reference 5, Mahil et al.

(2014), due to improved diagnostic tools, better treatment options, and increased knowledge of the disease among clinicians [13].

Several risk factors have been identified in the pathogenesis of glaucoma, including advanced age, elevated intraocular pressure (IOP), non-White ethnicity, a positive family history, and high myopia [14]. Although intraocular pressure is not always higher than population-based values, it is one of the most important and the only modifiable risk factors, as demonstrated by extensive clinical trials [15]. Understanding these risk factors is crucial for identifying individuals at higher risk and implementing preventive or therapeutic interventions to slow or prevent disease progression. Glaucoma exists on a spectrum, ranging from pre-perimetric stages with no detectable vision loss to end-stage blindness [16]. Diagnosis is challenging because patients often present at different points along this continuum, with early symptoms being subtle or absent.

**Figure 1. The glaucoma continuum, as described by Weinreb, outlines the progression of glaucoma as a disease, from initial, often asymptomatic changes in the optic nerve and retina to eventual visual field loss and blindness, with damage detected through newer, more sensitive perimetric tests.**

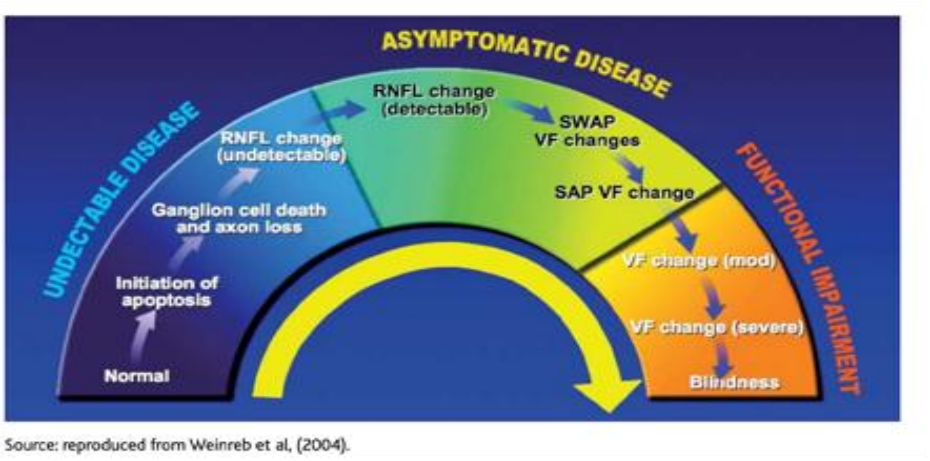


Source: reproduced from Weinreb et al, (2004).

*RNFL = Retinal Nerve Fibre Layer; SWAP = Short-Wavelength Automated Perimetry; SAP = Standard Automated Perimetry; VF = Visual Field*

## 1.2 The neurodegenerative nature of Glaucoma

Traditionally, glaucoma has been classified as an optic neuropathy caused by progressive retinal ganglion cell (RGC) death through a complex and silent apoptotic process. Emerging evidence suggests potential overlaps with Alzheimer's disease (AD), though a systemic neurodegenerative link remains unproven [17].

Some studies propose that glaucoma shares features like neuronal apoptosis and oxidative stress with AD, prompting comparisons to “Alzheimer’s of the eye” [18]. In a large national cohort, the authors found that persons with glaucoma had increased risks for AD, and all-cause dementia, particularly those diagnosed with glaucoma at older ages [19].

However, these features may reflect secondary effects of RGC loss or ageing rather than a primary systemic process [20]. Ongoing research focuses on retinal fibre layer thinning in the macular region as a potential early indicator of AD, though its specificity to glaucoma versus other CNS conditions is debated [21].

Martucci et al. explored overlaps between glaucoma and AD, identifying shared neuroimaging biomarkers [22]. Both conditions exhibit neurodegeneration, with glaucoma showing structural changes beyond the eye, including atrophy of the lateral geniculate nucleus (LGN) and alterations in optic radiation and visual cortex, resembling AD patterns. Diffusion tensor imaging and functional MRI reveal white matter disruption in glaucoma, potentially secondary to RGC loss or age-related changes [23]. Martucci et al. hypothesise shared mechanisms, such as amyloid-beta accumulation and trans-synaptic degeneration, but these may partly result from secondary degeneration rather than a systemic neurodegenerative process.

In glaucoma, RGC apoptosis initiates a self-propagating neurodegenerative cascade**.** This bystander cell death, or secondary degeneration, spreads via gap junctions and inflammatory mediators, amplifying neuronal loss [24]. This cycle explains why glaucomatous damage may persist despite controlled IOP, highlighting the need for early detection strategies [25].

## 1.3 The vascular insufficiency in Glaucoma

The vascular hypothesis suggests that reduced perfusion, vascular dysregulation, and endothelial dysfunction may contribute to disease progression, though its primary role remains debated [26].

Due to their high metabolic demands, retinal ganglion cells (RGCs) rely on precise autoregulation of ocular blood flow to maintain function. Impaired blood flow may increase hypoxic stress, potentially contributing to apoptosis of RGC; however, evidence for causality is limited [27].

Key vascular mechanisms potentially involved in glaucoma include:

- Reduced optic nerve head (ONH) perfusion: Optical coherence tomography angiography (OCTA) reveals decreased peripapillary and macular vessel density, particularly in normal-tension glaucoma (NTG), indicating a possible role as described Chan et al. 2019 in progression, though not necessarily primary [28].

- Mitochondrial dysfunction and hypoxia**:** Hypoxia may impair ATP production, thereby increasing oxidative stress and contributing to RGC damage, which can be potentially secondary to IOP or systemic factors [29].
- Impaired vascular autoregulation**:** Limited evidence suggests that altered endothelial function may reduce retinal blood flow adaptability, potentially leading to capillary dropout; however, robust longitudinal data are needed [30].
- Systemic vascular abnormalities**:** Cardiovascular risk factors (e.g., hypertension, smoking, obesity) and low ocular perfusion pressure are associated with increased glaucoma risk, suggesting systemic vascular contributions [31-35]. Additionally, glaucoma is an independent risk factor for cardiovascular disease, indicating shared vascular pathways [36].

These vascular factors, alongside evidence of systemic comorbidities and perfusion pressure associations, highlight the potential for biomarkers beyond intraocular pressure (IOP), such as vessel density metrics, to enhance risk assessment, and pending further validation [37,38].

## 1.4 Retinal Vascular Changes and Small Vessel Disease in Glaucoma

Recent studies suggest that vascular dysfunction, potentially linked to cerebral small vessel disease, may interact with neurodegenerative processes in glaucoma, though direct evidence remains limited [39].

The retina's microvascular structure, similar to that of cerebral vasculature, positions it as a potential marker of vascular health in glaucoma [40]. Optical coherence tomography angiography (OCTA) studies in glaucoma patients reveal reduced retinal capillary perfusion, which may be related to cerebral small vessel disease, although the specificity to glaucoma is unclear [41]. Specifically, lower retinal vessel density (VD) and perfusion metrics have been associated with:

- Reduced cognitive processing speed, a marker of neurodegeneration, though not unique to glaucoma [42].
- White matter abnormalities on MRI, such as increased free water content, in cerebral small vessel disease, are potentially relevant to glaucoma's vascular changes [43].
- Lower fractional anisotropy (FA), indicating reduced white matter integrity, which may align with vascular alterations in glaucoma [44].

These findings suggest possible vascular parallels between glaucoma and cerebral small vessel disease; however, their role in glaucoma progression requires further investigation [45]. Additional research is necessary to determine whether retinal vascular changes serve as specific biomarkers for glaucoma or represent a broader manifestation of small vessel disease [46].

## 1.5 The blood supply of the sensory eye

### 1.5.1 Retinal vascularisation

The ophthalmic artery, the first intracranial branch of the internal carotid artery, gives rise to the central retinal artery (CRA) and the short and long posterior ciliary arteries (PCA), both of which are responsible for retinal vascularisation. Retinal blood vessels from the central retinal artery (CRA) do not form any anastomoses and are considered terminal branches. It supplies the inner two-thirds of the retinal thickness. Figure 2, adapted from Dr. Kathrin Hirsh's thesis, provides a visual representation of the retinal vascularisation [47].

Immediately before leaving the optic nerve, the CRA divides into superior, inferior, temporal, and nasal branches. Occasionally (18% to 32% of eyes), a cilioretinal artery from the ciliary circulation irrigates the macula [48].

**Figure 2. Ocular blood supply.**

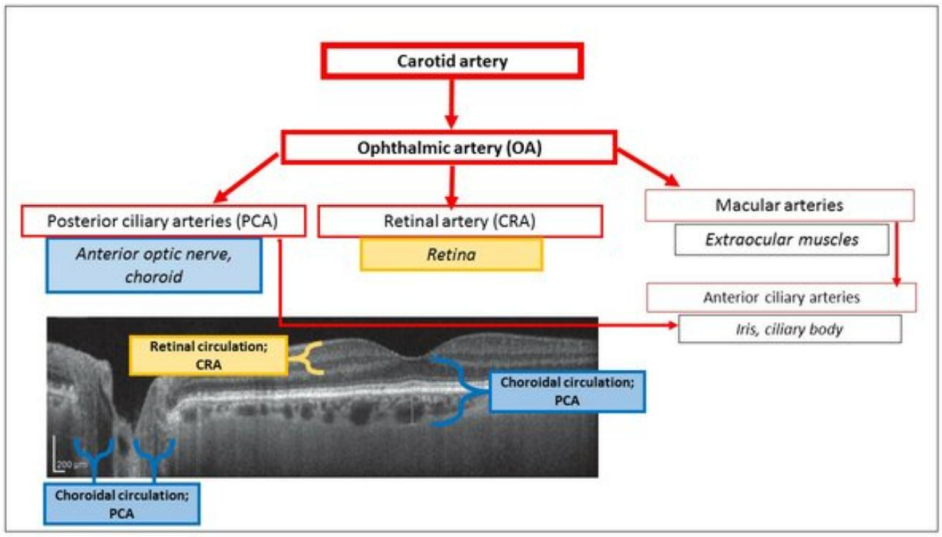


Four vascular networks are present in the retina of the posterior pole, similar to the pathway of the veins, which remain in the NFL:

1. The peripapillary radial capillary (PRC) network is in the nerve fibre layer and around the optic nerve head. These capillaries arise from single arterioles around the disc from the short PCA, not from vessels within the disc. Peripapillary capillaries have a radial distribution, rarely anastomose

(in contrast to other intraretinal capillaries) and have a limited extension to the posterior pole [49].

2. The plexus of superficial capillaries at the nerve fibre layer and the retinal ganglion cell layer. The vessels of the superficial capillaries' plexus resemble a spider's web. They present a linear and continuous shape [50].
3. The intermediate capillary plexus. The experts don't have a consensus on the exact location of this plexus [51].
4. The deep capillary plexus corresponds to the capillary beds on either side of the inner nuclear layer, including the intermediate and deep capillary plexus. It has a regular distribution around the foveal avascular zone (FAZ), with small and complex interconnections to ensure adequate perfusion of all cells in the inner retina, a "mesh" configuration. The capillaries are absent in the extreme periphery of the retina and the fovea, delimiting the FAZ, with a diameter of 400-500 µm in normal eyes.

Venous drainage from the retina usually accompanies arterial vascularisation. Retinal veins (especially venules) are also found in the inner retina. Occasionally, they cross with the corresponding arteries, sharing the adventitial layer. Its drainage is carried out into the central retinal vein, which receives blood from the optic nerve [52].

### 1.5.2 Optic nerve vascularisation

The blood supply of the optic nerve varies according to its different segments, as shown in Figure 3.

**Figure 3. The blood supply of the optic nerve head.**

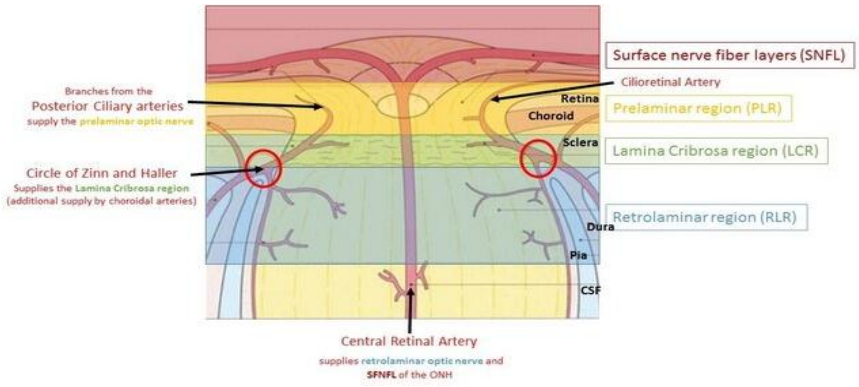


The retrolaminar portion of the optic nerve is primarily vascularised by the pila vessels, which originate from the internal carotid artery, and the short posterior cerebral artery (PCA), with a minor contribution from the central retinal artery (CRA) [53].

The laminar portion is supplied by the posterior short ciliary arteries or by branches of the Zinn-Haller arterial circle, an arterial ring located in the thickness of the sclera, surrounding the optic nerve head (supplied by paraaortic branches of the short posterior ciliary arteries). CRA does not contribute to the irrigation of this segment [54].

Finally, the short PCA (cilioretinal arteries, if present) and recurrent choroidal arteries supply the prelaminar nerve segment. The CRA supplies the nerve fibre layer [55].

### 1.5.3 Choroidal vascularisation

The choroid constitutes the most vascularised tissue of the eye, receiving its blood supply from the short and long PCAs, which branch from the ophthalmic artery [56]. Unlike the retinal circulation, the choroid exhibits limited autoregulation, with blood flow primarily driven by perfusion pressure and modulated by neural and humoral factors [57]. Histologically, the choroid is divided into five layers: 1) Bruch's membrane; 2) Choriocapillaris layer; 3) Sattler's layer; 4) Haller's layer; and 5) Suprachoroidal layer [58].

The choriocapillaris layer, a fine network of fenestrated, highly anastomosed capillaries in a single plane beneath the retinal pigment epithelium (RPE), supplies nutrients to the photoreceptors and RPE. It has a maximum capillary density, with a thickness of approximately 10 µm at the fovea, decreasing to 7 µm at the periphery [58]. Capillaries arise from arterioles in Sattler's layer, each feeding a hexagonal or lobular bed, creating the characteristic patch-like pattern of the choriocapillaris [59].

The Sattler's layer contains small and medium-sized arterioles, while Haller's layer comprises large-calibre vessels, both contributing to the choroid's vascular hierarchy [59]. Venous drainage occurs through the vortex veins, typically 4 to 7 per eye, which exit the choroid at the equator [60].

## 1.6 Current Challenges in Glaucoma Diagnosis and Management

Glaucoma diagnosis is hindered by intraocular pressure (IOP) variability, optic disc morphological differences, and the delayed onset of functional deficits relative to structural damage, with up to 50% of retinal ganglion cells lost before visual field defects emerge [61]. The intra-individual variability in the rate of progression (RoP) further complicates management, as some patients tolerate elevated IOP without vision loss, while others progress to blindness despite well-controlled pressures [62]. Early diagnosis, enabled by preventive strategies like targeted IOP screening for high-risk groups (e.g., those over 40, with family history, African descent, or high myopia), is crucial to halt disease progression [63]. Treatment options, including laser trabeculoplasty, topical IOP-lowering medications, or surgical interventions, aim to preserve vision, but undertreatment risks irreversible optic nerve damage [64].

At the same time, over-treatment may cause ocular surface disease or surgical complications [65].

**Figure 4. Evaluation of Functional loss/time for individualised treatment, adapted from the EGS Guidelines.**

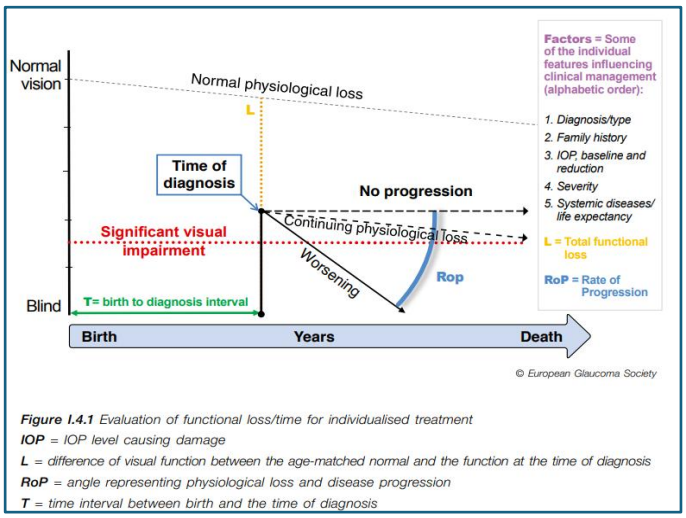


*Figure I.4.1 Evaluation of functional loss/time for individualised treatment*
*IOP = IOP level causing damage*
*L = difference of visual function between the age-matched normal and the function at the time of diagnosis*
*RoP = angle representing physiological loss and disease progression*
*T = time interval between birth and the time of diagnosis*

Regular monitoring to assess RoP, as illustrated in Figure 4 (adapted from EGS Guidelines), informs personalised treatment strategies, yet logistical barriers to screening, such as limited awareness and resources, underscore the need for advanced diagnostics like optical coherence tomography angiography (OCTA) to improve early detection [66].

## 1.7 Diagnosis tools and new imaging modalities

The diagnosis of glaucoma is based on IOP, VF, and imaging, all of which have their limitations. VF testing, being subjective, is influenced by environmental factors and physiological fluctuations, necessitating at least six tests over two years to establish the RoP and rule out rapid progression (≥−2 dB/year) for personalised treatment [67-71].

Colour fundus photography has been instrumental in the diagnosis of glaucoma for many decades. In 1926, Johan Nordenson and the Zeiss Camera Company introduced the first commercially available fundus camera, marking a significant advancement in retinal imaging. By capturing detailed images of the optic disc and retinal nerve fibre layer, clinicians could detect structural changes indicative of glaucoma, such as increased cup-to-disc ratios and optic disc notching. Over time, fundus photography has become a standard tool in ophthalmic practice for documenting and monitoring glaucomatous changes. Fundus photographs are inherently two-dimensional; generating a three-dimensional view requires two images taken at slightly different angles and binocular viewing, which is a logistically

cumbersome and challenging process to store and manage. We know from various studies that the quality of the image is crucial, as the level of expertise of the clinician still exhibits intra-individual variability in classifying the pictures [72,73].

Since its introduction in 1996, OCT has significantly advanced diagnosis and research in ophthalmology. The technology has rapidly evolved from time-domain OCT, which offered axial scan rates of up to 400 A-scans per second, to high-speed Spectral-Domain OCT (SD-OCT), reaching up to 120,000 A-scans per second. These systems enable detailed 3D retinal reconstructions (Figure 5) with automatic layer segmentation, enhancing optic nerve head analysis and improving microstructural visualisation.

The latest generation, Swept-Source OCT (SS-OCT), utilises a tunable laser light source with longer wavelengths, allowing for deeper tissue penetration and higher acquisition speeds, typically ranging from 100,000 to 200,000 A-scans per second, and in some systems, up to 400,000 A-scans per second. These SS-OCTs offer enhanced imaging of deep retinal and choroidal structures, making them ideal for comprehensive analysis of the posterior segment.

**Figure 5. Automatic Retina segmentation layers.**

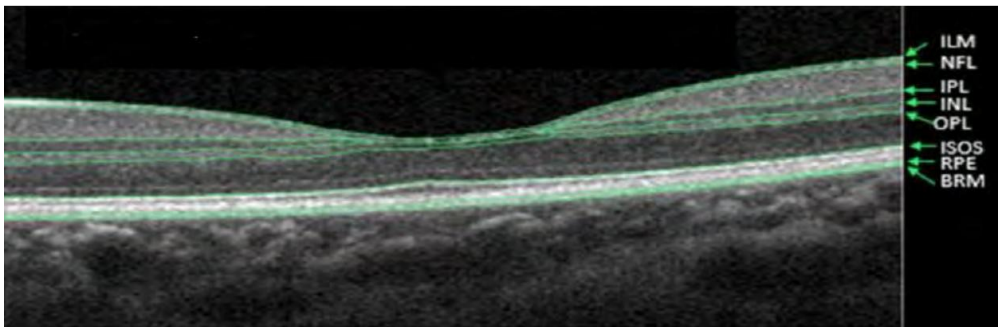


- Superficial (Upper limit = ILM; Lower limit = IPL-10μm)
- Deep (Upper limit = IPL-10μm; Lower Limit = OPL+10μm)
- Outer (Upper limit = OPL+10μm; Lower limit = BRM-10μm)
- Choroid (Upper limit = BRM-10μm; Lower limit = BRM+30μm)
- Retina (Upper limit = ILM; Lower limit = OPL+10μm)

SD-OCT, widely used in clinical practice and research, enables clinicians to view the inner retinal structures, similar to those observed in anatomical and histological studies (Figure 6), in a highly detailed, non-invasive manner. Picture 3 shows the histological comparison with the retina image obtained by SD-OCT [74].

**Figure 6. Comparison of the OCT to the anatomical structure of the retina.**

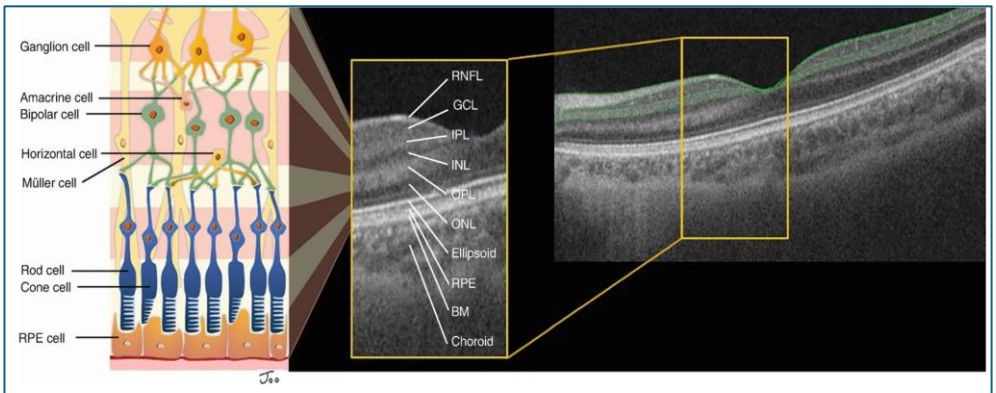


Human macular structure. Retinal layers (Left) and representative human macular structure imaged by swept-source optical coherence tomography (SS-OCT) (Middle and Right). Retinal nerve fiber layer (RNFL), ganglion cell layer (GCL), and inner plexiform layer (IPL) are annotated in green solid lines. The foveal structure in the yellow inset is magnified and each retinal layer is annotated. RNFL, retinal nerve fiber layer; GCL, ganglion cell layer; IPL, inner plexiform layer; INL, inner nuclear layer; OPL, outer plexiform layer; ONL, outer nuclear layer; RPE, retinal pigment epithelium; BM, Bruch's membrane

In glaucoma, OCT has been used to measure the thickness of the ganglion cell complex (GCC) in the macular area and to assess the morphology of the peripapillary and optic nerve head regions. The thickness is measured based on the EDTRS grid of the macula, as shown in Figure 7, adapted from the publication by Hasan et al. Journal of Ophthalmology 2024 [75].

**Figure 7: Early Treatment of Diabetic Retinopathy Study (ETDRS) grid RE.**

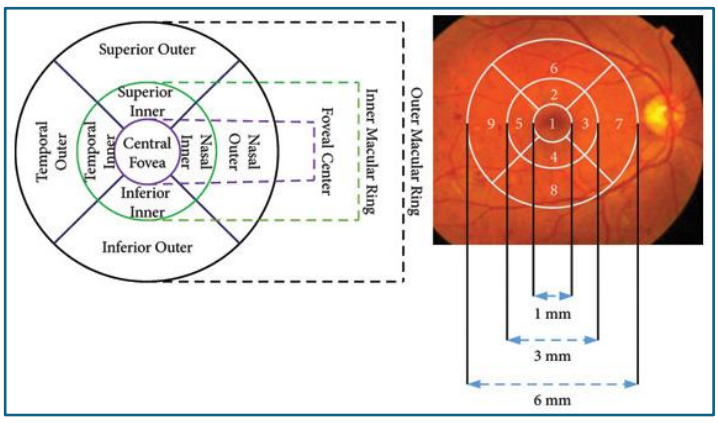


The GCC encompasses three layers of ganglion cells in the retina:

1. The RNFL comprises the ganglion cell axons.
2. The GCL comprises the ganglion cell bodies.
3. The IPL comprises the ganglion cell dendrites [76].

The GCC becomes thinner as ganglion cells die from glaucoma [77]. OCT measures FLV% (Focal Loss Volume) and GLV% (Global Loss Volume). FLV% quantifies the amount of significant GCC loss. As determined by volume, FLV is expressed as a percentage of the map area with significant ganglion cell loss. GLV% quantifies the average amount of GCC loss over the entire GCC map. GLV is the sum of the pixels where the fractional deviation map value is less than 0, divided by the total map area, to give a percentage loss of GCC thickness. The GCC deviation map is not stratified by any factor, such as age [78]. The OCT measurements on the disc comprise the Cup/Disc Area Ratio, Cup/Disc vertical and horizontal Ratios, Rim, disc, and Cup Areas ($mm^2$), as well as cup volume ($mm^3$). The disc margin is automatically detected (Figure 8) based on Bruch's Membrane Opening (BMO), and the cup and rim are measured within the BMO plane. The portion above the BMO plane is called the "rim," while the portion below is called the "cup" [79].

**Figure 8. Automatic Disc segmentation layers.**

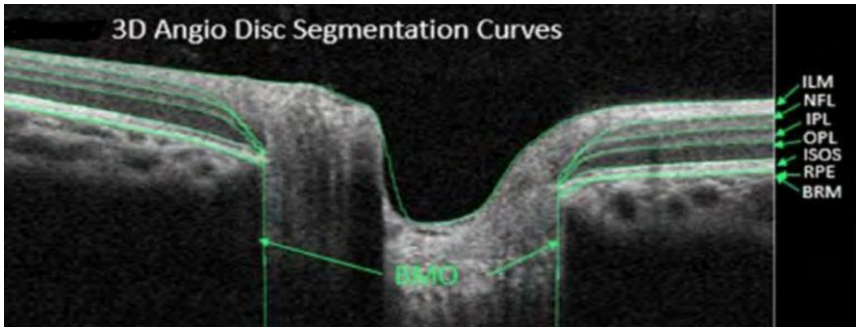


- Vitreous (Upper limit = ILM-2000µm; Lower limit = ILM)
- Superficial (Upper limit = ILM; Lower limit = IPL-10µm)
- RPC (Upper limit = ILM; Lower Limit = NFL): the nerve fibre layer containing the small branches of arterioles and venules.
- Choroid (Upper limit = BRM-10µm; Lower limit = BRM+30µm)
- Retina (Upper limit = ILM; Lower limit = OPL+10µm)

The RNFL thickness is measured across the image and on the Garway-Heath-based peripapillary grid (Figure 9) [80]. The peripapillary region is defined by two rings centred on the disc centre, 2.5mm and 4.5mm in diameter. The peripapillary sector is then divided into eight sectors to follow RNFL distribution and is sectored to provide more straightforward correlation with visual field testing.

**Figure 9 illustrates the connections between the Standard Automated Perimetry visual field sectors and the peripapillary OCT scan circle. Based on the research of Garway-Heath et al., this map indicates how the physical arrangement of the retinal nerve fibre bundles corresponds to regions of the visual field and the peripapillary retinal nerve fibre layer.**

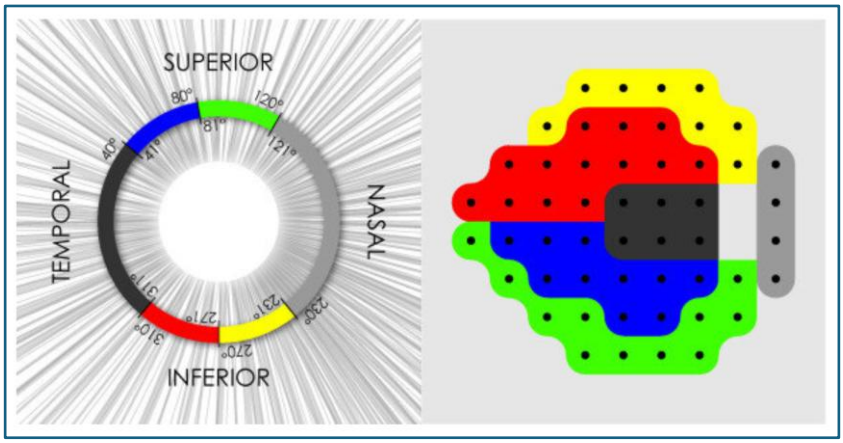


Optical coherence tomography (OCT) is limited by factors affecting image acquisition, such as media opacity and patient fixation, which can reduce quality [81]. OCT may fail to detect early glaucoma, as some pre-perimetric patients show visual field (VF) loss before OCT changes, particularly in normal-tension glaucoma with central damage [82]. In advanced glaucoma, the OCT 'floor effect' occurs when retinal nerve fibre layer (RNFL) thickness measurements plateau at a minimum due to residual non-neuronal tissue, masking further progression [83].

OCTA has been introduced as an add-on to the OCT system to replace traditional, invasive retinal fluorescein angiography. Unlike structural OCT, which primarily assesses retinal thickness, OCTA allows direct visualisation of microvascular changes. In glaucoma, vessel density loss has been strongly correlated with functional deficits, making OCTA an emerging biomarker for detecting and monitoring disease progression. OCTA maps the vascularisation in different layers of the retina. It visualises blood flow by detecting the motion of RBCs within ocular tissues [84]. It builds upon conventional OCT, which uses low-coherence interferometry to produce cross-sectional images (B-scans) of the retina with micrometre depth resolution [85].

OCTA acquires repeated OCT scans (A-scans or entire B-scans) at the exact location and then analyses the differences between those repeated scans over time (Figure 10). Stationary tissue yields little to no change in the OCT signal between consecutive scans. In contrast, moving RBCs produce fluctuations in the backscattered light intensity due to changes in scattering and speckle patterns. By detecting these temporal changes (motion contrast), OCTA can highlight the

locations of blood flow and reconstruct the vasculature. In essence, vessels are delineated because blood flow causes decorrelation (or variance) in the OCT signal compared to sequential scans, whereas static structures remain highly correlated [86]. The result is an in vivo map of the microvascular network, obtained without the need for dye injection, as the intrinsic motion of blood cells serves as the contrast agent.

**Figure 10. OCTA scans are built from repetitive B-scans at the exact location.**

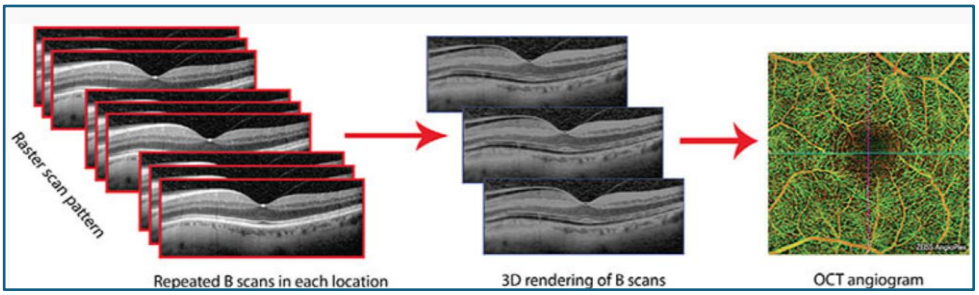


OCTA, acquired with standard OCT, co-registers structural and blood flow images, correlating pathology (e.g., atrophy) with vascular changes efficiently [87]. OCTA provides quantitative metrics such as VD and the percentage of vessel-occupied area to monitor progression [88]. Unlike OCT, which plateaus in advanced glaucoma due to RNFL thinning, OCTA detects ongoing vascular compromise [89]. However, OCTA's flow detection threshold (~0.3 mm/s) may miss slow capillary perfusion, and its static images lack temporal flow variability, which limits the sensitivity of AI models for early glaucoma detection [90]. This study used the upgraded Optovue Solix OCTA for detailed quantitative analysis.

## 1.8 OCTA demonstration of the retinal vasculature

The OCT-A follows the automatic OCT segmentation but can evaluate a layer of any thickness and depth (slabs) in the retina and choroid separately, representing them in a 3D model for the clinician. The automatic segmentation of most devices determines the presentation of four predefined face angiograms (Figure 11), based on the existence of two retinal vascular plexuses (superficial and deep).

## Figure11. Four predefined face angiograms of the retina.

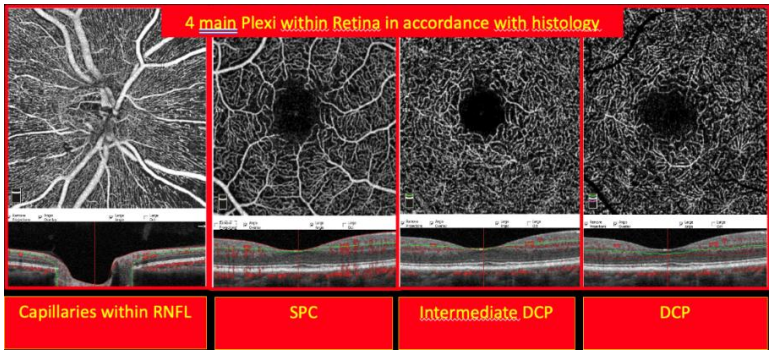


Zones of vascular dropout, as in Figure 12, on the choroidal slabs are a risk factor for glaucoma progression [90]. It is defined as the complete loss of choriocapillaris in localised parapapillary atrophy (PPA) regions, representing an actual perfusion defect.

**Figure 12. Choriocapillary dropout.**

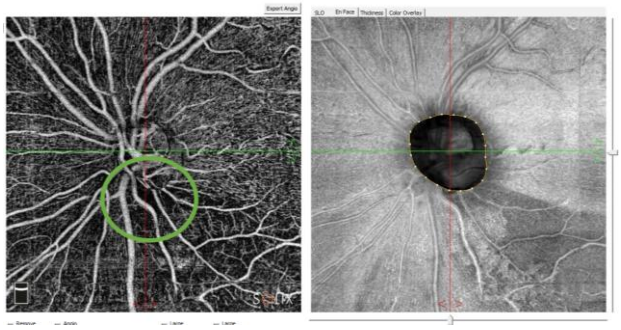

The choroid, supplied by multiple posterior ciliary arteries, exhibits limited autoregulation, which facilitates the detection of vascular density loss in conditions such as glaucoma [91].

OCTA measures VD in the peripapillary zone and the Radial Peripapillary Capillary (RPC). Loss in this layer seems to be implicated in the pathogenesis of glaucoma and most retinal vascular diseases [92]. It is associated with progressive RGC damage. Reduction in vasculature is reported to be more pronounced on the RPC slab than the deep retinal slabs in glaucomatous eyes [93]. It also measures the VD of the macula, FAZ in mm2 and its related parameters on the retinal slab. PERIM is the FAZ perimeter in mm and FD: vessel density of the 300μ μm width ring surrounding the FAZ, in %. FD is calculated by dividing the number of vessel pixels by the total number of pixels and then multiplying by 100%.

## 1.9 Discussion and Conclusion

While intraocular pressure (IOP) remains a key modifiable risk factor, glaucoma often progresses despite normal IOP, underscoring its multifactorial nature. Vascular insufficiency, mitochondrial dysfunction, oxidative stress, and impaired axonal transport likely contribute to disease progression beyond pressure-related mechanisms.

Despite advances in imaging, reliable biomarkers for personalised glaucoma care are still lacking. Optical coherence tomography angiography (OCTA) offers potential by capturing microvascular alterations that may precede structural loss, enabling earlier detection and better risk stratification.

A central, unresolved question persists: Does vascular dysfunction initiate ganglion cell loss, or does it result from it? Clarifying this causality is essential for developing targeted therapies.

OCTA shows promise in refining glaucoma monitoring, though it faces challenges such as motion artefacts, segmentation errors, and device variability. Standardisation and AI-enhanced analyses could help realise its clinical potential.

Transitioning from reactive to predictive care might help identify fast progressors and guide timely interventions.

The following chapters will explore the fundamentals of artificial intelligence in medicine (Chapter 2), followed by AI applications in glaucoma imaging (Chapter 3), model development (Chapter 4), normative dataset analysis (Chapter 5), and finally clinical integration and ethical reflections (Chapter 6)."

## References


1. Jonas JB, Aung T, Bourne RR, Bron AM, Ritch R, Panda-Jonas S. Glaucoma. Lancet. 2017;390(10108):2183-93. doi:10.1016/S0140-6736(17)31469-1.WHO (2019). World Report on Vision. Geneva: World Health Organization. Wiggs, J. (2015). Glaucoma genes and mechanisms. Prog. Mol. Biol. Transl. Sci. 134, 315–342.
2. Weinreb RN, Khaw PT. Primary open-angle glaucoma. Lancet. 2004;363(9422):1711-20. doi:10.1016/S0140-6736(04)16257-0.
3. Killer HE, Pircher A. Normal tension glaucoma: review of current understanding and mechanisms of optic neuropathy. Eye (Lond). 2018;32(5):924-30. doi:10.1038/s41433-018-0042-2.
4. Caprioli J. Glaucoma: a disease of early cellular senescence. Invest Ophthalmol Vis Sci. 2013;54(14):ORSF60-7. doi:10.1167/iovs.13-12716.
5. Malihi M, Moura Filho ER, Hodge DO, Sit AJ. Long-term trends in glaucoma-related blindness in Olmsted County, Minnesota. Ophthalmology. 2014 Jan;121(1):134-141. doi: 10.1016/j.ophtha.2013.09.003. Epub 2013 Oct 25. PMID: 24823760; PMCID: PMC4038428.
6. Varma R, Lee PP, Goldberg I, Kotak S. An assessment of the health and economic burdens of glaucoma. Am J Ophthalmol. 2011;152(4):515-22. doi:10.1016/j.ajo.2011.06.004.
7. Tan NYQ, Koh V, Girard MJA, Cheng CY. Imaging of the lamina cribrosa and its role in glaucoma: a review. Clin Exp Ophthalmol. 2018;46(2):177–88. doi:10.1111/ceo.13126.
8. Kapetanakis VV, Chan MP, Foster PJ, Cook DG, Owen CG, Rudnicka AR. Global variations and time trends in the prevalence of primary open angle glaucoma (POAG): a systematic review and meta-analysis. Br J Ophthalmol. 2016;100(1):86-93. doi:10.1136/bjophthalmol-2015-307223.
9. Day AC, Baio G, Gazzard G, Bunce C, Azuara-Blanco A, Munoz B, Friedman DS, Foster PJ. The prevalence of primary angle closure glaucoma in European derived populations: a systematic review. Br J Ophthalmol. 2012 Sep;96(9):1162-7. doi: 10.1136/bjophthalmol-2011-301189. Epub 2012 May 31. PMID: 22653314.
10. Cho HK, Kee C. Population-based glaucoma prevalence studies in Asians. Surv Ophthalmol. 2014 Jul-Aug;59(4):434-47. doi: 10.1016/j.survophthal. 2013.09.003. Epub 2014 May 13. PMID: 24837853.
11. George R, Panda S, Vijaya L. Blindness in glaucoma: primary open-angle glaucoma versus primary angle-closure glaucoma—a meta-analysis. Eye (Lond). 2022;36(11):2099-105. Published online 2021 Oct 13. doi:10.1038/s41433-021-01802-9.
12. Peters D, Bengtsson B, Heijl A. Lifetime risk of blindness in open-angle glaucoma. Am J Ophthalmol. 2013;156(4):724-30. doi:10.1016/j.ajo.2013.05.027.
13. Heijl A, Buchholz P, Norrgren G, Bengtsson B. Rates of visual field progression in clinical glaucoma care. Acta Ophthalmol. 2013;91(5):406-12. doi:10.1111/j.1755-3768.2012.02492.x.

14. Worley A, Grimmer-Somers K. Risk factors for glaucoma: what do they really mean? Aust J Prim Health. 2011;17(3):233-9. doi: 10.1071/PY10042. PMID: 21896259.
15. Leske MC, Heijl A, Hussein M, Bengtsson B, Hyman L, Komaroff E; Early Manifest Glaucoma Trial Group. Factors for glaucoma progression and the effect of treatment: the Early Manifest Glaucoma Trial. Arch Ophthalmol. 2003;121(1):48-56. doi:10.1001/archopht.121.1.48.
16. Weinreb RN, Friedman DS, Fechtner RD, Cioffi GA, Coleman AL, Girkin CA, Liebmann JM, Singh K, Wilson MR, Wilson R, Kannel WB. Risk assessment in the management of patients with ocular hypertension. Am J Ophthalmol. 2004 Sep;138(3):458-67. doi: 10.1016/j.ajo.2004.04.054. PMID: 15364230.
17. Gupta N, Yücel YH. Glaucoma as a neurodegenerative disease. Curr Opin Ophthalmol. 2007 Mar;18(2):110-4. doi: 10.1097/ICU.0b013e3280895aea. PMID: 17301611.
18. McKinnon SJ. Glaucoma: ocular Alzheimer’s disease? Front Biosci. 2003;8:s1140-56. doi:10.2741/1172.
19. Crump C, Sundquist J, Sieh W, Sundquist K. Risk of Alzheimer's Disease and Related Dementias in Persons with Glaucoma: A National Cohort Study. Ophthalmology. 2024 Mar;131(3):302-309. doi: 10.1016/j.ophtha.2023.10.014. Epub 2023 Oct 13. PMID: 37839560; PMCID: PMC11836936.
20. Lawlor M, Danesh-Meyer H, Levin LA, Davagnanam I, De Vita E, Plant GT. Glaucoma and the brain: trans-synaptic degeneration, structural change, and implications for neuroprotection. Surv Ophthalmol. 2018;63(3):296-306. doi:10.1016/j.survophthal.2017.09.010.
21. Chan JW, Chan NC, Sadun AA. Glaucoma as neurodegeneration in the brain. Eye Brain. 2021;13:21-8. doi:10.2147/EB.S293765.
22. Martucci A, Di Giuliano F, Minosse S, Pocobelli G, Nucci C, Garaci F. MRI and Cl inical Biomarkers Overlap between Glaucoma and Alzheimer's Disease. Int J Mol Sci. 2023 Oct 5;24(19):14932. doi: 10.3390/ijms241914932. PMID: 37834380; PMCID: PMC10573932.
23. Zhang Q, Wu S, Lu Q, Zhang Y, Zhang W, Liu Y, et al. Microstructural white matter abnormalities in primary open-angle glaucoma detected by diffusion tensor imaging. PLoS One. 2020;15(3):e0230977. doi:10.1371/journal.pone.0230977.
24. Akopian A, Kumar S, Ramakrishnan H, Roy K, Viswanathan S, Bloomfield SA. Targeting neuronal gap junctions in mouse retina offers neuroprotection in glaucoma. J Clin Invest. 2017 Jun 30;127(7):2647-2661. doi: 10.1172/JCI91948. Epub 2017 Jun 12. PMID: 28604388; PMCID: PMC5490768.
25. Nickells RW. The cell and molecular biology of glaucoma: mechanisms of retinal ganglion cell death. Invest Ophthalmol Vis Sci. 2012;53(5):2476-81. doi:10.1167/iovs.11-9310.
26. Flammer J, Mozaffarieh M. What is the present pathogenetic concept of glaucomatous optic neuropathy? Surv Ophthalmol. 2007;52(Suppl 2):S162-73. doi:10.1016/j.survophthal.2007.08.012.
27. Cherecheanu AP, Garhofer G, Schmidl D, Werkmeister R, Schmetterer L. Ocular perfusion pressure and ocular blood flow in glaucoma. Curr Opin Pharmacol. 2013 Feb;13(1):36-42. doi: 10.1016/j.coph.2012.09.003. Epub 2012 Sep 23. PMID: 23009741; PMCID: PMC3553552.

28. Chen HS, Liu CH, Wu WC, Tseng HJ, Lee YS. Optical Coherence Tomography Angiography of the Superficial Microvasculature in the Macular and Peripapillary Areas in Glaucomatous and Healthy Eyes. Invest Ophthalmol Vis Sci. 2017 Jul 1;58(9):3637-3645. doi: 10.1167/iovs.17-21846. PMID: 28728171.
29. Tezel G. Oxidative stress in glaucomatous neurodegeneration: mechanisms and consequences. Prog Retin Eye Res. 2006;25(5):490-513. doi:10.1016/j.preteyeres.2006.07.003.
30. Moore D, Harris A, Wudunn D, Kheradiya N, Siesky B. Dysfunctional regulation of ocular blood flow: A risk factor for glaucoma? Clin Ophthalmol. 2008;2(4):849-61. doi:10.2147/opth.s2774.
31. Flammer J, Konieczka K. The discovery of the Flammer syndrome: a historical and personal perspective. EPMA J. 2017 May 22;8(2):75-97. doi: 10.1007/s13167-017-0090-x. PMID: 28725290; PMCID: PMC5486542.
32. Kreft D, Doblhammer G, Guthoff RF, Frech S. Prevalence, incidence, and risk factors of primary open-angle glaucoma - a cohort study based on longitudinal data from a German public health insurance. BMC Public Health. 2019;19(1):851. doi:10.1186/s12889-019-7206-8.
33. Lin HC, Chien CW, Hu CC, Ho JD. Comparison of comorbid conditions between open-angle glaucoma patients and a control cohort: a case-control study. Ophthalmology. 2010;117(11):2088-95. doi:10.1016/j.ophtha.2010.03.003.
34. Talaat K, Fathi OT, Alamoudi SM, Alzahrani MG, Mukhtar RM, Khan MA. Types of glaucoma and associated comorbidities among patients at King Abdulaziz Medical City, Jeddah. Cureus. 2021;13(6):e15574. doi:10.7759/cureus.15574.
35. Wändell P, Carlsson AC, Ljunggren G. Systemic diseases and their association with open-angle glaucoma in the population of Stockholm. Int Ophthalmol. 2022;42(5):1481-9. doi:10.1007/s10792-021-02139-4.
36. Choi JA, Lee SN, Jung SH, Won HH, Yun JS. Association of glaucoma and lifestyle with incident cardiovascular disease: a longitudinal prospective study from UK Biobank. Sci Rep. 2023;13(1):2712. doi:10.1038/s41598-023-29775-8.
37. Harris A, Kagemann L, Ehrlich R, Rospigliosi C, Moore D, Siesky B. Measuring and interpreting ocular blood flow and metabolism in glaucoma. Can J Ophthalmol. 2008;43(3):328-36. doi:10.3129/i08-051.
38. Schmidl D, Garhofer G, Schmetterer L. The complex interaction between ocular perfusion pressure and ocular blood flow - relevance for glaucoma. Exp Eye Res. 2011;93(2):141-55. doi:10.1016/j.exer.2010.09.002.
39. Siesky B, Harris A, Carr J, Verticchio Vercellin A, Hussain RM, Parekh H, et al. Vascular dysregulation in glaucoma: current perspectives and future directions. Front Ophthalmol. 2022;2:874825. doi:10.3389/fopht.2022.874825.
40. Cheung CY, Chan VTT, Mok VC, Chen C, Wong TY. Potential retinal biomarkers for dementia: what is new? Curr Opin Neurol. 2019 Feb;32(1):82-91. doi: 10.1097/WCO.0000000000000645. PMID: 30566412.
41. Ma F, Su J, Shang Q, Ma J, Zhang T, Wang X, et al. Changes in retinal vasculature and thickness in the cortex correlate with cognitive impairment in patients with cerebral small vessel disease. Front Neurol. 2021;12:640217. doi:10.3389/fneur.2021.640217.
42. Wang J, Li T, Zhou P, Wang N, Xian J, He H. Altered functional connectivity within and between the default model network and the visual network in primary open-

angle glaucoma: a resting-state fMRI study. Brain Imaging Behav. 2017;11(4):1154-63. doi:10.1007/s11682-016-9597-3.
43. Prins D, Hanekamp S, Cornelissen FW. Structural brain MRI studies in eye diseases: are they clinically relevant? A review of current findings. Acta Ophthalmol. 2016;94(2):113-21. doi:10.1111/aos.12825.
44. Giorgio A, Zhang J, Costantino F, De Stefano N, Frezzotti P. Diffuse brain damage in normal tension glaucoma. Hum Brain Mapp. 2018;39(1):532-41. doi:10.1002/hbm.23862.
45. Graham SL, Butlin M, Lee M, Avolio AP. Central blood pressure, arterial waveform analysis, and vascular risk factors in glaucoma. J Glaucoma. 2013;22(2):98-103. doi:10.1097/IJG.0b013e3182254bc0.
46. Lawlor M, Danesh-Meyer H, Levin LA, Davagnanam I, De Vita E, Plant GT. Glaucoma and the brain: trans-synaptic degeneration, structural change, and implications for neuroprotection. Surv Ophthalmol. 2018;63(3):296-306. doi:10.1016/j.survophthal.2017.09.010.
47. K. Hirsch. Structural and haemodynamic differences between emmetropic and highly myopic eyes. Theses. Aston University 2019.
48. Hayreh, S. S. (1975). The central artery of the retina: Its role in the blood supply of the retina. British Journal of Ophthalmology, 59(7), 392–401.
49. Henkind, P. (1967). Radial peripapillary capillaries of the retina: I. Anatomy: Human and comparative. *British Journal of Ophthalmology*, 51(2), 115–123.
50. Campbell, J., Zhang, M., Hwang, T. *et al.* Detailed Vascular Anatomy of the Human Retina by Projection-Resolved Optical Coherence Tomography Angiography. *Sci Rep* 7, 42201 (2017). .
51. Garrity, S. T., Paques, M., Gaudric, A., Freund, K. B., & Sarraf, D. (2017). Considerations in the understanding of venous outflow in the retinal capillary plexus. *Retina*, 37(10), 1809–1812.
52. Levin, L. A., Nilsson, S. F. E., Ver Hoeve, J., Wu, S., Kaufman, P. L., & Alm, A. (2011). Adler's Physiology of the Eye: Clinical Application (11th ed.). Elsevier.
53. Hayreh, S. S. (2001). The blood supply of the optic nerve head and the evaluation of it - Myth and reality. *Progress in Retinal and Eye Research*, 20(5), 563–593.
54. Onda, E., Cioffi, G. A., Bacon, D. R., & Van Buskirk, E. M. (1995). Microvasculature of the human optic nerve. *American Journal of Ophthalmology*, 120(1), 92–102.
55. Lieberman, M. F., Maumenee, A. E., & Green, W. R. (1976). Histologic studies of the vasculature of the anterior optic nerve. *American Journal of Ophthalmology*, 82(3), 405–423.
56. Hayreh, S. S. (1975). The ophthalmic artery: III. Branches. *British Journal of Ophthalmology*, 59(8), 460–470.
57. Nickla DL, Wallman J. The multifunctional choroid. Prog Retin Eye Res. 2010 Mar;29(2):144-68. doi: 10.1016/j.preteyeres.2009.12.002. Epub 2009 Dec 29. PMID: 20044062; PMCID: PMC2913695.
58. Hogan, M. J., Alvarado, J. A., & Weddell, J. E. (1971). *Histology of the Human Eye: An Atlas and Textbook*. W.B. Saunders.
59. Fryczkowski AW. Anatomical and functional choroidal lobuli. Int Ophthalmol. 1994;18(3):131-41. doi: 10.1007/BF00915961. PMID: 7852018.

60. Olver JM. Functional anatomy of the choroidal circulation: methyl methacrylate casting of human choroid. Eye (Lond). 1990;4 ( Pt 2):262-72. doi: 10.1038/eye.1990.38. PMID: 2379644.
61. Quigley, H. A., Dunkelberger, G. R., & Green, W. R. (1989). Retinal ganglion cell atrophy correlated with automated perimetry in human eyes with glaucoma. *American Journal of Ophthalmology*, 107(5), 453–464.
62. Weinreb RN, Aung T, Medeiros FA. The pathophysiology and treatment of glaucoma: a review. JAMA. 2014 May 14;311(18):1901-11. doi: 10.1001/jama.2014.3192. PMID: 24825645; PMCID: PMC4523637.
63. European Glaucoma Society. (2020). *Terminology and Guidelines for Glaucoma* (5th ed.).
64. Kass MA, Heuer DK, Higginbotham EJ, Johnson CA, Keltner JL, Miller JP, Parrish RK 2nd, Wilson MR, Gordon MO. The Ocular Hypertension Treatment Study: a randomized trial determines that topical ocular hypotensive medication delays or prevents the onset of primary open-angle glaucoma. Arch Ophthalmol. 2002 Jun;120(6):701-13; discussion 829-30. doi: 10.1001/archopht.120.6.701. PMID: 12049574.
65. Baudouin C, Labbé A, Liang H, Pauly A, Brignole-Baudouin F. Preservatives in eyedrops: the good, the bad and the ugly. Prog Retin Eye Res. 2010 Jul;29(4):312-34. doi: 10.1016/j.preteyeres.2010.03.001. Epub 2010 Mar 17. PMID: 20302969.
66. Tan NYQ, Friedman DS, Stalmans I, Ahmed IIK, Sng CCA. Glaucoma screening: where are we and where do we need to go? Curr Opin Ophthalmol. 2020 Mar;31(2):91-100. doi: 10.1097/ICU.0000000000000649. PMID: 31904596.
67. William C. Stewart, Hurshell H. Hunt, Threshold variation in automated perimetry, Survey of Ophthalmology, Volume 37, Issue 5,1993, Pages 353-361, ISSN 0039-6257.
68. Chauhan BC, Garway-Heath DF, Goñi FJ, Rossetti L, Bengtsson B, Viswanathan AC, Heijl A. Practical recommendations for measuring rates of visual field change in glaucoma. Br J Ophthalmol. 2008 Apr;92(4):569-73. doi: 10.1136/bjo.2007.135012. Epub 2008 Jan 22. PMID: 18211935; PMCID: PMC2564806.
69. Lieberman MF, Congdon NG, He M. The value of tests in the diagnosis and management of glaucoma. Am J Ophthalmol. 2011 Dec;152(6):889-899.e1. doi: 10.1016/j.ajo.2011.06.029. Epub 2011 Sep 14. PMID: 21924398.
70. Caprioli J, Garway-Heath DF; International Glaucoma Think Tank. A critical reevaluation of current glaucoma management: International Glaucoma Think Tank, July 27-29, 2006, Taormina, Sicily. Ophthalmology. 2007 Nov;114(11 Suppl):S1-41. doi: 10.1016/j.ophtha.2007.08.032. PMID: 17980762.
71. Spry PG, Johnson CA. Senescent changes of the normal visual field: an age-old problem. Optom Vis Sci. 2001 Jun;78(6):436-41. doi: 10.1097/00006324-200106000-00017. PMID: 11444634.
72. Varma R, Steinmann WC, Scott IU. Expert agreement in evaluating the optic disc for glaucoma. Ophthalmology. 1992 Feb;99(2):215-21. doi: 10.1016/s0161-6420(92)31990-6. PMID: 1553210.
73. Pourjavan S, Bourguignon GH, Marinescu C, Otjacques L, Boschi A. Evaluating the Influence of Clinical Data on Inter-Observer Variability in Optic Disc Analysis

for AI-Assisted Glaucoma Screening. Clin Ophthalmol. 2024 Dec 27;18:3999-4009. doi: 10.2147/OPTH.S492872. PMID: 39741794; PMCID: PMC11687089
74. Kamalipour A, Moghimi S. Macular Optical Coherence Tomography Imaging in Glaucoma. J Ophthalmic Vis Res. 2021 Jul 29;16(3):478-489. doi: 10.18502/jovr.v16i3.9442. PMID: 34394875; PMCID: PMC8358749.
75. Hasan, Md. Asif, Islam, Sheikh Md. Rabiul, Pathan, Md. Arif Hayat Khan, Retrospective Study of Diabetic Retinopathy and Macular Edema in Southern Part of Bangladesh, Journal of Ophthalmology, 2024, 8437947, 16 pages, 2024. doi.org/10.1155/2024/8437947.
76. Curcio CA, Allen KA. Topography of ganglion cells in human retina. J Comp Neurol. 1990 Oct 1;300(1):5-25. doi: 10.1002/cne.903000103. PMID: 2229487.
77. Tan O, Chopra V, Lu AT, Schuman JS, Ishikawa H, Wollstein G, Varma R, Huang D. Detection of macular ganglion cell loss in glaucoma by Fourier-domain optical coherence tomography. Ophthalmology. 2009 Dec;116(12):2305-14.e1-2. doi: 10.1016/j.ophtha.2009.05.025. Epub 2009 Sep 10. PMID: 19744726; PMCID: PMC2787911.
78. Kim NR, Lee ES, Seong GJ, Kim JH, An HG, Kim CY. Structure-function relationship and diagnostic value of macular ganglion cell complex measurement using Fourier-domain OCT in glaucoma. Invest Ophthalmol Vis Sci. 2010 Sep;51(9):4646-51. doi: 10.1167/iovs.09-5053. Epub 2010 Apr 30. PMID: 20435603.
79. Reis AS, Sharpe GP, Yang H, Nicolela MT, Burgoyne CF, Chauhan BC. Optic disc margin anatomy in patients with glaucoma and normal controls with spectral domain optical coherence tomography. Ophthalmology. 2012 Apr;119(4):738-47. doi: 10.1016/j.ophtha.2011.09.054. Epub 2012 Jan 4. PMID: 22222150; PMCID: PMC3319857.
80. Garway-Heath, D. F., Poinoosawmy, D., Fitzke, F. W., & Hitchings, R. A. (2000). Mapping the visual field to the optic disc in normal tension glaucoma eyes. Ophthalmology, 107(10), 1809–1815. doi.org/10.1016/S0161-6420(00)00284-0
81. Stein JD, Talwar N, Laverne AM, Nan B, Lichter PR. Trends in use of ancillary glaucoma tests for patients with open-angle glaucoma from 2001 to 2009. Ophthalmology. 2012 Apr;119(4):748-58. doi: 10.1016/j.ophtha.2011.09.045. Epub 2012 Jan 3. PMID: 22218146; PMCID: PMC3319788.
82. Park SC, De Moraes CG, Teng CC, Tello C, Liebmann JM, Ritch R. Initial parafoveal versus peripheral scotomas in glaucoma: risk factors and visual field characteristics. Ophthalmology. 2011 Sep;118(9):1782-9. doi: 10.1016/j.ophtha.2011.02.013. Epub 2011 Jun 12. PMID: 21665283.
83. Hood, D. C., & Kardon, R. H. (2007). A framework for comparing structural and functional measures of glaucomatous damage. *Progress in Retinal and Eye Research*, 26(6), 688–710. https://doi.org/10.1016/j.preteyeres.2007.08.001
84. Braun M, Saini C, Sun JA, Shen LQ. The Role of Optical Coherence Tomography Angiography in Glaucoma. Semin Ophthalmol. 2024 Aug;39(6):412-423. doi: 10.1080/08820538.2024.2343049. Epub 2024 Apr 20. PMID: 38643350.
85. Koustenis A Jr, Harris A, Gross J, Januleviciene I, Shah A, Siesky B. Optical coherence tomography angiography: an overview of the technology and an assessment of applications for clinical research. Br J Ophthalmol. 2017 Jan;101(1):16-20. doi: 10.1136/bjophthalmol-2016-309389. Epub 2016 Oct 4. PMID: 27707691.

86. Le PH, Kaur K, Patel BC. Optical Coherence Tomography Angiography. [Updated 2024 Oct 6]. In: StatPearls [Internet]. Treasure Island (FL): StatPearls Publishing; 2025 Jan.
87. Jia Y, Bailey ST, Hwang TS, McClintic SM, Gao SS, Pennesi ME, Flaxel CJ, Lauer AK, Wilson DJ, Hornegger J, Fujimoto JG, Huang D. Quantitative optical coherence tomography angiography of vascular abnormalities in the living human eye. Proc Natl Acad Sci U S A. 2015 May 5;112(18):E2395-402. doi: 10.1073/pnas.1500185112. Epub 2015 Apr 20. PMID: 25897021; PMCID: PMC4426471.
88. Yarmohammadi A, Zangwill LM, Diniz-Filho A, Suh MH, Manalastas PI, Fatehee N, Yousefi S, Belghith A, Saunders LJ, Medeiros FA, Huang D, Weinreb RN. Optical Coherence Tomography Angiography Vessel Density in Healthy, Glaucoma Suspect, and Glaucoma Eyes. Invest Ophthalmol Vis Sci. 2016 Jul 1;57(9):OCT451-9. doi: 10.1167/iovs.15-18944. PMID: 27409505; PMCID: PMC4968912.
89. Liu L, Jia Y, Takusagawa HL, Pechauer AD, Edmunds B, Lombardi L, Davis E, Morrison JC, Huang D. Optical Coherence Tomography Angiography of the Peripapillary Retina in Glaucoma. JAMA Ophthalmol. 2015 Sep;133(9):1045-52. doi: 10.1001/jamaophthalmol.2015.2225. PMID: 26203793; PMCID: PMC4950955.
90. Spaide RF, Fujimoto JG, Waheed NK, Sadda SR, Staurenghi G. Optical coherence tomography angiography. Prog Retin Eye Res. 2018 May;64:1-55. doi: 10.1016/j.preteyeres.2017.11.003. Epub 2017 Dec 8. PMID: 29229445; PMCID: PMC6404988.
91. Lee EJ, Lee KM, Lee SH, Kim TW. Parapapillary Choroidal Microvasculature Dropout in Glaucoma: A Comparison between Optical Coherence Tomography Angiography and Indocyanine Green Angiography. Ophthalmology. 2017 Aug;124(8):1209-1217. doi: 10.1016/j.ophtha.2017.03.039. Epub 2017 Apr 19. PMID: 28433445.
92. Kollia E, Christou EE, Patsea E, Papadonta SA, Papaconstantinou D. Radial peripapillary capillary density as a predictive factor for glaucoma in eyes with ocular hypertension. An observational, comparative, single-centred study. F1000Res. 2023 Nov 10;12:1456. doi: 10.12688/f1000research.140453.1. PMID: 38161427; PMCID: PMC10755262.
93. Liu L, Jia Y, Takusagawa HL, Pechauer AD, Edmunds B, Lombardi L, Davis E, Morrison JC, Huang D. Optical Coherence Tomography Angiography of the Peripapillary Retina in Glaucoma. JAMA Ophthalmol. 2015 Sep;133(9):1045-52. doi: 10.1001/jamaophthalmol.2015.2225. PMID: 26203793; PMCID: PMC4950955.

# Chapter 2: Fundamentals of Artificial Intelligence in Medicine: An overview and applications in Ophthalmology

In the following sections, I outline the evolution of artificial intelligence in medicine, with a focus on ophthalmology. The chapter distinguishes between machine learning and deep learning, introduces key algorithms, and highlights the use of convolutional neural networks (CNNs) in image-based diagnostics. It concludes with a discussion of multimodal and foundation models and their potential role in glaucoma care and clinical integration.

## 2.1 Introduction: The rise of AI in medicine

Artificial intelligence (AI) is a rapidly evolving field that encompasses a broad range of computational approaches designed to emulate human cognitive functions. In the context of ophthalmology, AI has demonstrated increasing potential to aid in diagnosis, prediction, and clinical decision-making, particularly in imaging-intensive domains such as glaucoma management. In this chapter, we delineate the different subfields of AI, describe its evolution in ophthalmology, and explain how it underpins the methods developed in this thesis.

In this thesis, “artificial intelligence” refers to a broad set of computational techniques that allow systems to perform tasks typically requiring human intelligence. This includes both classical machine learning (ML) and more recent deep learning (DL) methods. The methods implemented in this thesis are specifically supervised learning algorithms, including convolutional neural networks (CNNs) for classification and support vector regression (SVR) for age prediction.

## 2.2 Early Beginnings till modern application: The Foundations of AI in Medicine

This section presents a structured, non-systematic historical overview of AI in medicine, highlighting key conceptual milestones, particularly those that have influenced ophthalmology. At the same time, although not a formal systematic review, selected examples illustrate how AI evolved into the methods used in this thesis.

The concept of artificial intelligence, in which machines simulate human cognition, was first formalised in the 1950s by pioneers such as Alan Turing and John McCarthy. Turing’s seminal paper, Computing Machinery and Intelligence (1950), posed the question: Can machines think? A notion that later shaped medical computing [1].

By the 1960s and 1970s, the first medical AI systems emerged in the form of expert systems, built to replicate human decision-making. DENDRAL, developed at Stanford in the mid-1960s, helped chemists in deducing molecular structures from mass spectrometry data. It was the first AI expert system and relied on hand-coded if-then rules-static knowledge, not learned from data.

Following this, MYCIN was created in the 1970s to diagnose bacterial infections and recommend antibiotics [2]. Although it showcased the power of AI to support medical reasoning, its adoption was limited by its complexity and the computing constraints of the era.

CASNET (Causal Associational Network Model) was one of the earliest AI applications in ophthalmology. Developed in the 1970s, it assisted glaucoma diagnosis by modelling medical knowledge as causal links between symptoms, intermediate states, and diseases [3]. Unlike simple rule-based systems, CASNET mimicked structured clinical reasoning, which is symbolic, not data-driven.

Rule-based AI systems faced scalability issues. Thousands of rules were required to account for real-world complexity, making them rigid, difficult to update, and incapable of learning from new data. These limitations led to the rise of machine learning (ML), which gradually replaced expert systems.

By the 1980s and 1990s, ML enabled computers to learn patterns from data, paving the way for diagnostic decision support systems driven by clinical datasets rather than static rules. Meanwhile, advances in medical imaging, such as CT, MRI, and OCT, have produced large volumes of data, prompting the integration of AI tools in radiology and ophthalmology. In the early 2000s, deep learning (DL) and big data analytics triggered a significant shift. DL architectures, inspired by the brain's neural networks, became central to AI-driven medicine. The availability of large, labelled datasets and increasing computational power enabled AI to surpass traditional approaches.

By the 2010s, convolutional neural networks (CNNs) revolutionised medical imaging, particularly in ophthalmology, dermatology, and radiology [4]. A significant milestone was the FDA approval of IDx-DR in 2018, the first AI system authorised to make autonomous diagnoses without clinician input. It analyses fundus images to detect diabetic retinopathy (DR), referring patients to ophthalmologists if signs of more than mild DR are detected or scheduling follow-up in one year [5]. With a sensitivity of over 87% and a specificity above 90%, IDx-DR is a highly effective screening tool. Its clinical adoption, especially in underserved areas, illustrates how AI can improve early detection and reduce vision loss [6].

## 2.3 Definition and Terminology

### 2.3.1 Artificial Intelligence (AI)

Artificial intelligence (AI) is a broad field that encompasses various techniques enabling machines to simulate aspects of human intelligence, such as reasoning, problem-solving, and pattern recognition. In this chapter, I adopt the definition used by Russell and Norvig, describing AI as the study of systems that perceive their environment and take actions to maximise success [7].

### 2.3.2 Machine Learning (ML)

Machine learning (ML) is a subset of AI that involves a set of algorithms that learn from data to make predictions or decisions, thereby improving performance over time without requiring explicit programming for every scenario. Traditional ML methods typically require handcrafted features, that is, variables selected by clinical experts (e.g., intraocular pressure, RNFL thickness, or visual field indices). These techniques have been successfully applied in ophthalmology for diagnosis, risk stratification, and monitoring disease progression, especially in glaucoma [8,9].

- Support Vector Machines (SVM): A supervised algorithm that separates data into classes (e.g., glaucoma vs. non-glaucoma) by finding an optimal decision boundary (hyperplane) with maximum margin.
- Random Forests and Decision Trees: Decision Trees classify patients based on a sequence of risk-factor decisions. Random Forests enhance accuracy and reduce overfitting by combining many such trees and using majority voting (for classification) or averaging (for regression). They handle missing data well and balance the influence of different clinical variables (e.g., VF, IOP, OCT).
- K-Nearest Neighbors (KNN): A simple yet effective method for early disease detection. KNN compares new cases to similar existing ones. If a majority of the nearest neighbours have glaucoma, the algorithm predicts risk for the new patient.
- Gradient Boosting & XGBoost: Advanced decision-tree models that build trees sequentially, improving on previous errors. XGBoost is known for its speed and efficiency and is used in estimating progression and optimising treatment strategies.

Despite their success, classical ML models depend heavily on manual feature engineering and struggle with generalisation [10]. Deep learning has addressed many of these limitations.

### 2.3.3 Multilayer Perceptron (MLP)

A Multilayer Perceptron (MLP) is a type of feedforward artificial neural network. It consists of an input layer, one or more hidden layers, and an output layer. Each node (also called a neuron) in one layer is connected to every node in the next layer through weighted connections.

MLPs are widely used for processing structured, tabular data, such as IOP, age or CCT). They learn patterns in the data by adjusting the weights during training, typically through backpropagation [11].

In the context of this thesis, MLPs are used to process non-image inputs. They are integrated with imaging features (from OCT/OCTA) in intermediate or late fusion strategies, depending on the model architecture.

### 2.3.4 Deep Learning (DL)

Deep learning (DL), a subfield of ML, differs in that it does not require handcrafted features. It utilises artificial neural networks with multiple layers (hence "deep") to process and learn from large datasets. These networks are designed to automatically identify patterns, extract features, and make predictions without requiring explicit programming for each task [12,13].

Although loss functions and backpropagation are used across various ML approaches, they are especially critical in deep learning models because the model optimises performance through iterative feedback mechanisms. The loss function, which quantifies prediction error and Backpropagation, which adjusts internal weights to reduce this error over time. This process parallels human learning: just as a clinician refines diagnostic accuracy through experience and feedback, a DL model improves with exposure to labelled data. Over time, both build more accurate internal representations.

Convolutional Neural Networks (CNNs) are the backbone of most DL models in medical imaging. They are especially suited for 2D image data (like fundus or OCT scans) and operate via:

- Convolutional Layers to extract spatial features (edges, patterns).
- Pooling Layers to reduce dimensionality while preserving key features.
- Fully Connected Layers to aggregate features and output classifications.

CNNs remain dominant in ophthalmology despite the recent rise of attention-based models and vision transformers [14,15]. However, CNNs' "Black-Box" nature raises concerns about interpretability. To address this, explainability techniques such as Grad-CAM (Gradient-weighted Class Activation Mapping) visually highlight influential image regions. At the same time, SHAP (SHapley Additive exPlanations)

quantifies the contribution of each feature to a prediction. This concern will be explained later in this chapter.

DL has proven superior to traditional ML for several reasons:

- End-to-End Learning: can learn directly from raw images, eliminating the need for manual feature selection and reducing bias.
- Higher Accuracy and Robustness: demonstrated high performance in glaucoma detection, with area under the curve (AUC) values exceeding 95% when using OCT/OCTA data [16].
- Adaptability: It continues to improve as they are exposed to more data, making them well-suited to dynamic and evolving datasets.
- Integrates multiple data modalities (e.g., combining OCT with fundus images improves VF prediction [17].
- Automated Feature Extraction: Reduces bias from manual feature selection.
- Handling Complex Imaging Data.
- Scalability with Big Data: It improves its accuracy with large datasets.

### 2.3.5 Understanding the learning process of AI

To train a model, different learning approaches are used depending on the type and data availability:

- Supervised Learning (SL): Models learn from labelled datasets, such as labelled OCT images, which learn to classify glaucoma versus healthy eyes. In this thesis, SL was applied.
- Unsupervised Learning: Models find patterns in unlabelled data. In ophthalmology, this can help discover subtypes of glaucoma or identify novel patient clusters.
- Semi-Supervised Learning (SSL): Combines a small number of labelled samples with a large set of unlabelled data. This is particularly useful in medical imaging, where labels (such as glaucoma diagnoses) are expensive to obtain. SSL techniques, such as pseudo-labelling or consistency regularisation, can enhance model performance by leveraging unlabelled datasets. In this thesis, SSL remains a promising direction for future clinical applications, particularly in scenarios with limited annotated data.
- Reinforcement Learning: Models learn by receiving feedback from their actions. While less common in imaging, it has potential in robotic surgery and treatment optimisation.

## 2.4 Evolution of AI in Medical Imaging: Key Milestones

Pivotal milestones have marked the evolution of AI in medicine, none more influential than the breakthrough of AlexNet in 2012 [18]. By dramatically reducing classification

error in the ImageNet competition (from ~26% to ~15%), AlexNet demonstrated the power of CNNs and catalysed their adoption across fields, including medical imaging. Although the competition ended in 2017 due to performance saturation (error <3%), its impact remains foundational [19].

In medical imaging, architectures like U-Net, ResNet, and AlexNet remain central. U-Net enables precise image segmentation, particularly useful in delineating retinal layers or lesions [20]. ResNet's residual connections allow for deeper networks without vanishing gradients, and AlexNet remains a benchmark for image classification. While these models provided the necessary groundwork, this thesis emphasises clinically driven model development over architectural benchmarking.

**Table 1. Historical development of AI in healthcare and Ophthalmology.**

| Year | Event | Importance |
|---|---|---|
| 1965 | DENDRAL | First expert system for molecular structure analysis; inspired medical reasoning tools. |
| 1972 | MYCIN | Rule-based AI for infectious diseases. First clinical decision support system. |
| 1970s | CASNET | First AI model in ophthalmology (glaucoma); used causal network mapping. |
| 1980s–90s | Symbolic AI peak | Logic-based systems that lacked scalability and adaptability. |
| 1998 | LeNet | One of the first CNNs for digit recognition inspired visual AI. |
| 2012 | AlexNet / ImageNet victory | Sparked the deep learning era by revolutionising computer vision. |
| 2015–2018 | U-Net, ResNet, VGG | DL architectures, widely adopted in medical imaging. |
| 2017 | Transformer architecture | Shifted AI toward self-attention and LLM. |

| | | |
|---|---|---|
| 2020s | Multimodal & Explainable AI | AI models integrating multiple data types (OCT, VF, IOP) (like GlauOCTA-AI) |
| Future | Foundation Models | Universal AI models for personalised medicine |

## 2.5 Synergy between AI, Medical Imaging and Big Data

Deep learning, particularly through CNNs and emerging transformers, is revolutionising medical imaging by enhancing automation, precision, and efficiency. Unlike human specialists, these models are immune to fatigue and inter-observer variability, making them ideal for high-volume diagnostics. They can detect early indicators, such as optic nerve cupping or RNFL thinning, often beyond human perception [21,22]. Several studies demonstrate expert-level performance in diagnosing ophthalmic and systemic conditions, thereby reshaping workflows in imaging-intensive fields such as ophthalmology and radiology [23,24].

AI thrives on large-scale datasets, and healthcare generates vast amounts of structured and unstructured data:

- Medical Imaging Datasets: Repositories of OCT, CT, MRI, and histopathology images allow AI to generalise across diverse patient populations.
- Electronic Health Records (EHRs): These enable AI to track longitudinal trends and predict disease progression [25].
- Genomic and Multimodal Data: Integration of genetic, clinical, and imaging data paves the way for personalised medicine [26].

Together, these developments underscore how AI, empowered by both high-quality imaging and diverse clinical data, is transforming ophthalmology and other diagnostic-heavy specialities.

## 2.6 Transformers: The Next Frontier in Medical AI

In recent years, transformer-based architectures, originally developed for natural language processing (e.g., BERT, GPT), have demonstrated strong performance across diverse domains, including vision and medical imaging. Unlike CNNs, which rely on spatially local filters, transformers leverage a self-attention mechanism to capture global dependencies across the input. This enables the better integration of multimodal data, such as combining image features from OCT/OCTA with clinical records and underpins the recent development of medical foundation models.

While transformers require large datasets and computational power, they offer promising flexibility and have already shown strong results in medical tasks such as retinopathy detection, histopathology, and multimodal fusion. As transformer models evolve, they may complement or even outperform CNNs in specific glaucoma-related applications.

Transformers currently represent the most advanced and flexible architecture in artificial intelligence, powering state-of-the-art foundation models and multimodal systems that can simultaneously understand vision, language, and clinical signals. Transformers rely on attention rather than convolution to prioritise relevant images and clinical features regardless of position or scale.

Table 2 summarises the core differences between key AI model types discussed in this chapter, highlighting their respective strengths, limitations, and real-world applications in glaucoma research. This overview also positions multimodal and transformer-based models as the next frontier in clinical decision support.

**Table 2. Overview of different AI models and their application in Glaucoma research.**

| Model Type | Description | Strengths | Limitations | Example in Ophthalmology |
|---|---|---|---|---|
| **ML (e.g., SVM, XGBoost)** | Traditional rule-based learning using handcrafted features | Interpretable, good with small data | Needs manual feature extraction | Predicting glaucoma risk from IOP, CCT |
| **DL (e.g., MLP)** | Learns features automatically via deep layers | Handles complex patterns | Requires more data, less interpretable | Predicting VF loss from structural data |
| **CNN** | Special DL model for image input using convolutional layers | Excellent at image feature extraction | Local spatial focus, needs labelled data | OCT/OCTA analysis, RNFL segmentation |
| **Multimodal AI** | Combines several data types (e.g., images + clinical) | Captures complex phenotypes | Challenging Data fusion | Your GlauOCTA-AI architecture |
| **Transformer** | Uses self-attention for global data relationships | Best for sequences MM input | Needs huge datasets and compute | Multimodal AI, foundation models (e.g., MedPaLM) |

## 2.7 AI applications in Ophthalmology

AI methods, including ML, DL, and emerging vision transformer models, are increasingly utilised in ophthalmology, particularly in imaging-intensive conditions such as glaucoma [27]. By leveraging AI for early diagnosis, progression monitoring, and risk prediction, clinicians can make more precise, data-driven decisions, improving patient outcomes. There are several CNNs widely adopted in ophthalmology, such as ResNet, which enables deep OCT classification while avoiding vanishing gradients. Other notable CNNs include the Visual Geometry Group Network (VGGNet), a structured and effective model for fundus image classification, and U-Net, designed for segmentation tasks such as optic disc and RNFL mapping.

### 2.7.1 Glaucoma Detection from Imaging

AI-based analysis of OCT and OCTA enables the early detection of glaucoma, even before functional loss occurs. ML models utilise features such as RNFL thickness or cup-to-disc ratio, whereas CNN-based DL models extract image patterns without requiring manual feature selection. CNN-enhanced models have demonstrated high sensitivity and specificity in identifying subtle changes [28].

### 2.7.2 IOP Prediction & Progression Risk Assessment

ML models trained on clinical parameters (e.g., IOP, RNFL, vascular density) predict pressure fluctuations and assess the likelihood of disease progression [29]. These tools support more precise risk stratification and treatment planning.

### 2.7.3 Structure–Function Correlation and VF Prediction

AI systems can analyse longitudinal visual field (VF) and OCT data to predict disease trajectories and correlate structural loss with functional deficits. This improves early detection of fast progressors and supports targeted interventions [30].

### 2.7.4 Transformers and Generative AI in Ophthalmology

Vision Transformers (ViTs) utilise self-attention mechanisms to model global dependencies across an image, providing advantages in integrating multimodal data (e.g., OCT/OCTA and clinical records). These models are emerging as strong alternatives to CNNs, particularly for large-scale, multimodal datasets [31].

Generative AI models, including diffusion models and GANs, are also being explored for data augmentation, synthetic imaging, and anomaly detection in ophthalmology. Though still largely experimental, these techniques may enhance training for rare diseases or improve model robustness by generating diverse, high-quality training data [32].

Large Language Models (LLMs), such as ChatGPT, are increasingly applied for study design, protocol drafting, and hypothesis generation. In projects like those at Owkin, LLMs support collaborative biomedical research by accelerating study setup

and facilitating multimodal reasoning across imaging, genomics, and clinical data [33].

### 2.7.5 Towards Personalised AI-Driven Glaucoma Care

AI is transforming glaucoma care by enabling earlier and more personalised intervention strategies. It detects preclinical structural and vascular changes before functional vision loss, supports longitudinal monitoring of RNFL thinning and vascular density, and integrates multimodal clinical data to stratify the risk of progression. This facilitates the development of tailored follow-up and treatment plans. Furthermore, AI models can predict treatment response by analysing patient history and imaging biomarkers, guiding the timing of surgical intervention when appropriate [34–37].

These advancements lay the foundation for the glaucoma-specific AI models developed in this thesis. The methodological design presented in the next chapter builds directly on these applications, ensuring conceptual and structural continuity with the work reviewed above.

## 2.8 Limitations & Challenges

Despite these advances, several limitations hinder AI's full integration into clinical practice. One critical challenge is data bias. Many models are trained on datasets predominantly from Western populations, which limits their generalizability across ethnicities and raises concerns about equity [38].

A second challenge is the lack of standardisation in imaging data. OCT and OCTA devices from different manufacturers (e.g., Heidelberg, Optovue, Zeiss) employ proprietary processing pipelines, which makes model interoperability challenging. Without harmonised acquisition protocols, AI deployment across clinical centres remains limited [39].

The third major challenge is interpretability, often referred to as the "black box" problem. DL models, especially CNN, can produce highly accurate results but usually lack transparency in how predictions are made. This opacity leads to hesitation among clinicians, who are expected to justify their decisions based on understandable reasoning. To address this, the field of explainable AI (XAI) has introduced tools such as saliency maps and Grad-CAM, which visually highlight the regions of an OCT or fundus image that most influenced the model's output. These visualisations are intuitive for clinicians and align well with the pattern-based thinking used in ophthalmic diagnostics [40].

In the case of machine learning models like XGBoost, explanation is achieved using SHAP (SHapley Additive exPlanations), a method that assigns a contribution value to each input variable. For example, SHAP can show how much RNFL thickness, IOP, or mean deviation in the VF contributed to a particular "glaucoma" or "healthy" classification. One notable study by Oh et al. (2021) demonstrated how SHAP,

combined with radar and gauge chart visualisations, enabled clinicians to identify which features influenced a model's diagnosis precisely. This level of transparency is vital for building trust in AI-assisted decision-making [41].

Reliability of ground truth labels also impacts supervised learning models. In glaucoma, diagnostic criteria and progression definitions can vary among clinicians, introducing label noise [42]. Consensus-based datasets and longitudinal outcomes may help improve model robustness and generalisation.

## 2.9 Application of AI in our study Glau-OCTA-AI

In our Glau-OCTA study, AI was applied in a phased manner to support glaucoma detection and risk prediction. The project began with traditional supervised ML models trained on OCT and OCTA features to distinguish between glaucomatous and healthy eyes. Despite multiple validation strategies, including 5-fold cross-validation, the models plateaued in specificity (~70%), suggesting limitations in the manually selected features.

This led to a transition to deep learning using CNNs. The GlauOCTA model enhanced diagnostic performance by directly learning from raw images, achieving an AUC of 96.94% in the optimal configuration. CNNs enabled automated feature extraction and efficient training through weight optimisation and backpropagation.

To further enhance performance, GlauOCTA-AI will integrate multimodal inputs, combining OCT, OCTA and VF images with clinical parameters such as IOP fluctuations, gender and CCT.

## 2.10 Conclusion

The future of AI in glaucoma hinges on advances in interpretability, data privacy, and generalisability. Explainable AI (XAI), federated learning, and foundation models, especially those utilising self-supervised learning, promise to push these boundaries, enabling scalable and personalised diagnostics.

Despite ongoing research success, clinical adoption remains limited due to validation gaps, regulatory barriers, and cost. This is particularly evident in healthcare systems like Belgium's, where reimbursement and equitable access must align with innovation.

My optimism toward integrating AI in ophthalmology is shaped by the perspective of a Generation X clinician who witnessed the evolution from paper-based records and manual calculations to digital imaging and partially automated diagnostics. While today's AI engineers, many of whom come from a generation where intelligent systems are the default, may find the pace of medical integration frustratingly slow, clinicians see this evolution as rapid and transformative. This optimism does not ignore current limitations; it is rooted in lived progress. The gap between research and clinical implementation is real, but so is the trajectory. From where we began, the momentum is unmistakable.

This chapter provided a technical foundation for understanding the core AI architectures used in this thesis. The following chapters apply these models to glaucoma datasets to explore their diagnostic and predictive capabilities.

Chapter 3 will narrow this focus to applying classical machine learning and CNN models on our glaucoma datasets, serving as a first diagnostic benchmark.

# References


1. A.M.Touring. Computing Machinery and Intelligence. 1950 Mind 49: 433-460.
2. 1984 book, Rule-Based Expert Systems: The MYCIN Experiments of the Stanford Heuristic Programming Project (edited by Bruce G. Buchanan and Edward H. Shortliffe)
3. Sholom Weiss, Casimir A. Kulikowski, Aran Safir, Glaucoma consultation by computer, Computers in Biology and Medicine,Volume 8, Issue 1,1978, Pages 25-40, ISSN 0010-4825, doi:10.1016/0010-4825(78)90011-2.
4. Turaga SC, Murray JF, Jain V, Roth F, Helmstaedter M, Briggman K, Denk W, Seung HS. Convolutional networks can learn to generate affinity graphs for image segmentation. Neural Comput. 2010 Feb;22(2):511-38. doi: 10.1162/neco.2009.10-08-881. PMID: 19922289.
5. J., F., Engelberts, J., Luger, A. M., & Van Grinsven, M. J. (2022). Performance of a deep learning system for detection of referable diabetic retinopathy in real clinical settings. ArXiv. https://arxiv.org/abs/2205.05554
6. Khan Z, Gaidhane AM, Singh M, Ganesan S, Kaur M, Sharma GC, Rani P, Sharma R, Thapliyal S, Kushwaha M, Kumar H, Agarwal RK, Shabil M, Verma L, Sidhu A, Ab Manan NB, Bushi G, Mehta R, Sah S, Satapathy P, Samal SK. Diagnostic Accuracy of IDX-DR for Detecting Diabetic Retinopathy: A Systematic Review and Meta-Analysis. Am J Ophthalmol. 2025 Feb 20:S0002-9394(25)00081-9. doi: 10.1016/j.ajo.2025.02.022. Epub ahead of print. PMID: 39986640.
7. Russell, S., & Norvig, P. (2010). Artificial Intelligence: A Modern Approach (3rd ed.). Prentice Hall.
8. Bowd C, Weinreb RN, Balasubramanian M, Lee I, Jang G, Yousefi S, Zangwill LM, Medeiros FA, Girkin CA, Liebmann JM, Goldbaum MH. Glaucomatous patterns in Frequency Doubling Technology (FDT) perimetry data identified by unsupervised machine learning classifiers. PLoS One. 2014 Jan 30;9(1):e85941. doi: 10.1371/journal.pone.0085941. PMID: 24497932; PMCID: PMC3907565.
9. Yousefi S, Goldbaum MH, Balasubramanian M, Jung TP, Weinreb RN, Medeiros FA, Zangwill LM, Liebmann JM, Girkin CA, Bowd C. Glaucoma progression detection using structural retinal nerve fiber layer measurements and functional visual field points. IEEE Trans Biomed Eng. 2014 Apr;61(4):1143-54. doi: 10.1109/TBME.2013.2295605. PMID: 24658239; PMCID: PMC4248722.
10. Ting DSW, Pasquale LR, Peng L, Campbell JP, Lee AY, Raman R, Tan GSW, Schmetterer L, Keane PA, Wong TY. Artificial intelligence and deep learning in ophthalmology. Br J Ophthalmol. 2019 Feb;103(2):167-175. doi: 10.1136/bjophthalmol-2018-313173. Epub 2018 Oct 25. PMID: 30361278; PMCID: PMC6362807.

11. Rumelhart DE, Hinton GE, Williams RJ. Learning representations by back-propagating errors. Nature. 1986;323(6088):533-6. doi: 10.1038/323533a0.
12. LeCun Y, Bengio Y, Hinton G. Deep learning. Nature. 2015;521(7553):436–444.
13. Litjens G, Kooi T, Bejnordi BE, et al. A survey on deep learning in medical image analysis. Medical Image Analysis. 2017;42:60–88
14. Ran AR, Tham CC, Chan PP, Cheng CY, Tham YC, Rim TH, Cheung CY. Deep learning in glaucoma with optical coherence tomography: a review. Eye (Lond). 2021 Jan;35(1):188-201. doi: 10.1038/s41433-020-01191-5. Epub 2020 Oct 7. Erratum in: Eye (Lond). 2021 Jan;35(1):357. doi: 10.1038/s41433-020-01244-9. PMID: 33028972; PMCID: PMC7852526.
15. Li Z, He Y, Keel S, Meng W, Chang RT, He M. Efficacy of a Deep Learning System for Detecting Glaucomatous Optic Neuropathy Based on Color Fundus Photographs. Ophthalmology. 2018 Aug;125(8):1199-1206. doi: 10.1016/j.ophtha.2018.01.023. Epub 2018 Mar 2. PMID: 29506863.
16. Pourjavan S, Bourguignon GH, Marinescu C, Otjacques L, Boschi A. Evaluating the Influence of Clinical Data on Inter-Observer Variability in Optic Disc Analysis for AI-Assisted Glaucoma Screening. Clin Ophthalmol. 2024 Dec 27;18:3999-4009. doi: 10.2147/OPTH.S492872. PMID: 39741794; PMCID: PMC11687089.
17. Kihara Y, Montesano G, Chen A, et al. Policy-driven, multimodal deep learning for predicting visual fields from the optic disc and OCT imaging. Ophthalmology. 2022;129(7):781-791. doi:10.1016/j.ophtha.2022.02.017
18. Krizhevsky A, Sutskever I, Hinton GE. ImageNet classification with deep convolutional neural networks. Adv Neural Inf Process Syst. 2012;25:1097-105. doi: 10.5555/2999134.2999257.
19. Russakovsky O, Deng J, Su H, et al. ImageNet Large Scale Visual Recognition Challenge. Int J Comput Vis. 2015;115(3):211-52. doi: 10.1007/s11263-015-0816-y.
20. Ronneberger O, Fischer P, Brox T. U-Net: Convolutional networks for biomedical image segmentation. In: Navab N, Hornegger J, Wells WM, Frangi AF, editors. Medical Image Computing and Computer-Assisted Intervention – MICCAI 2015. Cham: Springer; 2015. p. 234-41. doi: 10.1007/978-3-319-24574-4_28.
21. Hemelings R, Elen B, Barbosa-Breda J, Lemmens S, Meire M, Pourjavan S, Vandewalle E, Van de Veire S, Blaschko MB, De Boever P, Stalmans I. Accurate prediction of glaucoma from colour fundus images with a convolutional neural network that relies on active and transfer learning. Acta Ophthalmol. 2020 Feb;98(1):e94-e100. doi: 10.1111/aos.14193. Epub 2019 Jul 25. PMID: 31344328.
22. Hemelings, R., Elen, B., Schuster, A.K. et al. A generalizable deep learning regression model for automated glaucoma screening from fundus images. npj Digit. Med. 6, 112 (2023). https://doi.org/10.1038/s41746-023-00857-0

23. Zhou Y, Wagner SK, Chia MA, et al. A foundation model for generalizable disease detection from retinal images. Nature. 2023;622(7981):156-63. doi: 10.1038/s41586-023-06555-x.
24. Hosny A, Parmar C, Quackenbush J, Schwartz LH, Aerts HJWL. Artificial intelligence in radiology. Nat Rev Cancer. 2018;18(8):500-10. doi: 10.1038/s41568-018-0016-5.
25. Rajkomar A, Dean J, Kohane I. Machine Learning in Medicine. N Engl J Med. 2019 Apr 4;380(14):1347-1358. doi: 10.1056/NEJMra1814259. PMID: 30943338.
26. Luo H, Xu G, Li C, et al. Big data analytics for genomic medicine. Int J Mol Sci. 2017;18(2):412. doi: 10.3390/ijms18020412.
27. da Costa DR, Medeiros FA. Big data for imaging assessment in glaucoma. Taiwan J Ophthalmol. 2024 Sep 13;14(3):299-318. doi: 10.4103/tjo.TJO-D-24-00079. PMID: 39430345; PMCID: PMC11488812.
28. Shi N.N., Li T., Cheng S., Wong T.Y. Quantifying the Performance of Artificial Intelligence (AI) in Detecting Glaucoma Using Spectral Domain Optical Coherence Tomography (SD-OCT) Images. Int. J. Ophthalmol. 2024;17:100–110.
29. Martin KR, Mansouri K, Weinreb RN, Wasilewicz R, Gisler C, Hennebert J, Genoud D; Research Consortium. Use of Machine Learning on Contact Lens Sensor-Derived Parameters for the Diagnosis of Primary Open-angle Glaucoma. Am J Ophthalmol. 2018 Oct;194:46-53. doi: 10.1016/j.ajo.2018.07.005. Epub 2018 Jul 25. PMID: 30053471.
30. Mohammadzadeh V, Wu S, Besharati S, Davis T, Vepa A, Morales E, Edalati K, Rafiee M, Martinyan A, Zhang D, Scalzo F, Caprioli J, Nouri-Mahdavi K. Prediction of Visual Field Progression with Baseline and Longitudinal Structural Measurements Using Deep Learning. Am J Ophthalmol. 2024 Jun;262:141-152. doi: 10.1016/j.ajo.2024.02.007. Epub 2024 Feb 12. PMID: 38354971; PMCID: PMC11226195.
31. Xu, H., et al. (2022). "Multimodal Learning with Transformers: A Survey." arXiv preprint. arXiv:2206.06488.
32. Zheng C, Xie X, Zhou K, Chen B, Chen J, Ye H, Li W, Qiao T, Gao S, Yang J, Liu J. Assessment of Generative Adversarial Networks Model for Synthetic Optical Coherence Tomography Images of Retinal Disorders. Transl Vis Sci Technol. 2020 May 27;9(2):29. doi: 10.1167/tvst.9.2.29. PMID: 32832202; PMCID: PMC7410116.
33. Thirunavukarasu AJ, Ting DSJ, Elangovan K, Gutierrez L, Tan TF, Ting DSW. Large language models in medicine. Nat Med. 2023 Aug;29(8):1930-1940. doi: 10.1038/s41591-023-02448-8. Epub 2023 Jul 17. PMID: 37460753.
34. Ling XC, Chen HS, Yeh PH, Cheng YC, Huang CY, Shen SC, Lee YS. Deep Learning in Glaucoma Detection and Progression Prediction: A Systematic Review and Meta-Analysis. Biomedicines. 2025 Feb 10;13(2):420. doi: 10.3390/biomedicines13020420. PMID: 40002833; PMCID: PMC11852503.

35. Tonti E, Tonti S, Mancini F, Bonini C, Spadea L, D'Esposito F, Gagliano C, Musa M, Zeppieri M. Artificial Intelligence and Advanced Technology in Glaucoma: A Review. J Pers Med. 2024 Oct 16;14(10):1062. doi: 10.3390/jpm14101062. PMID: 39452568; PMCID: PMC11508556.
36. Herbert P, Hou K, Bradley C, Hager G, Boland MV, Ramulu P, Unberath M, Yohannan J. Forecasting Risk of Future Rapid Glaucoma Worsening Using Early Visual Field, OCT, and Clinical Data. Ophthalmol Glaucoma. 2023 Sep-Oct;6(5):466-473. doi: 10.1016/j.ogla.2023.03.005. Epub 2023 Mar 20. PMID: 36944385; PMCID: PMC10509314.
37. Wang, R., Bradley, C., Herbert, P. et al. Deep learning-based identification of eyes at risk for glaucoma surgery. Sci Rep 14, 599 (2024). doi.org/10.1038/s41598-023-50597-0.
38. Kelly CJ, Karthikesalingam A, Suleyman M, Corrado G, King D. Key challenges for delivering clinical impact with artificial intelligence. BMC Med. 2019 Oct 29;17(1):195. doi: 10.1186/s12916-019-1426-2. PMID: 31665002; PMCID: PMC6821018.
39. Beede E, Baylor E, Hersch F, et al. A human-centered evaluation of a deep learning system deployed in clinics for the detection of diabetic retinopathy. In: Proceedings of the 2020 CHI Conference on Human Factors in Computing Systems. New York, NY: ACM; 2020. p. 1-12. doi: 10.1145/3313831.3376718.
40. Hasan MM, Phu J, Wang H, Sowmya A, Kalloniatis M, Meijering E. OCT-based diagnosis of glaucoma and glaucoma stages using explainable machine learning. Sci Rep. 2025 Jan 28;15(1):3592. doi: 10.1038/s41598-025-87219-w. PMID: 39875492; PMCID: PMC11775169.
41. Oh S, Park Y, Cho KJ, Kim SJ. Explainable machine learning model for glaucoma diagnosis and its interpretation. Diagnostics (Basel). 2021;11(3):510. doi: 10.3390/diagnostics11030510
42. Pourjavan S, Gouverneur F, Macq B, Van Drooghenbroeck T, De Potter P, Boschi A, El Maftouhi A. Advanced Analysis of OCT/OCTA Images for Accurately Differentiating Between Glaucoma and Healthy Eyes Using Deep Learning Techniques. Clin Ophthalmol. 2024 Nov 26;18:3493-3502. doi: 10.2147/OPTH.S472231. PMID: 39618988; PMCID: PMC11607993.

# Chapter 3: AI theory to clinical application: GlauOCTA and GlauOCTA-AI, a Multimodal Approach for glaucoma diagnosis and risk assessment

Artificial intelligence in medicine leverages machine learning, deep learning, and big data analytics to enhance diagnostic precision, predict disease progression, and inform clinical decision-making. In glaucoma, AI holds particular promise due to the disease's heavy reliance on imaging and quantifiable biomarkers.

Glaucoma is an ideal candidate for AI-driven analysis. The diagnosis and monitoring of this chronic, progressive optic neuropathy depend on structural and functional markers identifiable via OCT, OCTA, and visual field (VF) testing. These imaging modalities provide quantifiable parameters, such as RNFL thickness and capillary density, that AI can rapidly analyse. Importantly, AI can detect subtle changes long before they are recognisable to the human eye [1,2].

Early detection is critical in glaucoma care. AI models, especially convolutional neural networks (CNNs), have shown high accuracy in recognising glaucomatous changes from fundus photographs and OCT scans, facilitating pre-perimetric diagnosis [3,4]. Beyond detection, AI enables effective disease monitoring by analysing longitudinal data to predict structural and functional deterioration, identify fast progressors, and guide timely interventions.

By integrating multimodal data, including OCT, OCTA, IOP fluctuations, VF outcomes, and potentially genetic markers, AI supports comprehensive risk assessment and personalised management. This data-driven approach provides an objective complement to traditional, often subjective, testing methods, enabling clinicians to reduce variability and improve outcomes.

Despite these advances, managing early-stage glaucoma remains challenging. At the time of diagnosis, distinguishing patients at risk of rapid progression is often uncertain. AI offers a means to navigate these clinical grey zones, enabling earlier, targeted treatment to preserve vision [5].

The remainder of this chapter presents the development and application of our GlauOCTA and GlauOCTA-AI frameworks, demonstrating how theoretical AI models were translated into multimodal tools for glaucoma detection and risk stratification of progression.

## 3.1 The Challenge of Diagnosing Glaucoma Suspects

Classifying glaucoma suspects presents a significant challenge for AI and experienced clinicians. While current AI models achieve high accuracy in distinguishing clear-cut glaucoma cases from healthy eyes, their performance

deteriorates when faced with borderline cases, reflecting the challenges that human clinicians also face.

This limitation is well-documented in the literature; In a study by Lim et al., a multimodal AI model integrating fundus photographs and OCT-derived parameters showed a high area under the receiver operating characteristic curve (AUROC) of 93.9% in classifying normal, preperimetric glaucoma (PPG), and glaucoma cases. However, while the AI achieved high sensitivity for advanced glaucoma (86.13%), it performed poorly in PPG cases (30.27%), struggling to differentiate early-stage disease from normal eyes despite transitioning from ML (SVM, Random Forest) to DL-based models [6]. A study by Muhammad et al. demonstrated that while AI models performed with high accuracy (above 90%) in distinguishing advanced glaucoma from healthy eyes, sensitivity dropped significantly (to ~70%) in glaucoma suspect cases [7]. Because glaucoma suspects lack clear structural or functional damage, making classification inherently difficult, just like for human experts. An experienced glaucoma specialist considers various biomarkers before making a decision. This reinforces the need for multimodal AI approaches that incorporate functional and vascular biomarkers alongside structural OCT data to enhance diagnostic certainty in borderline cases. By leveraging a combination of these biomarkers, AI models may improve diagnostic certainty and reduce misclassification rates in suspect cases.

## 3.2 Selecting the Appropriate AI Model for Glaucoma Detection

The foundation of this work was established through my observations during a small-scale glaucoma screening campaign [8]. Despite standardised training and adherence to the European Glaucoma Guidelines, a small group of experienced clinicians exhibited significant interobserver variability in diagnosing glaucoma. This highlights the subjectivity inherent in clinical evaluation and the potential role of AI in mitigating such inconsistencies.

Commercially available AI algorithms now facilitate remote fundus image analysis, delivering automated diagnostic feedback within minutes. For example, Netra.AI, developed in collaboration with the Sankara Eye Foundation, is a cloud-based platform for assessing retinal risk. Initially designed for diabetic retinopathy screening, Netra.AI has expanded its capabilities to include the detection of glaucoma. Analysing retinal images generates a comprehensive report within two minutes, enabling early detection and timely referrals. Similarly, Remidio's Fundus on Phone provides portable, AI-assisted glaucoma screening.

Despite these advancements, the clinical applicability of such models remains limited due to several key challenges:

- Lack of transparency in ground truth labelling: The datasets used to train these models often lack clear documentation on diagnostic criteria and external validation.

- Limited generalisability: AI models trained on homogeneous populations may underperform in multiethnic cohorts, necessitating rigorous external validation.
- Algorithmic variability across imaging platforms: Differences between OCT manufacturers (e.g., Optovue, Heidelberg, Topcon) can lead to inconsistencies in AI model outputs.
- The black-box nature of deep learning: The lack of interpretability in many DL-based models raises concerns regarding clinical trust and implementation. To address these concerns, Explainable AI (XAI) is being increasingly explored to enhance transparency and trust in AI-driven clinical decision-making.

### 3.3 Clinical Implications: Predicting Fast Progressors and Personalising Treatment

One of the most pressing challenges in clinical practice is predicting which patients will progress rapidly. Traditional risk assessment incorporates parameters such as age, ethnicity, maximum IOP, and family history, but these provide only a probabilistic estimate of disease progression [9,10]. This risk assessment method doesn't fit all patients, and the rate of progression (RoP) is not linear, varying for each patient.

AI-based models can stratify patients more precisely by integrating structural (RNFL thinning), functional (VF RoP), and vascular (OCTA density) parameters. A study designed a customised CNN based on longitudinal macular OCTA images to detect glaucoma progression [11]. The DL model performed well, suggesting that CNNs can effectively analyse OCTA data to monitor glaucoma progression. Such predictive capabilities would enable targeted intervention before irreversible damage occurs.

The ultimate goal is to develop AI-driven tools that enable clinicians to estimate the VF loss trajectory from a single OCT/OCTA exam, without requiring multiple years of follow-up data. Implementing predictive AI algorithms in routine clinical practice would facilitate personalised treatment strategies and improve patient adherence by providing tangible risk projections.

### 3.4 Publication I – Interobserver Variability Study

## Evaluating the Influence of Clinical Data on Inter-Observer Variability in Optic Disc Analysis for AI-Assisted Glaucoma Screening.

## *Pourjavan S, Bourguignon G, Marinescu C et al.*

Accurately assessing the optic nerve head (ONH) remains one of the fundamental challenges in glaucoma diagnosis. Despite standardized guidelines and extensive

clinician training, significant inter-observer variability persists, particularly in borderline cases. Even among glaucoma specialists trained within the same institution and adhering to European Guidelines, diagnostic discrepancies remain widespread. This inconsistency is partially driven by differences in individual weighting of risk factors such as intraocular pressure (IOP), visual field progression, and optic disc morphology. Interestingly, instead of improving diagnostic consensus, including additional clinical information sometimes heightened confusion. Certain clinicians relied more heavily on structural parameters. In contrast, others prioritised functional tests, highlighting the subjective nature of clinical decision-making.

Given these inconsistencies, integrating AI-based assessment tools could provide a more standardised approach to ONH evaluation. By leveraging deep learning models trained on large datasets, AI has the potential to reduce subjective bias and enhance diagnostic reproducibility. The following study investigates how AI models compare to human experts in assessing the optic disc, shedding light on the extent of inter-clinician variability and the potential role of AI in establishing a more objective diagnostic framework for glaucoma.

Clinical Ophthalmology

Dovepress
Taylor & Francis Group

Open Access Full Text Article

ORIGINAL RESEARCH

# Evaluating the Influence of Clinical Data on Inter-Observer Variability in Optic Disc Analysis for AI-Assisted Glaucoma Screening

Sayeh Pourjavan[1,2], Gen-Hua Bourguignon[1], Cristina Marinescu[2], Loic Otjacques[2], Antonella Boschi[1]

[1]Department of Ophthalmology, Cliniques Universitaires Saint Luc, UCL, Brussels, Belgium; [2]Department of Ophthalmology, Chirec Hospital Groups, Delta Hospital, Brussels, Belgium

Correspondence: Sayeh Pourjavan, Email Sayeh.pourjavan@saintluc.uclouvain.be



**Purpose:** This study aims to evaluate the inter-observer variability in assessing the optic disc in fundus photographs and its implications for establishing ground truth in AI research.

**Methods:** Seventy subjects were screened during a screening campaign. Fundus photographs were classified into normal (NL) or abnormal (GS: glaucoma and glaucoma suspects) by two masked glaucoma specialists. Referrals were based on these classifications, followed by intraocular pressure (IOP) measurements, with rapid decisions simulating busy outpatient clinics.In the second stage, four glaucoma specialists independently categorized images as normal, suspect, or glaucomatous. Reassessments were conducted with access to IOP and contralateral eye data.

**Results:** In the first stage, the agreement between senior and junior specialists in categorizing patients as normal or abnormal was moderately high. Knowledge of IOP emerged as an independent factor influencing the decision to refer more patients. In the second stage, agreement among the four specialists varied, with greater concordance observed when additional clinical information was available. Notably, there was a statistically significant variability in the assessment of optic disc excavation.

**Conclusion:** The inclusion of various risk factors significantly influences the classification accuracy of specialists. Risk factors like IOP and bilateral data influence diagnostic consistency among specialists. Reliance solely on fundus photographs for AI training can be misleading due to inter-observer variability. Comprehensive datasets integrating multimodal clinical information are essential for developing robust AI models for glaucoma screening.

**Plain Language Summary:** Glaucoma is a leading cause of irreversible blindness, and early detection is critical in preventing blindness. Screening for glaucoma using fundus photographs is one approach, but there is significant variability in how specialists interpret these images. This study evaluated how consistently different eye specialists assess these photographs and what this variability means for developing artificial intelligence (AI) tools to detect glaucoma.

The study involved 70 individuals screened for glaucoma using fundus photographs. Two specialists initially classified the images as either normal or abnormal (including glaucoma suspects). The agreement between the specialists was moderate, showing that different clinicians sometimes reach different conclusions based on the same images. The study also tested how additional information, like intraocular pressure (IOP), affects these classifications. Surprisingly, including IOP data introduced more variability, making agreement between the specialists even lower.

The research highlights that relying solely on fundus photos without considering other clinical factors, like IOP or data from both eyes, could be misleading when developing AI tools. For AI to effectively assist in glaucoma detection, it must be trained on comprehensive datasets that include more than just fundus images.

These findings emphasize the importance of using a broad range of clinical data when training AI models for glaucoma screening to improve accuracy and reliability in real-world settings.

**Keywords:** artificial intelligence, diagnostic imaging, glaucoma screening, clinical decision support, multimodal diagnostic

Received: 24 October 2024
Accepted: 20 December 2024
Published: 27 December 2024

## Introduction

Glaucoma is the leading cause of irreversible blindness worldwide, affecting 3.5% of individuals aged 40 to 80 years.[1] Over half of cases remain undiagnosed due to the asymptomatic nature of early disease,[2] often leading to advanced stages with significant visual impairment, impacting the quality of the patient's life. Additionally, the economic burden associated with late-stage disease is substantial; the direct care costs for advanced glaucoma (stages 4–5, Bascom Palmer system) are 1.7 times higher than for early-stage disease.[3] These challenges highlight an urgent need for improved strategies for early detection to prevent blindness.

However, mass screening faces logistical and clinical challenges, including reliance on skilled personnel, limited diagnostic tools, and high patient volumes in underserved regions. Inter-observer variability in optic disc assessment further complicates glaucoma diagnosis, emphasizing the need for innovative tools to enhance accuracy.

Recent advancements in artificial intelligence (AI), particularly deep learning, have demonstrated diagnostic performance exceeding 95% AUC in internal datasets.[4–6] AI has the potential to reduce variability and provide consistent evaluations, making it invaluable in busy clinics and resource-limited settings.

This study originated from a glaucoma screening campaign conducted on World Sight Day. Seventy individuals were screened, and fundus photographs were rapidly classified as normal or abnormal, reflecting the time constraints typical of a busy outpatient clinic condition. The observed unexpected variability during this rapid decision-making process among trained professionals motivated further investigation with masked evaluations by experienced colleagues, transforming this campaign into a research opportunity.

## Purpose

To evaluate inter-observer variability in optic disc classification using colour fundus photographs, with and without intraocular pressure (IOP) data, and to assess the reliability of ground truth labels based solely on fundus images for the external validation of AI algorithms in glaucoma detection.

## Methods

This cross-sectional observational study was conducted at our hospital in accordance with the principles of the Declaration of Helsinki. The Institutional Ethical Commission of the Cliniques Universitaires Saint-Luc in Brussels approved the study protocol (OVO-AI Study: Observer Variability in Optic disc and AI Implications). This research adheres to the principles outlined in the Declaration of Helsinki for studies involving human subjects. It complies with all relevant national ethical guidelines, including the General Data Protection Regulation (GDPR) for data privacy and confidentiality within Europe. While HIPAA is specific to the United States, the GDPR ensures similar standards in the European context. Written informed consent was obtained from each participant before inclusion in the study.

Fundus images from both eyes were obtained from a cohort of 70 individuals presenting randomly during a glaucoma screening campaign in the hospital. The only two exclusion criteria were age and a confirmed diagnosis of glaucoma. The minimum age for screening was set at 30 years due to the racial heterogeneity (Caucasians, Asians, Latinos, and African descendants) in Brussels. The clinical parameters were age, bilateral fundus pictures, taken with a Crystalvue NFC600 camera and intraocular pressure measured with air tonometry, NIDEK Tonoref III.

The Crystalvue NFC600 camera is equipped with MONA AI-driven software capable of providing a probability score for glaucoma based on fundus images. MONA, a Belgian healthcare AI startup, is a spin-off of KULeuven and VITO (the Flemish technology agency). Initially developed for detecting diabetic retinopathy (DR) and diabetic macular edema (DME), MONA AI was trained on an extensive dataset of over 273,000 retinal images. The system achieved a sensitivity of 90% and specificity of 95% for referable DR and similarly high accuracy for DME detection. Its convolutional neural network (CNN) architecture leverages these vast datasets to identify subtle pathological changes with high consistency. Although specific details about MONA's glaucoma training dataset are unavailable, it likely employs a comparable AI framework, assigning optic disc scores from 0.0 to 1.0, with higher scores indicating a greater likelihood of glaucoma.

While the MONA AI system is not yet commercially available, its use in this study was dictated by camera availability. AI-generated probability scores were accessed post hoc for supplementary analysis and were not part of the initial evaluations. The inclusion of MONA was not intended as validation or a comparative assessment of the software.

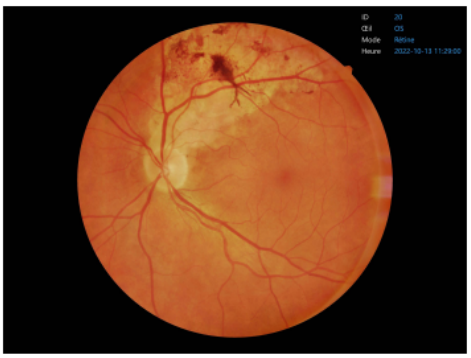


**Figure 1** Asymptomatic patient during screening with branch occlusion and vasculitis caused by recent toxoplasmosis infection.

Fundus photographs were visually evaluated by two masked glaucoma specialists (SP and GB) who categorized the images as normal (NL) or abnormal (GS) including glaucoma and glaucoma suspects, in real-time, simulating the time constraints of a busy outpatient clinic. The classification adhered to the European Glaucoma Society (EGS) guidelines,[7] using parameters such as optic disc size and rim, vessel bearing, peripapillary haemorrhages, and cup-to-disc ratio.

Intraocular pressure (IOP) was subsequently measured using an air tonometer (NIDEK Tonoref III), which underwent routine calibration per manufacturer recommendations to ensure accuracy. Elevated IOP values were defined as >21 mmHg. Patients with abnormal fundus classifications (GS) and/or elevated IOP were referred for further ophthalmological evaluation. During the screening, one asymptomatic patient showed an important branch occlusion (Figure 1) and was directly sent to the Ophthalmology emergency for further examination and was diagnosed with a toxoplasmosis-caused occlusion. He was discarded from the study.

In the second phase, the fundus photographs of 138 optic discs were reanalyzed by four ophthalmologists (three glaucoma specialists and one resident). The images were categorized into three groups: normal (N), glaucoma-suspect (S), and glaucomatous (G) per EGS guidelines. Vertical Cup-to-Disc Ratio (VCDR) values were recorded for each optic nerve. The classifications were conducted in a masked manner without knowledge of IOP or the condition of the contralateral disc. Following unblinding, IOP and contralateral disc appearance were revealed sequentially, allowing observers to update their classifications.

### Statistical Analysis

The Kappa coefficients were used to assess the agreement among different specialists for categorical variables and the Weighted Kappa coefficients for categorical ordinal variables. Kappas with their standard error are reported.

Intraclass correlation coefficients (ICC) were used to evaluate agreement in VCDR scoring on the image level for continuous variables.

## Results

138 images of 69 subjects were taken. The statistical descriptive data of the continuous variables are shown in Table 1.

### Results from the Hospital Screening

During the screening in the hospital, the flow of incoming patients limited the decision and scoring time. It was nearly instantaneous, less than one minute per eye mimicking a normal clinical setting.

Of the total 138 right and left eye pictures, 120 were labelled NL (61/ 69 for the RE, 61 and 59/ 69 for the LE). Eighteen subjects were referred for further examination based solely on their fundus photographs when either observer classified one or both eyes as GS. The number of referred subjects increased to 27, based on their initial allocation to the

**Table 1** Descriptive Analysis of the Participants

| F/M | 47.7/52.3% | |
|---|---|---|
| **Variable** | **Mean ± SD** | **Min-max** |
| Age (years) | 57 ± 12 | 33–82 |
| IOP RE | 15.5 ± 4.5 | 10–28 |
| IOP LE | 15.8 ± 4.4 | 10–30 |

**Table 2** Number of Referred Patients with or Without Knowledge of the IOP

| | **Referral Based on Pictures** | **Referral Based on Pictures and IOP** |
|---|---|---|
| SP | 5 | 4 |
| GB | 8 | 6 |
| Both | 5 | 17 |
| total | 18 | 27 |

**Table 3** Reproducibility Between SP & GB Based on Fundus Pictures

| | **Cohen's Weighted Kappas** | ***p*** |
|---|---|---|
| RE | 0.53 ± 0.17 | 0.001 |
| LE | 0.57 ± 0.15 | < 0.001 |
| BE | 0.55 ± 0.11 | <0.001 |

**Table 4** Reproducibility Between SP & GB Based on Fundus Pictures with or Without IOP

| | **Cohen's Weighted Kappas** | | ***p*** | |
|---|---|---|---|---|
| | **Without IOP** | **With IOP** | **Without IOP** | **With IOP** |
| RE | 0.38 ± 0.12 | 0.24 ± 0.13 | 0.001 | 0.015 |
| LE | 0.35 ± 0.19 | 0.29 ± 0.14 | < 0.001 | 0.007 |

GS group and, or high IOP, after revealing the eye pressure (Table 2). It indicates that IOP, for clinicians, is considered a crucial and independent risk factor for further investigation.

The concordance between the 2 masked observers (Table 3) during the screening, where the observers took the pictures and scored them only as NL or GS without knowing the IOP, is quantified by the kappa's values for both eyes (kappa ± SE = 0.55 ± 0 0.11, $p < 0.001$). It means an acceptable reproducibility between the glaucoma specialist (SP) and her junior resident (GB) score.[8]

The Kappa values for the initial assessment (without IOP) indicate "moderate" agreement (Table 4).

The values of the weighted Kappa's decline when the IOP is revealed. The lower Kappa values after including IOP fall into the "fair" agreement category, suggesting less consistency when IOP data is factored in. This reduction in Kappa

values suggests that the inclusion of IOP data may have introduced some variability in the assessment, leading to a lower level of agreement between the observers. This variability could arise from differing interpretations of the significance of IOP values in the context of fundus images.

## Results from the Masked Picture Analysis

In the second phase of the study, three glaucoma specialists (SP, LO, CM) and one glaucoma resident (GB) independently reviewed the fundus photographs under various conditions to assess classification consistency. The evaluations were performed in the following scenarios:

1. Separate Classification: Each eye was assessed individually without additional information or time constraints.
2. Incorporating Contralateral Eye Information: Observers compared the images of both eyes from the same subject.
3. With and Without IOP Consideration: Observers classified the images without IOP data initially, followed by a second round where IOP values were revealed, allowing for potential reclassification.

The images were categorized into three groups: Normal (N), Suspect (S), and Glaucoma (G). Additionally, the vertical cup-to-disc ratio (VCDR) was recorded for each optic disc. Table 5 and Table 6 summarize the descriptive analysis of classifications and inter-observer agreement, respectively.

The comparison of classification performance across the different conditions is summarized below:

**Table 5** Descriptive Analysis of Patient Classifications Across Different Conditions and Comparisons, with Data Provided by Multiple Observers. N= Normal, S= Suspect, G= Glaucoma

| | RE | | | RE + IOP | | | RE Compared to LE | | | RE+IOP Compared to LE | | | LE | | | LE + IOP | | | LE Compared to RE | | | LE + IOP Compared to RE | | |
|---|---|---|---|---|---|---|---|---|---|---|---|---|---|---|---|---|---|---|---|---|---|---|---|---|
| | N | S | G | N | S | G | N | S | G | N | S | G | N | S | G | N | S | G | N | S | G | N | S | G |
| SP | 60 | 8 | 1 | 60 | 8 | 1 | 60 | 7 | 2 | 60 | 7 | 2 | 59 | 8 | 2 | 59 | 8 | 2 | 59 | 8 | 2 | 59 | 8 | 2 |
| GB | 59 | 8 | 2 | 60 | 7 | 2 | 60 | 6 | 3 | 60 | 9 | 3 | 59 | 9 | 1 | 61 | 8 | 0 | 57 | 10 | 2 | 58 | 10 | 1 |
| LO | 56 | 10 | 1 | 54 | 13 | 1 | 53 | 13 | 1 | 53 | 14 | 1 | 57 | 8 | 2 | 55 | 13 | 0 | 54 | 11 | 2 | 55 | 12 | 1 |
| CM | 56 | 10 | 3 | 49 | 16 | 3 | 56 | 9 | 4 | 55 | 9 | 4 | 57 | 9 | 3 | 47 | 19 | 3 | 54 | 12 | 3 | 53 | 12 | 3 |

**Table 6** Comparison of Classification Performance Across Different Conditions and Among Different Specialists. The Bolded Values Reflect the Highest Agreement for Each Specialist

| Weighted Kappas ± SE | | | | | | | | |
|---|---|---|---|---|---|---|---|---|
| | Condition 1 | | Condition 2 | | Condition 3 | | Condition 4 | |
| | Separate Classification for Each Eye (With & Without IOP Consideration) | | Classification with Contralateral Eye Consideration (With & Without IOP) | | Classification with and Without Consideration of the Other Eye (IOP unknown) | | Classification with and Without Consideration of the Other Eye (IOP known) | |
| | RE | LE | RE | LE | RE | LE | RE | LE |
| SP | 0,42±0,19 | 0,56±0,15 | **1,00±0,00** | **1,00±0,00** | 0,84±0,09 | 0,71±0,10 | 0,39±0,19 | 0,45±0,16 |
| GB | **0,95±0,05** | **0,82±0,09** | 0,91±0,07 | 0,82±0,08 | 0,91±0,06 | 0,77±0,08 | 0,95±0,05 | 0,77±0,10 |
| LO | 0,72±0,11 | 0,61±0,11 | 0,42±0,12 | 0,57±0,10 | **0,87±0,08** | **0,87±0,08** | 0,72±0,09 | 0,77±0,09 |
| CM | 0,80±0,08 | 0,69±0,10 | 0,74±0,09 | 0,71±0,09 | **0,96±0,03** | **0,89±0,06** | 0,89±0,06 | 0,92±0,05 |

- SP (Senior Specialist) achieved perfect agreement (Kappa = 1.00) when using contralateral eye information (Condition 2). However, performance declined when relying solely on IOP or without any additional information.
- GB (Resident) demonstrated consistently high performance across all conditions, indicating robust diagnostic capability irrespective of data inputs.
- LO (Specialist) showed significant improvement when contralateral eye information was available (Conditions 2 and 3) but lower agreement when relying only on IOP.
- CM (Specialist) consistently performed well in all conditions, with the highest agreement observed when both contralateral eye information and IOP were included (Condition 3).

Table 6 shows that SP performs perfectly when the other eye's information is available (Condition 2), but its performance is lower when relying solely on IOP or without any additional information. GB performs consistently well across all conditions, indicating its robustness to various data inputs. LO performance benefits most when the other eye's information is available (Conditions 2 and 3) but shows lower performance when relying solely on IOP. CM performs strongly in all conditions, with the highest agreement when other eye information is available (Conditions 2 and 3).

In Condition 3, where classifications were based on contralateral eye information but excluded IOP, emerged as the optimal scenario, showing high inter-observer agreement. This condition provides a balance where all raters perform well, suggesting that using the other eye's information without IOP gives the most reliable classification across the board and makes it the most robust scenario for ground truth classification. In conclusion, including contralateral eye information significantly improved classification reliability across all observers. In contrast, including IOP often introduced variability, leading to lower agreement in several conditions. Condition 3—leveraging contralateral eye data without IOP—proved to be the most reliable for establishing ground truth. The consistently high performance of GB and CM further highlights the potential for enhanced diagnostic accuracy when incorporating bilateral information.

## Results from VCDR Scoring

Estimation of the optic disc excavation by all the raters is shown in Table 7.

This table shows that the more "experimented" ophthalmologists rate the excavations smaller than the "younger" colleagues.

Figure 2 shows the Vertical Cup to Disc scoring (VCDR) for each rater.

**Table 7** Estimation of the Optic Disc Excavation by All the Raters

| | Nr | Minimum C/D | Maximum C/D | Average C/D ±SD | |
|---|---|---|---|---|---|
| SP OD | 69 | 0.00 | 0.60 | 0.27 | 0.13 |
| SP OG | 69 | 0.10 | 0.60 | 0.27 | 0.12 |
| GB OD | 69 | 0.00 | 0.75 | 0.30 | 0.19 |
| GB OG | 69 | 0.00 | 0.75 | 0.32 | 0.18 |
| LO OD | 67 | 0.00 | 0.70 | 0.33 | 0.16 |
| LO OG | 67 | 0.00 | 0.70 | 0.33 | 0.18 |
| CM OD | 69 | 0.10 | 0.65 | 0.27 | 0.16 |
| CM OG | 69 | 0.10 | 0.65 | 0.29 | 0.16 |
| Valid Nr | 67 | | | | |

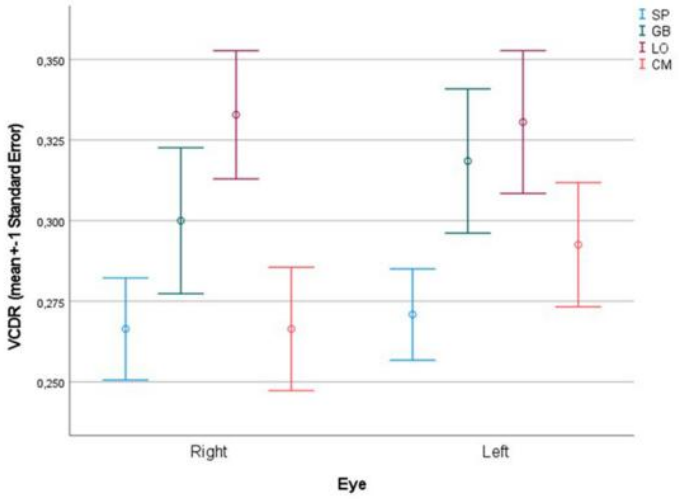


**Figure 2** Shows the Vertical Cup to Disc scoring (VCDR) for each rater.

## Result from AI-MONA

The MONA algorithm analyzes fundus images to assess the likelihood of glaucoma, as shown in Figure 3. While the system does not provide a numeric image-quality score, it automatically rejects poor-quality images where the optic nerve head is not visible or is improperly centred. For acceptable images, MONA generates a probability score between 0 and 1, where higher scores indicate a greater likelihood of glaucoma.

- The algorithm operates with a defined threshold: Scores below 0.73: Classified as healthy and Scores of 0.73 or higher: Indicate a high probability of glaucoma.

**Figure 3** The original picture and the processed picture by MONA.

**Table 8** The Descriptive Analysis by MONA, Based on Risk Scores. The Higher the Risk Scores, the Higher the Possibility of Having Glaucoma

| Risk Score | Mean ± SD | Min | Max | Rejected |
|---|---|---|---|---|
| RE | 0,587,494,512 ± 0,11,121,722 | 0,282,902,298 | 0,282,902,298 | 7/69 |
| LE | 0,586,386,255 ± 0,12,020,194 | 0,319,392,204 | 0,831,739,731 | 1/69 |

Notably, the algorithm does not classify images as "Suspect", focusing only on binary outcomes (healthy or glaucomatous). Table 8 provides a descriptive analysis of the risk scores generated by MONA, illustrating the distribution of scores and their correlation with the likelihood of glaucoma (Table 8). Figure 4 shows the Scatter Plot of MONA- AI risk factors for both eyes separately.

The Pearson correlation coefficient between the RE and LE is 0.23 indicating a weak positive correlation.

Figure 5 shows the different histograms and kernel density estimates (KDEs) for both eyes to represent the distribution differences.

## Discussion

Initially designed as an awareness campaign, this study uncovered significant inter-observer variability in clinical glaucoma diagnostics. Despite shared training and adherence to standardized methodologies, the findings highlighted the inherently subjective nature of optic disc evaluation. Notably, each specialist's diagnostic reasoning, shaped by individual experience and cognitive processes, operated like a distinct "black box", even within a structured framework. For example, while intraocular pressure (IOP) often introduced complexity, assessing both optic discs simultaneously improved diagnostic accuracy in some cases, further illustrating the variability in clinical approaches.

The small sample size of 70 subjects reflects the practical limitations of data collection during the campaign. However, the results provide valuable insights into diagnostic variability and decision-making processes under real-world conditions. The increase in referrals from 18 to 27 when intraocular pressure (IOP) data was included underscores IOP's role as an independent glaucoma risk factor, though its inclusion introduced more significant variability and lowered agreement among observers. Notably, Condition 3, where bilateral fundus information was available, but IOP was excluded, showed the highest inter-observer agreement, indicating its potential as a reliable framework for establishing ground truth.

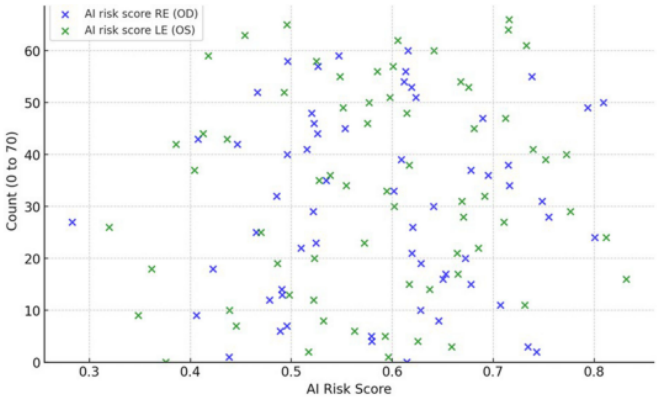


**Figure 4** The Scatter Plot of MONA- AI risk factors for both eyes separately.

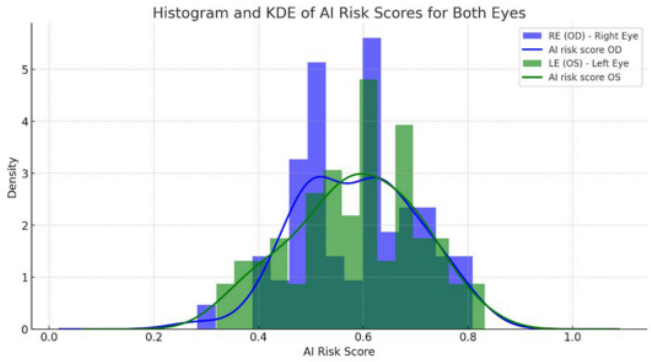


**Figure 5** Histograms and kernel density estimates (KDEs) for both eyes to represent the.

## Clinical and AI Implications

The moderate agreement observed in this study highlights limitations in using fundus photographs as the sole basis for training and validating AI models. Despite employing the European Glaucoma Society (EGS) Guidelines, subjective interpretations of these criteria led to inconsistencies, complicating comparisons between AI and human evaluations. These findings align with prior research showing that AI models trained on datasets with comprehensive clinical parameters demonstrate superior generalizability compared to those reliant solely on fundus photo-based labels.

While not a validation focus in this study, the MONA AI system generated probability scores post hoc, revealing a weak positive correlation between scores for both eyes. This contrasts with the higher agreement among clinicians when bilateral images were evaluated together. MONA's inability to classify "Suspects" or identify non-glaucomatous pathologies, such as visible vasculitis, underscores the limitations of narrow task-specific training. This further emphasizes the need for broader and more diverse clinical datasets to enhance AI robustness and generalizability.

AI employment in clinical decision-making as a support system faces several challenges. Several studies indicate that high image quality is essential for accurately classifying fundus images.[9,10] Standard fundus cameras lack integrated software to assess image quality. In contrast, optical coherent tomography (OCT) and angio-OCT devices provide an image quality score and recommend discarding images that fall below a certain threshold.[11] The determination of image quality in fundus photography is often subjective. An observer may choose to classify the optic disc even if the image exhibits mild blurriness. Additionally, many patients participating in screening programs are elderly and may have cataracts or corneal ageing, leading to inherently lower image quality. The data's quality should represent the expected data level that the model will encounter in practice,[12] meaning elderly with mild to pronounced blurriness of the media. Therefore, the ground truth is fundamentally subjective by default.

Consequently, comparing the performance of AI algorithms to such variability becomes complex. These findings are in keeping with our previous work,[13,14] where the performance of a robust glaucoma-AI model trained on a dataset with ground truth labels based on deep phenotyping including all available clinical parameters had excellent generalizability in various external databases, but with the least good performance in datasets which had ground truth labels bases on only fundus photo evaluation.

In this study, other important clinical parameters, such as visual field, optic nerve head measurements with optical coherence tomography, and corneal thickness, were not performed to confirm the presence of glaucoma at the end. In a similar study by Al Aswad. et al,[15] the deep learning AI (Pegasus) could be compared to a gold standard of glaucoma versus healthy diagnosis because the testing was performed on a known database of patients: fundus images randomly selected from the Singapore Malay Eye Study (SiMES).[16]

This study utilized a small cohort of 69 subjects obtained during a glaucoma screening campaign. While small sample sizes can be useful for initial exploratory studies, they pose significant generalizability and statistical power limitations. In glaucoma screening, the disease prevalence may vary across different populations, making it essential to have a representative sample size to draw accurate conclusions. A larger patient sample would improve the robustness and external validity of the results, allowing for better assessments of AI performance and generalizability to real-world clinical settings. In comparison, in a large systematic review of 2021 including 6 original studies comparing the performance of ophthalmologists and AI, the rate of included patients with glaucomatous optic neuropathy ranged from 41.4% to 50%. In our study, the subjects were in hospital for different reasons with a much lower rate of glaucoma, closer to the actual prevalence in the population. This difference in prevalence in our cohort was also a source of lower inter-observer reproducibility.

VCDR scoring, we observed considerable variation in how clinicians rated excavation. In this study, the longer a clinician had been practicing, the smaller their evaluation of the excavation tended to be, highlighting both inter- and possible intra-clinician variability in C/D ratings.[17,18]

## Conclusion

The limitations of inter-observer variability and small cohort highlighted in this discussion, emphasize the need for cautious interpretation of studies evaluating AI systems for glaucoma screening in clinical practice solely based on fundus photos. These observations should remind AI researchers that the performance of AI algorithms relies on the robustness of the ground truth labels. We should consider a hybrid approach, for example, supplementing "Condition 3" with other clinically relevant information in this study. Future research should address these limitations by incorporating larger and more diverse patient cohorts considering multiple diagnostic parameters: specifically for glaucoma, it is recommended to determine the ground truth based on not only fundus pictures but also additional metadata such as visual field examinations or Optical Coherence Tomography scans.[19] Our findings resonate with experiences in other medical domains, where AI has been shown to complement rather than replace human expertise. Studies demonstrate that while AI and specialists independently achieve similar diagnostic accuracy for recognizing a disease, their combined efforts significantly outperform either alone. This underscores AI's strength in analyzing vast and diverse datasets, particularly for rare conditions, while clinicians bring a holistic perspective grounded in clinical experience. Similarly, in glaucoma diagnostics, AI has the potential to enhance the accuracy of human assessments by mitigating inter-observer variability and identifying subtle features that may be overlooked in busy clinical settings". By addressing these challenges, the potential of AI for glaucoma screening in clinical settings should be more effectively evaluated.

## Acknowledgments

We wish to express our appreciation to MONA Health for generously granting access to the algorithm and for the prompt and insightful responses to our queries.

## Funding

A grant has been awarded for the doctorate thesis of the first author of which this article is one of the publications. Glaucoma Centre Ophthalmologists Zaventem outpatient financially supported the publication of this article.

## Disclosure

Gen-Hua Bourguignon is the co-author. All authors declare no competing interests.

## References

1. Tham YC, Li X, Wong TY, Quigley HA, Aung T, Cheng CY. Global prevalence of glaucoma and projections of glaucoma burden through 2040: a systematic review and meta-analysis. *Ophthalmology*. 2014;121(11):2081-90. doi:10.1016/j.ophtha.2014.05.013
2. Soh Z, Yu M, Betzler BK, et al. The global extent of undetected glaucoma in adults: a systematic review and meta-analysis. *Ophthalmology*. 2021;128(10):1393-404. doi:10.1016/j.ophtha.2021.04.009
3. Lee PP, Walt JG, Doyle JJ, et al. A multicenter, retrospective pilot study of resource use and costs associated with severity of disease in glaucoma. *Arch Ophthalmol Chic Ill*. 2006;124(1):12-9.

4. Chaurasia AK, Greatbatch CJ, Hewitt AW. Diagnostic accuracy of artificial intelligence in glaucoma screening and clinical practice. *J Glaucoma*. 2022;31(5):285. doi:10.1097/IJG.0000000000002015
5. Buisson M, Navel V, Labbé A, et al. Deep learning versus ophthalmologists for screening for glaucoma on fundus examination: a systematic review and meta-analysis. *Clin Experiment Ophthalmol*. 2021;49(9):1027-38. doi:10.1111/ceo.14000
6. Islam M, Poly TN, Yang HC, Atique S, Li YCJ. Deep learning for accurate diagnosis of glaucomatous optic neuropathy using digital fundus image: a meta-analysis. *Stud Health Technol Inform*. 2020;270:153-7. doi:10.3233/SHTI200141
7. Spaeth GL. European glaucoma society terminology and guidelines for glaucoma, 5th edition. *Br J Ophthalmol*. 2021;105(Suppl 1):1-169. doi:10.1136/bjophthalmol-2021-egsguidelines
8. Altman DG. *Practical Statistics for Medical Research*. London: Chapman and Hall; 1991.
9. Gonçalves MB, Nakayama LF, Ferraz D, et al. Image quality assessment of retinal fundus photographs for diabetic retinopathy in the machine learning era: a review. *Eye*. 2024;38:426–433. doi:10.1038/s41433-023-02717-3
10. Sabottke CF, Spieler BM. The effect of image resolution on deep learning in radiography. *Radiol Artif Intell*. 2020;2(1):e190015. doi:10.1148/ryai.2019190015
11. Pradhan ZS, Sreenivasaiah S, Srinivasan T, et al. The importance of signal strength index in optical coherence tomography angiography: a study of eyes with pseudoexfoliation syndrome. *Clin Ophthalmol*. 2022;16:3481–3489. doi:10.2147/OPTH.S378722
12. Dow ER, Keenan TDL, Lad EM, et al. Collaborative community for ophthalmic imaging executive committee and the working group for artificial intelligence in age-related macular degeneration. from data to deployment: the collaborative community on ophthalmic imaging roadmap for artificial intelligence in age-related macular degeneration. *Ophthalmology*. 2022;129(5):e43–e59. doi:10.1016/j.ophtha.2022.01.002
13. Tan NYQ, Friedman DS, Stalmans I, Ahmed IIK, Sng CCA. Glaucoma screening: where are we and where do we need to go? *Curr Opin Ophthalmol*. 2020;31(2):91. doi:10.1097/ICU.0000000000000649
14. Hemelings R, Elen B, Barbosa-Breda J, et al. Accurate prediction of glaucoma from colour fundus images with a convolutional neural network that relies on active and transfer learning. *Acta Ophthalmol*. 2020;98(1):e94-100. doi:10.1111/aos.14193
15. Al-Aswad LA, Kapoor R, Chu CK, et al. Evaluation of a deep learning system for identifying glaucomatous optic neuropathy based on color fundus photographs. *J Glaucoma*. 2019;28(12):1029-34. doi:10.1097/IJG.0000000000001319
16. Rosman M, Zheng Y, Lamoureux E, et al. Review of key findings from the Singapore Malay Eye Study (SiMES-1). *Singapore Med J*. 2012;53(2):82-7.
17. Lichter PR. Variability of expert observers in evaluating the optic disc. *Trans Am Ophthalmol Soc*. 1976;74:532–572.
18. Kwon YH, Adix M, Zimmerman MB, et al. Variance owing to observer, repeat imaging, and fundus camera type on cup-to-disc ratio estimates by stereo planimetry. *J Glaucoma*. 2009;18(4):305–310. doi:10.1097/IJG.0b013e318181545e
19. Pourjavan S, Gouverneur F, Macq B, et al. Advanced analysis of OCT/OCTA images for accurately differentiating between glaucoma and healthy eyes using deep learning techniques. *Clin Ophthalmol*. 2024;18:3493–3502. doi:10.2147/OPTH.S472231

**Clinical takeaway: Interobserver variability study**

*This study reveals the high inter- and intra-observer variability among glaucoma experts and how new information reshapes their assessments. Each clinician applies a different personal cognitive weighting, akin to deep neural reasoning, illustrating how backpropagation-like mental adjustments occur in real-time. It highlights the challenge of defining ground truth, particularly for subtle structural changes.*

## 3.5 Bridging the Gap: From Expert Variability to AI-Driven Biomarkers

Our first study revealed significant inter-clinician variability in optic disc assessment—even among experienced glaucoma specialists using the same guidelines. Despite structured protocols, diagnostic interpretations varied: some clinicians prioritised structural indicators like the cup-to-disc ratio, others focused more on IOP, and in several cases, additional clinical information increased rather than reduced uncertainty. This variation reflects the influence of personal experience and interpretative bias, especially in borderline cases.

Such inconsistency highlights the need for more objective, standardised diagnostic tools. AI addresses this challenge by analysing large-scale imaging datasets to uncover subtle patterns invisible to the human eye. In addition to established markers like RNFL thickness, vascular biomarkers derived from OCTA—such as reduced vessel density—have shown promise for detecting early glaucomatous damage, even when structural metrics appear normal.

However, clinical implementation of vascular biomarkers is still evolving. Differences in image quality, device-specific variability, and limited understanding of how vascular loss relates to disease progression present ongoing challenges. AI-based multimodal models that integrate structural, vascular, and functional data offer a path forward—delivering more individualised and reproducible glaucoma risk assessments.

Having demonstrated the limitations of human interpretation, our work pivots to AI as a scalable, objective tool for diagnostic standardisation and early risk prediction in glaucoma.

## 3.6 Publication II – Glau-OCTA CNN with Intermediate Fusion

# Deep convolutional neural network prediction for glaucoma detection using OCT and OCTA disc- and macula- centred images and their combined power.

## *Gouverneur F, Pourjavan S et Macq B.*

Integrating deep learning in ophthalmology has led to significant advancements in AI-driven glaucoma detection, mainly through the use of CNNs for image-based classification. Our study introduces an optimised deep learning pipeline for glaucoma detection by leveraging multimodal imaging, combining OCT and OCTA data.

Initial tests by the author with late fusion architectures showed suboptimal diagnostic performance, likely due to the model's inability to capture synergistic interactions between structural and vascular features when they are merged only at the classification layer. Based on these findings and prior literature, the team opted for intermediate fusion. This architecture enables the model to learn cross-modal relationships during feature extraction, resulting in more robust representations and enhanced diagnostic accuracy. It merges disc- and macula-centred OCT and OCTA inputs in a shared encoding stream before branching into modality-specific refinements, offering a flexible yet integrated learning strategy [12,13].

Unlike conventional AI models that rely on a single imaging modality, this study explores the synergistic potential of structural (OCT) and vascular (OCTA) biomarkers to improve diagnostic accuracy. We employed a multi-input CNN framework, termed Glau-OCTA, which processes disc- and macula-centred scans to enhance the early detection of glaucomatous changes. The model architecture follows a hierarchical approach:

- Convolutional Layers: Extract low to high-level image features, identifying structural (RNFL thinning) and vascular (capillary dropout) changes.
- Pooling Layers: Perform dimensionality reduction while preserving critical spatial information.
- Fully Connected Layers: Aggregate extracted features and execute final classification (glaucoma vs. non-glaucoma).

### 3.6.1 Model Architecture and Training Strategy

This study presents a convolutional neural network (CNN) model designed to classify glaucoma from multimodal imaging (OCT and OCTA), based on macula and disc-centred scans. The model integrates structural and vascular information, aiming to support early detection.

Key training elements and contributions include:

- Model design and fusion strategy
    - A multi-input CNN was used to process each scan separately before fusing extracted features at an intermediate level.
    - Intermediate fusion was preferred over early and late fusion, based on internal comparisons, due to its ability to preserve modality-specific information while enabling joint learning.
    - The final classification was based on fully connected layers aggregating these multimodal features.
- Training optimisation
    - The model was trained using the Adam optimiser with a learning rate of 0.001.
    - Training was conducted over 50 epochs with a batch size of 16.
    - Transfer learning was applied using pre-trained CNN backbones to stabilise training and improve generalisation.
    - Data augmentation (e.g. flipping, rotation, contrast variation) addressed class imbalance, particularly the under-representation of early glaucoma.
- Diagnostic focus
    - The model was tested on a dataset of macula- and disc-centred OCT and OCTA scans.
    - The aim was to support the detection of early-stage disease, where biomarkers are often subtle.
    - Diagnostic performance was evaluated using 5-fold cross-validation and bootstrapping.
    - External validation and statistical comparison between fusion types were not included in this first phase and are planned for future work.

This multimodal approach reflects an effort to combine the strengths of structural and vascular imaging, while remaining cautious about interpretability and generalisation beyond the original dataset. The following section presents the results of this CNN framework as published in the second article of this thesis.

### 3.6.2 Limitations and Post-Publication Reflections

While Publication II highlighted the feasibility and potential of intermediate fusion in a multimodal CNN framework for glaucoma detection, several limitations remain. The model was trained on a single-centre dataset with an imbalanced age and gender distribution, which limited its generalisability despite the use of stratified 5-fold cross-validation, bootstrapping, and subject-level grouping to minimise data leakage.

The inclusion of moderate to advanced glaucoma cases (with MD values up to –20 dB) may have favoured OCTA-based detection due to more evident vascular dropout, potentially influencing the model's apparent reliance on OCTA features. As such, conclusions regarding the contribution of modality should be interpreted cautiously.

Fusion strategies were compared internally, with late fusion yielding suboptimal results. However, no formal statistical tests (e.g., DeLong's, McNemar's) or metrics like F1-score were included to quantify these differences. External validation and further comparative analyses are planned to support the broader applicability of this approach.

All our publications in peer-reviewed journals have been accepted after careful evaluation, and there were no comments regarding the content and data of our submitted manuscripts, which were accepted for publication.

# DEEP CONVOLUTIONAL NEURAL NETWORK PREDICTION FOR GLAUCOMA DETECTION USING OCT AND OCT-ANGIOGRAPHY DISC- AND MACULA-CENTERED IMAGES AND THEIR COMBINED POWER

*Gouverneur François*[a], *Pourjavan Sayeh*[b], *Macq Benoit*[a]

[a]ICTEAM, UCLouvain, Belgium
[b]Cliniques Universitaires Saint-Luc, Bruxelles, Belgium

## ABSTRACT

This study evaluates the effectiveness of deep convolutional neural networks (CNN) in glaucoma detection based on a multimodal approach using Optical Coherence Tomography (OCT) and OCT Angiography (OCTA) images centered on the disc and macula regions. The research focuses on binary classification for glaucoma diagnosis. The study introduces a novel intermediate fusion architecture, named GlauOCTA, which enables the modeling of interactions between features of different modalities while offering adaptability to varying numbers of input images. The results demonstrate that the combination of disc- and macula-centered images from both the OCT and OCTA technologies consistently outperforms individual region images. Specifically, when considering only the disc or macula, OCT+OCTA yields the best accuracy and area under the curve (AUC). However, when both the disc and macula images are available, OCTA alone provides the most accurate results. These findings provide valuable insights for enhancing diagnostic precision in glaucoma classification and have potential implications for improving glaucoma detection in clinical practice.

***Index Terms***— OCT, OCTA, glaucoma, deep learning, GlauOCTA

## 1. INTRODUCTION

Glaucoma, a degenerative neuro-ophthalmic disease, poses a significant global health challenge due to its progressive nature, characterized by the gradual loss of retinal ganglion cells. Glaucoma results in the deterioration of the visual field (VF) and, ultimately, irreversible blindness [1]. The gravity of the situation is underscored by the fact that glaucoma ranks as the second leading cause of blindness worldwide, with projections estimating its impact on approximately 110 million individuals by the year 2040 [2]. Alarmingly, a significant proportion of affected individuals, particularly in Asia and Africa, remain unaware of their condition due to the subtle nature of its symptoms [2]. The diagnostic landscape of glaucoma is further complicated by anatomical differences among individuals, leading to both intra- and inter-observer variations in diagnosis [3]. Identifying glaucoma at an early stage is crucial, as the disease can be effectively managed if detected promptly. However, the challenge lies in the fact that, glaucoma presents itself with ambiguous symptoms, making accurate and timely diagnosis difficult.

One of the primary risk factors for glaucoma is elevated intraocular pressure (IOP), with advancing age being the second most significant factor [4]. As IOP is a treatable risk factor, its monitoring and management are critical in preventing the progression of glaucoma. Early detection of glaucoma becomes imperative, as studies have demonstrated that early intervention significantly reduces the rate of disease progression [5].

Addressing the diagnostic challenges in glaucoma, the application of Deep Learning (DL) offers promising avenues for more accurate and timely diagnoses. DL, especially Convolutional Neural Networks (CNN), has already demonstrated considerable efficiency in various medical imaging domains [6] [7].

CNNs, known for their effectiveness as image classifiers, have the capability to automatically capture essential image features relevant to glaucoma diagnosis [8]. The utilization of non-clinical features correlated with vascular mechanisms in the pathogenesis of glaucoma during CNN training further enhances their potential as efficient glaucoma detectors.

In the context of anatomical eye structure imaging, three prominent methods stand out: Fundus, Optical Coherence Tomography (OCT), and OCT Angiography (OCTA), each providing distinct information about the eyes. Fundus photography (FP) offers a comprehensive view of retinal and optic nerve conditions, but its limitation lies in its two-dimensional nature, lacking depth assessment and featuring low-resolution images. Moreover the images are interpreted in a subjective and qualitative manner [9]. OCT, on the other hand, provides structural images showing the distinct layers of the retina, aiding in diagnosis through thickness mapping [10]. In OCT en-face images, the reflectance intensity reveals the retinal nerve fiber thickness (RNFL), and this reflectance is positively linked to RNFL thickness. Additionally, subtle ar-

979-8-3503-4939-9/24/$31.00 ©2024 IEEE 

In OCT en-face images, the reflectance intensity reveals the retinal nerve fiber thickness (RNFL), and this reflectance is positively linked to RNFL thickness. Additionally, subtle arcuate RNFL defects, often unnoticed in FP, can be detected. OCTA produces vascular images by capturing the movement of red blood cells, featuring parameters like vessel density (VD), foveal avascular zone (FAZ) size, and microvascular drop-out for glaucoma detection [11]. Our main investigation is to identify when glaucoma-related changes, structural and vascular, occur and to determine whether OCT, OCTA or their combination is more effective to predict these changes. This helps us to understand when these changes happen in glaucoma and which imaging method is more effective for early detection.

These imaging modalities offer visualizations of two distinct regions of interest (ROI): the disc and macula, as illustrated respectively on the left and right sides of Figure 1. Additionally, these images can represent various layers of the eye, such as the superficial, choroidal, deep layers, among others.

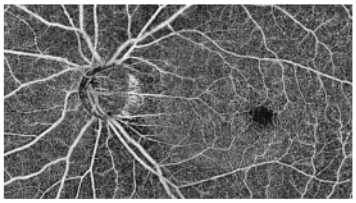

**Fig. 1**. OCTA en-face image of disc (left) and macula (right), superficial layer, from a left eye of a glaucoma patient

### 1.2. Related Works

In the context of OCT data, RNFL around the optic nerve head (ONH) has long been a key focus for glaucoma detection, known for its accuracy [12]. However, the diagnostic challenges of RNFL for advanced glaucoma, as emphasized by Bowd et al. [13] prompt the exploration of alternative approaches. In previous studies, OCT parameters have been pivotal in constructing classification models for glaucoma. Specifically, [14] and [15] utilized OCT parameters to develop models distinguishing between glaucoma and non-glaucoma cases while [16] employed these parameters to stratify subjects into categories of early and suspected glaucoma. Certain studies employ deep learning models on 2D images, as demonstrated by [17] and [18]. Conversely, other researchers apply these models to OCT volumetric 3D scans, as evidenced by works such as [19] and [20]. Additionally, tailored CNNs for myopic macular eyes have been developed to enhance diagnostic accuracy [21]. Notably, a model integrating both OCT parameters and images, focused on either the disc or the macula region, has demonstrated remarkable efficacy in early glaucoma detection, even preceding visual field loss [22]. This diverse array of approaches underscores the ongoing efforts to optimize glaucoma classification using OCT data.

In the realm of retinal disease detection, OCTA images have proven valuable. Nagasato et al. [23] achieved a remarkable AUC of 0.98 using VGG16 and SVM for non-perfusion area detection in retinal vein occlusion, while Le et al. [24] applied VGG16 to diagnose diabetic retinopathy, yielding AUCs of 0.97–0.98. Similarly, Heisler et al. [25] utilized an ensemble method on FAZ area for diabetic retinopathy, with VGG19 showing the best performance (AUC=0.91). Despite these advancements, OCTA images' application in glaucoma detection is in the proof-of-concept stage [26], hindered by small datasets, lack of standardized data pre-processing, and the absence of standardized results interpretation over the last decade. In contrast, GlauNet, a convolutional neural network tailored for glaucoma diagnosis using OCTA images from the disc and macula regions, demonstrated robust performance with an AUC of 0.89 [27]. Notably, it maintained high sensitivity (82.4%) and specificity (80.3%) even when tested on poor-quality images, indicating its potential for reliable glaucoma detection. Furthermore, a comparative study examined $3\times3mm^2$ and $6\times6mm^2$ macula OCTA scans for glaucoma classification, revealing superior performance in distinguishing healthy from mild glaucoma for the $6\times6mm^2$ scan's outer area (AUC=0.79) [28].

Regarding the comparison between OCT and OCTA, Rao et al. [29] highlighted that OCTA parameters, especially those related to vessel density (VD), exhibit a stronger correlation with visual field loss than retinal nerve fiber layer (RNFL) thickness in advanced glaucoma. In a comprehensive study, Bowd et al. [30] contrasted the effectiveness of a VGG16 CNN analyzing OCTA images (of $4.5x4.5mm^2$ size) with a gradient boosting classifier (GBC) model using separate OCT and OCTA parameters for glaucoma classification. Notably, the VGG16 model, focusing on en-face vessel density images, surpassed GBC models individually trained on distinct OCTA and OCT measurements, emphasizing its superiority in leveraging OCTA imaging for glaucoma diagnosis. In another study [31], a GBC assessed the combination of OCT (RNFL thickness) and OCTA (vessel density) parameters for glaucoma detection. Outperforming standard parameters, the Full GBC, which combined all measures, achieved the highest diagnostic accuracy (AUC=0.93). This suggests that combining OCT and OCTA images in a deep learning model could enhance glaucoma prediction.

Given the diverse information in OCT and OCTA images, their combination demands caution. This is approached through three distinct modalities: early fusion, intermediate fusion, and late fusion. Early fusion combines modalities at the input level, intermediate fusion integrates information in intermediate layers, and late fusion merges modalities at the final layers, influencing how the network processes multi-

modal data. In the medical imaging domain, fusion techniques have been applied in various scenarios. For instance, early fusion has been employed in glaucoma classification using disc images [32]. Intermediate fusion has found application in predicting Alzheimer's disease [33], while late fusion has been utilized for the diagnosis of prostate cancer [34].

Lee et al. [35], in their study, compared CNN models using macula-centered OCT and OCTA images from highly myopic patients. The ImageNet-based assessment across different layers revealed an AUC of 0.946 with OCTA superficial layers, comparable to OCT GCL+ (ganglion cell layer + inner plexiform layer) at 0.982. Both models significantly outperformed OCTA deep layer images (AUC = 0.779). This suggests that using a CNN based on OCTA images from the superficial layer is a more effective diagnostic strategy than using those from the deep layer. A similar conclusion can be drawn from the study by Schottenhamml et al. [36], where a CNN based on 3x3mm$^2$ images from different layers was compared.

To summarize this section, CNNs are increasingly used to predict diseases by processing images. Their ability to identify non-clinical details has shown impressive results in AUC performance. Importantly, combining OCT and OCTA parameters improves predictive outcomes compared to using them separately, suggesting a potential application of a similar approach for images. The choice of fusion strategy of the different modalities depends on the nature of them. Notably, CNNs applied to 6x6mm$^2$ images from the superficial layer offer a powerful diagnostic strategy.

### 1.3. Contribution

This study investigates the efficacy of DL models applied to OCT and OCTA images centered on disc and on macula regions. The primary focus is on binary classification for glaucoma diagnosis, glaucoma/healthy, aiming to identify the most accurate image combination for predicting glaucoma. This research provides essential insights to assist ophthalmologists in patient detection and treatment decisions. By evaluating the performance of the various image combinations, using an intermediate CNN fusion approach, our study contributes to enhancing diagnostic precision in the context of binary glaucoma classification.

## 2. METHODOLOGY

### 2.1. Study setting and population

In this retrospective cross-sectional study, approved by the Institutional Ethical Commission of the *Cliniques Universitaires Saint-Luc* in Brussels, subjects were exclusively recruited from the same institution. The study included individuals aged 18 and above, who had consultations between January 1, 2020, and December 31, 2023, during which disc- and macula-centered OCT and OCTA images were captured. Initially, 157 subjects were selected, contributing to a total of 1106 eye scans. Exclusion criteria involved poor scan quality, Quality Index (QI) $< 6$ and/or Signal Strength Index (SSI) $< 48$, and scans with more than 10% outlier parameter values. The ground truth for scans was determined by a specialized glaucoma ophthalmologist. Detailed demographic information for the final dataset of 96 subjects is available in Table 1. It is crucial to emphasize that a single subject may have multiple eye scans obtained at various time points. Consequently, the count of eyes exceeds twice the total number of subjects in our dataset.

### 2.2. Data acquisition and image pre-processing

En-face images were collected using the Solix machine (V1.1.100.20 FullRang AngioVue Expert 8/2020). These images, obtained through OCT and OCTA technology, focused on both the disc and macula regions, with the downloaded layer being the superficial one. This choice was motivated by its superior diagnostic efficacy, as highlighted in studies by Lee et al. [35] and Schottenhamml et al. [36]. The collected images were in a 6x6mm$^2$ format for disc-centered and 6.4x6.4mm$^2$ for macula-centered scans, with a resolution of 512x512 pixels in black and white color. For computational efficiency, the images were resized to 128x128 pixels and normalized from a range of $0 - 255$ to $0 - 1$. Furthermore, the dataset was stratified into a 5-fold classification, with 190 eyes allocated for training and 48 eyes for testing.

### 2.3. GlauOCTA's intermediate fusion architecture

This paper introduces a novel intermediate CNN fusion architecture for glaucoma detection from OCT and OCTA images, namely GlauOCTA architecture (illustrated in Figure 2). The selection of an intermediate fusion approach arises from the varied image modalities and the flexible combination possibilities inherent in the study [37]. This architecture is designed to model interactions between features of different modalities, allowing, for instance, the consideration of a vessel on the left edge of a disc-centered image present on the right side of a macula-centered image (for a left eye), which is not possible with late fusion. Unlike early fusion, our approach accommodates predictions even when not all modalities are present, providing adaptability to diverse scenarios where a combination of one to four images may be available.

| | Glaucoma | Healthy | Total |
|---|---|---|---|
| Number of subjects | 45 | 51 | 96 |
| Number of eyes | 135 | 103 | 238 |
| Age (y); mean (SD) | 64.76 (11.63) | 48.02 (17.75) | 55.87 (17.29) |
| Gender; women/men (%) | 47.7/52.3 | 72.6/27.4 | 61.1/38.9 |
| RNFLT ($\mu$m); mean (SD) | 67.95 (15.47) | 93.22 (9.73) | 81.38 (17.93) |
| VF MD (dB); mean (SD) | -6.24 (7.57) | -0.32 (1.46) | -4.08 (6.72) |

**Table 1**. Final subjects and eyes characteristics of our study

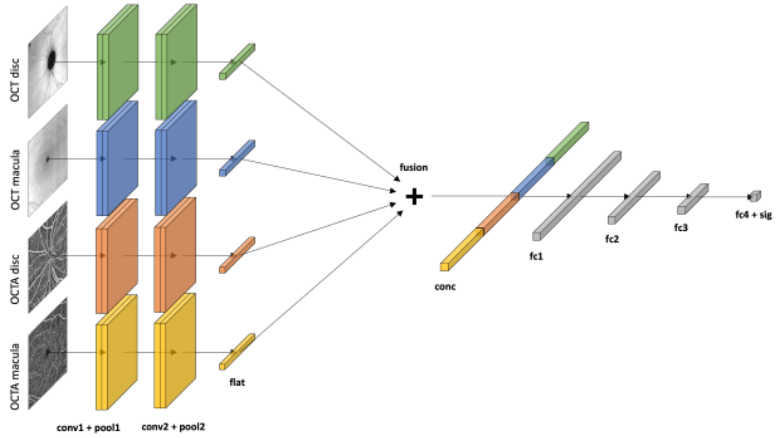


**Fig. 2**. GlauOCTA's intermediate fusion CNN architecture for glaucoma detection with four image types as input

The architecture comprises two convolutional + pooling layers and one flatten layer for each image type (OCT disc, OCTA disc, OCT macula, and OCTA macula). Specifically, the first convolutional + pooling layer (conv1 & pool1) processes 128x128x1-size input images. Subsequently, the second convolutional + pooling layer (conv2 & pool2) operates on a 64x64x4-size input. The flatten layer (flat) generates an output size of 16,384. Concatenating these flattened vectors for each image type (conc) yields an output size equal to the product of the size of flat vector and the number of image types. Following this, four fully connected layers (fc1 to fc4) and a sigmoïd function (sig) are applied, culminating in a binary output that classifies the eye as either healthy or affected by glaucoma.

The goal is to compare different combinations of image types, leading to variable concatenated vector dimensions depending on the number of input images. In contrast, the fully connected network (fc1 to fc4) maintains a constant structure irrespective of the quantity of distinct input images.

## 3. RESULTS AND DISCUSSION

### 3.1. Experimental Setup

Our proposed GlauOCTA model was implemented using the PyTorch framework with the Adam optimizer. The learning rate was set to 0.001, and the training process involved 50 epochs with a batch size of 16. Stratified 5-fold cross-validation was employed to split eye images into training and testing sets. To ensure robustness, 20 runs of 5-fold cross-validation were conducted. Notably, for a specific run, the same folds were consistently used across all image combinations, facilitating meaningful comparisons.

Currently, there is a lack of consensus regarding the optimal region of interest (ROI), either the disc or macula, for effective glaucoma detection. Researchers vary in their choices of ROI and layer of interest. Given our objective to identify the optimal combination, we will systematically compare the disc and macula regions, as well as their combinations. We conducted a comparison involving nine distinct combinations of image types. Four configurations included single inputs: OCT disc, OCT macula, OCTA disc, and OCTA macula. Another set of four configurations combined two inputs: OCT disc + macula, OCTA disc + macula, OCT + OCTA disc, and OCT + OCTA macula. The final configuration encompassed all four inputs: OCT + OCTA disc + macula and is represented on Figure 2. Evaluation metrics comprised accuracy (ACC), area under the ROC curve (AUC), sensitivity (SE), and specificity (SP).

To compute metrics for each method, the bootstrap method was employed. Specifically, for a given combination, in each of the 20 runs, each subject was included exactly once in the test fold, and their prediction (a continuous value between 0 and 1) was recorded. The mean of these 20 predictions was then assigned as the average prediction for a patient. Subsequently, the sample was resampled 1000 times (with replacement), and the four metrics were calculated along with a 95% confidence interval. This method is advantageous as it obviates dependencies on assumptions regarding population distribution or parameters; it exhibits robustness against

outliers and skewed data, surpassing parametric methods [1]. Moreover, it demonstrates efficacy with small sample sizes, as is the case in our study.

### 3.2. Results

The achieved accuracy ranged from 82.35% to 92.44%, AUC values between 91.40% and 96.94%, sensitivity ranged from 83.74% to 94.71%, and specificity from 77.7% to 89.34%. The detailed results, including the 95% confidence intervals obtained through bootstrap resampling, are presented in Table 2.

Regarding the comparison between disc and macula images, for OCT images, disc+macula outperformed disc and macula alone in three of the four metrics (all except specificity). For OCTA images, disc+macula surpassed disc which itself outperforms macula in all metrics. In the case of OCT+OCTA images, disc+macula consistently outperformed both macula and disc alone across all metrics. Moreover, macula surpassed disc in all the evaluated metrics.

In the comparison between OCT and OCTA, for disc images, OCTA exhibited superior performance in accuracy, sensitivity, and specificity compared to OCT+OCTA and OCT alone, while AUC was higher for OCT+OCTA than the two others. In macula images, OCT+OCTA outperformed OCTA alone which itself surpassed OCT alone in all metrics except specificity, where OCT surpassed OCT+OCTA and OCTA. For combined disc+macula images, OCTA outperformed both OCT+OCTA and OCT across all metrics, the same conclusion can be drawn for OCT+OCTA who surpassed OCT alone for all metrics.

Overall, the combination of OCTA disc+macula images exhibited the best performance across all metrics, followed by the complete combination of OCT+OCTA disc+macula.

### 3.3. Discussion

In our comprehensive evaluation of nine image combinations, the cumulative evidence consistently supports the superior performance of combined disc and macula images (disc+macula) across all metrics, with only a minor exception in the specificity of OCT macula, which is marginally (<0.1%) better than that of OCT disc+macula. This finding emphasizes the significance of considering both disc and macula regions for effective glaucoma detection, as Manassakorn et al. did in their paper [27], which combined disc and macula images.

Furthermore, focusing on the AUC, OCTA emerges as the most effective modality for disc+macula, while OCT+OCTA demonstrates superior performance when evaluating disc and macula individually. The best average AUC for each of the regions, disc, macula and disc+macula, are represented on Figure 3.

[1] https://fastercapital.com/keyword/bootstrap-method.html

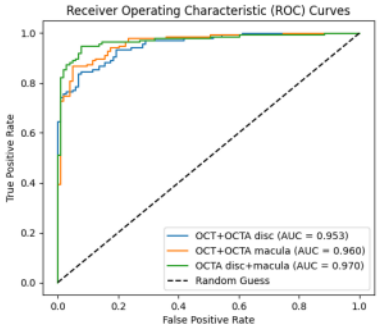


**Fig. 3**. Best average AUC scores for each of the region, disc in blue, macula in orange, disc+macula in green

As modern machines increasingly integrate OCT and OCTA modalities, acquiring both types of images for the same eye has become more common. However, obtaining disc- and macula-centered images for the same patient remains less systematic. Our study provides valuable insights, suggesting that when only one image from either region is available, relying on the combination of OCT and OCTA images is preferable (in terms of AUC). Conversely, when both regions are present, prioritizing solely OCTA images as model inputs is recommended. For now, most current research practices in OCT and OCTA imaging involve selecting either the disc or macula region [21] [35].

## 4. CONCLUSION

GlauOCTA's intermediate fusion architecture facilitates the comparison of various image types used in glaucoma detection, including OCT disc, OCT macula, OCTA disc, and OCTA macula. The combination of disc and macula regions proves crucial for effective glaucoma detection. Utilizing OCTA images alone, compared to OCT or OCT+OCTA, yields superior results, particularly when considering both disc and macula regions.

Given the scarcity of confirmed glaucoma specialists, this study sheds light on critical images for glaucoma detection, with potential future implications for equipping OCT/OCTA machines with deep learning software to aid non-subspecialist ophthalmologists in diagnosis. Model performance can be enhanced through parameter fine-tuning, increased diversity incorporation (ethnicity, severity, etc.), and inclusion of scans quantitative parameters.

| | OCT | | | OCTA | | | OCT + OCTA | | |
|---|---|---|---|---|---|---|---|---|---|
| | Disc | Macula | Disc + Macula | Disc | Macula | Disc + Macula | Disc | Macula | Disc + Macula |
| ACC | 0.8235 | 0.8445 | *0.8782* | 0.8950 | 0.8697 | **0.9244** | 0.8697 | 0.8866 | *0.8992* |
| (95% CI) | (0.774 - 0.873) | (0.797 - 0.892) | (0.836 - 0.920) | (0.857 - 0.933) | (0.827 - 0.912) | (0.89 - 0.958) | (0.829 - 0.91) | (0.846 - 0.927) | (0.861 - 0.937) |
| AUC | 0.9140 | 0.9262 | *0.9549* | 0.9501 | 0.9380 | **0.9694** | 0.9534 | 0.9604 | *0.9692* |
| (95% CI) | (0.878 - 0.950) | (0.895 - 0.957) | (0.932 - 0.978) | (0.923 - 0.977) | (0.906 - 0.97) | (0.948 - 0.99) | (0.931 - 0.976) | (0.938 - 0.983) | (0.951 - 0.988) |
| SE | 0.8584 | 0.8374 | *0.8966* | 0.9329 | 0.9112 | **0.9471** | 0.9184 | *0.9261* | *0.9261* |
| (95% CI) | (0.801, 0.916) | (0.775, 0.899) | (0.844, 0.949) | (0.892, 0.974) | (0.863, 0.959) | (0.91, 0.984) | (0.874, 0.963) | (0.882, 0.971) | (0.883, 0.97) |
| SP | 0.777 | *0.8552* | 0.8546 | 0.8446 | 0.8166 | **0.8934** | 0.8057 | 0.8377 | *0.8651* |
| (95% CI) | (0.701, 0.853) | (0.788, 0.922) | (0.785, 0.924) | (0.775, 0.915) | (0.74, 0.893) | (0.835, 0.952) | (0.73, 0.882) | (0.768, 0.907) | (0.801, 0.93) |

**Table 2**. Nine models average bootstrap metrics and 95% confidence interval. Best metric for each subcategory, OCT, OCTA and OCT+OCTA, are in italics while best model among all is in bold

## 5. REFERENCES


[1] Harry A. Quigley and Aimee Teo Broman, "The number of people with glaucoma worldwide in 2010 and 2020," *British Journal of Ophthalmology*, vol. 90, pp. 262 – 267, 2006.

[2] Yih-Chung Tham, Xiang Li, T-Y Wong, Harry Quigley, Tin Aung, and Ching-yu Cheng, "Global prevalence of glaucoma and projections of glaucoma burden through 2040 a systematic review and meta-analysis," *Ophthalmology*, vol. 121, 06 2014.

[3] Henry Jampel, David Friedman, Harry Quigley, Susan Vitale, Rhonda Miller, Frederick Knezevich, and Yulan Ding, "Agreement among glaucoma specialists in assessing progressive disc changes from photographs in open-angle glaucoma patients," *American journal of ophthalmology*, vol. 147, pp. 39–44.e1, 10 2008.

[4] Bruce E Prum, Lisa F Rosenberg, Steven J Gedde, Steven L Mansberger, Joshua D Stein, Sayoko E Moroi, Leon W Herndon, Michele C Lim, and Ruth D Williams, "Primary open-angle glaucoma preferred practice pattern® guidelines," *Ophthalmology*, vol. 123, no. 1, pp. P41–P111, 2016.

[5] Anders Heijl, M Cristina Leske, Bo Bengtsson, Leslie Hyman, Boel Bengtsson, Mohamed Hussein, Early Manifest Glaucoma Trial Group, et al., "Reduction of intraocular pressure and glaucoma progression: results from the early manifest glaucoma trial," *Archives of ophthalmology*, vol. 120, no. 10, pp. 1268–1279, 2002.

[6] Huanhuan Zhang and Yufei Qie, "Applying deep learning to medical imaging: A review," *Applied Sciences*, vol. 13, no. 18, pp. 10521, 2023.

[7] Heang-Ping Chan, Ravi K Samala, Lubomir M Hadjiiski, and Chuan Zhou, "Deep learning in medical image analysis," *Deep Learning in Medical Image Analysis: Challenges and Applications*, pp. 3–21, 2020.

[8] Shafeeq Ahmed Haja and Vidyadevi Mahadevappa, "Advancing glaucoma detection with convolutional neural networks: a paradigm shift in ophthalmology," *Romanian Journal of Ophthalmology*, vol. 67, no. 3, pp. 222, 2023.

[9] Abegaile Bartolome Lim, Ji-Hye Park, Jae Hoon Jung, Chungkwon Yoo, and Yong Yeon Kim, "Characteristics of diffuse retinal nerve fiber layer defects in red-free photographs as observed in optical coherence tomography en face images," *BMC ophthalmology*, vol. 20, pp. 1–7, 2020.

[10] Marco Zeppieri, Stefania Marsili, Ehimare Samuel Enaholo, Ayishetu Oshoke Shuaibu, Ngozi Uwagboe, Carlo Salati, Leopoldo Spadea, and Mutali Musa, "Optical coherence tomography (oct): A brief look at the uses and technological evolution of ophthalmology," *Medicina*, vol. 59, no. 12, pp. 2114, 2023.

[11] Richard F. Spaide, James G. Fujimoto, Nadia K. Waheed, Srinivas R. Sadda, and Giovanni Staurenghi, "Optical coherence tomography angiography," *Progress in Retinal and Eye Research*, vol. 64, pp. 1–55, 2018.

[12] P Sathyan, Shilpa Shilpa, and Anitha Anitha, "Optical coherence tomography in glaucoma," *Journal of Current Glaucoma Practice*, vol. 6, no. 1, pp. 1, 2012.

[13] Christopher Bowd, Linda M Zangwill, Robert N Weinreb, Felipe A Medeiros, and Akram Belghith, "Estimating optical coherence tomography structural measurement floors to improve detection of progression in advanced glaucoma," *American journal of ophthalmology*, vol. 175, pp. 37–44, 2017.

[14] Ryo Asaoka, Hiroshi Murata, Kazunori Hirasawa, Yuri Fujino, Masato Matsuura, Atsuya Miki, Takashi Kanamoto, Yoko Ikeda, Kazuhiko Mori, Aiko Iwase, et al., "Using deep learning and transfer learning to accurately diagnose early-onset glaucoma from macular optical coherence tomography images," *American journal of ophthalmology*, vol. 198, pp. 136–145, 2019.

[15] Jinho Lee, Young Kook Kim, Ki Ho Park, and Jin Wook Jeoung, "Diagnosing glaucoma with spectral-domain optical coherence tomography using deep learning classifier," *Journal of glaucoma*, vol. 29, no. 4, pp. 287–294, 2020.

[16] Hassan Muhammad, Thomas J Fuchs, Nicole De Cuir, Carlos G De Moraes, Dana M Blumberg, Jeffrey M Liebmann, Robert Ritch, and Donald C Hood, "Hybrid deep learning on single wide-field optical coherence tomography scans accurately classifies glaucoma suspects," *Journal of glaucoma*, vol. 26, no. 12, pp. 1086, 2017.

[17] Atalie C Thompson, Alessandro A Jammal, Samuel I Berchuck, Eduardo B Mariottoni, and Felipe A Medeiros, "Assessment of a segmentation-free deep learning algorithm for diagnosing glaucoma from optical coherence tomography scans," *JAMA ophthalmology*, vol. 138, no. 4, pp. 333–339, 2020.

[18] Xi Wang, Hao Chen, An-Ran Ran, Luyang Luo, Poemen P Chan, Clement C Tham, Robert T Chang, Suria S Mannil, Carol Y Cheung, and Pheng-Ann Heng, "Towards multi-center glaucoma oct image screening with semi-supervised

**Clinical takeaway**

*This study highlights the potential of intermediate fusion in deep learning. Instead of combining predictions at the decision level (late fusion), the model integrates OCTA macula and disc features at an earlier stage, enabling the learning of richer interactions across regions. While other fusion strategies were not statistically compared, this design improved binary glaucoma classification within this dataset and laid the conceptual foundation for the later multimodal GlauOCTA-AI model.*

## 3.7 Beyond Numerical Metrics: Deep Learning-Driven Insights from OCTA in Glaucoma.

Our second study demonstrated the potential of deep CNNs in integrating multimodal imaging for glaucoma detection, emphasising the benefits of leveraging both structural (OCT) and vascular (OCTA) information. The study aimed to improve classification accuracy across varying disease severities by incorporating optimised deep learning pipelines. However, the practical application of these findings necessitates further validation in larger, heterogeneous populations. The challenges in distinguishing early glaucoma from healthy eyes also underline the need for refined AI models to handle ambiguous cases better.

Notably, our study demonstrated that deep learning-augmented OCTA analysis outperformed deep learning-enhanced structural OCT metrics in glaucoma classification. Rather than relying solely on numerical vascular density values, the CNN model extracted complex vascular features with superior diagnostic performance. This suggests that AI-driven analysis of vascular architecture, rather than structural metrics alone, may offer a more sensitive and nuanced approach to detecting glaucomatous changes.

While our previous study demonstrated the power of deep learning for structural and vascular analysis, this next study focuses on clinical applicability and validation in real-world settings.

## 3.8 Publication III. Towards Clinical Implementation: AI-Driven OCT and OCTA Analysis in Glaucoma.

### Advanced analysis of OCT/OCTA images for accurately differentiating between glaucoma and healthy eyes using deep learning techniques.

### *Pourjavan S, Gouverneur F, Macq B et al.*

Building on the foundation of AI-driven multimodal imaging analysis, our third study investigates the diagnostic performance of deep learning models applied to OCT and OCTA images to distinguish glaucoma from healthy eyes.

Unlike previous studies, which focused primarily on technical optimisations, this research adopts a clinically relevant perspective, assessing the efficacy of deep learning models in real-world patient cohorts. By incorporating en-face images of the superficial layers alongside peripapillary and macular vessel density measurements, the study seeks to determine the most effective image combination for glaucoma diagnosis.

Furthermore, it provides insights into how different image modalities contribute to AI-based classification accuracy, reinforcing the clinical value of multimodal integration.

Clinical Ophthalmology Dovepress

Open Access Full Text Article ORIGINAL RESEARCH

# Advanced Analysis of OCT/OCTA Images for Accurately Differentiating Between Glaucoma and Healthy Eyes Using Deep Learning Techniques

Sayeh Pourjavan[1], François Gouverneur[2], Benoit Macq[2], Thomas Van Drooghenbroeck[2], Patrick De Potter[1], Antonella Boschi[1], Adil El Maftouhi[3]

[1]Department of Ophthalmology, Cliniques Universitaires Saint Luc, UCL, Brussels, Belgium; [2]Institute for Information and Communication Technologies, Electronics, and Applied Mathematics (ICTEAM), Louvain School of Engineering, UCLouvain, Louvain-la-Neuve, Belgium; [3]Centre Ophtalmologique de RIVE, Geneve, Switzerland

Correspondence: Sayeh Pourjavan, Email Sayeh.pourjavan@saintluc.uclouvain.be



**Purpose:** To evaluate the discriminative power of optical coherence tomography (OCT) and optical coherence tomography angiography (OCTA) images, identifying the best image combination for differentiating glaucoma from healthy eyes using deep learning (DL) with a convolutional neural network (CNN).

**Methods:** This cross-sectional study included 157 subjects contributing 1,106 eye scans. We used en-face images of the superficial and choroid layers for OCTA-based vessel density and OCT-based structural thickness of the macula (M) and optic disc (D). Images were preprocessed, resized, and normalized for CNN analysis. The CNN architecture had two components: one extracted features for each image type (OCT-D, OCT-M, OCTA-D, OCTA-M), while the second combined these features to classify eyes as healthy or glaucomatous. Performance was measured by accuracy, sensitivity, specificity, and area under the curve (AUC).

**Results:** For OCT images, the D+M combination outperformed disc (D) or macula (M) alone in three of the four metrics. For OCTA images, D+M also performed better than D or M alone, with D+M outperforming disc (D) in all criteria. Across all metrics for combined OCT+OCTA images, D+M performed better than D or M alone, and the macula (M) outperformed the disc (D). In disc (D) imaging, OCTA outperformed both OCT and OCT+OCTA in accuracy, sensitivity, and specificity, while OCT+OCTA had a higher AUC. OCTA consistently outperformed OCT and OCT+OCTA across all metrics for combined D+M images.

**Conclusion:** The OCTA D+M combination performed best, followed by the OCT+OCTA D+M combination. When both en-face images are available, OCTA is preferred. Always include both disc and macula images for optimal diagnosis.

**Keywords:** glaucoma, OCTA, optic disc, macula, vessel density, deep learning, AI-Glau-OCTA, health expenditure

## Introduction

Glaucoma is a degenerative neuro-ophthalmic disease, characterized by progressive loss of retinal ganglion cells. It causes morphological changes in the optic nerve head and the deterioration of the visual field, which if untreated can ultimately lead to irreversible blindness. It is one of the leading causes of blindness worldwide.[1] Due to its subtle symptoms, 50% of patients do not know that they are affected by the disease.[2,3] Intraocular pressure (IOP), next to advancing age, is the most important and the only treatable risk factor.[4]

Individual anatomical differences in optic nerve head appearances, complicate the diagnosis of glaucoma, resulting in discrepancies in diagnosis between and within observers. Accurate and prompt diagnosis of glaucoma is challenging since the condition frequently exhibits equivocal symptoms in its early stages.[5,6]

It has been shown that early treatment can significantly reduce the progression of the disease,[7] allowing patients to maintain quality of life and social activities.[8,9] Early intervention also positively impacts economic health expenditure and decreases the cost of blindness.[10] Therefore, early diagnosis is a "golden tool".

Received: 4 April 2024
Accepted: 4 November 2024
Published: 26 November 2024

The diagnosis of glaucoma is based on examination of the optic disc, visual field, and IOP. Multiple factors, IOP & non-IOP related, can cause structure and functional changes in, contrast sensitivity, visual field, and visual acuity.[11] Therefore, tools that enable early diagnosis are essential in glaucoma treatment to prevent irreversible vision loss.

Fundus pictures, optical coherence tomography (OCT), and optical coherence tomography angiography (OCTA) are the three main imaging modalities commonly utilized to identify glaucoma with each of their characteristics. Although fundus photography provides a thorough understanding of retinal and optic nerve disorders, it is limited by its two-dimensionality, lack of depth perception, and low-resolution image quality. Additionally, the interpretation of the pictures is qualitative and subjective.[12]

OCT allows us to measure quantitatively the retina nerve fibre layer (RNFL) thickness on peripapillary and macular zones and to detect early loss of RNFL before the symptomatic visual field's loss.[13]

OCTA is a relatively new diagnostic tool that reflects the vascular density of the optic disc and macula, both of which are important in developing glaucoma. It also shows complete choriocapillaris loss in areas of localized peripapillary atrophy, the so-called deep microvascular dropout.[14]

While OCT provides high-resolution cross-sectional images for structural analysis, fundus imaging provides a complete view of the ocular's constituent parts. On the other hand, OCTA detects abnormal perfusion by displaying the vasculature in every layer of the optic disc and retina and the macula (Figure 1).

Several investigations have employed Deep Learning (DL), especially Convolutional Neural Networks (CNN), for analyses of OCT and OCTA readings to identify ocular illnesses such as retinal vein occlusion or diabetic retinopathy. However, although DL has already been used on OCT images to detect glaucoma, this is much rarer in the case of OCTA images.[15,16]

CNNs can automatically extract key image features that are pertinent to the diagnosis of glaucoma. CNNs are well-known for their efficacy as image classifiers. Their potential as effective glaucoma detectors are further enhanced by the use of non-clinical variables related to vascular pathways in glaucoma during CNN training.[17]

We aimed to develop and evaluate a CNN architecture for both OCT and OCTA, compare their diagnostic accuracy and secondly assess the value of CNN-derived combined OCT+OCTA images in diagnosing glaucoma.

## Participant

The Institutional Ethical Commission of the Cliniques Universitaires Saint-Luc in Brussels approved the study protocol. This research adheres to the principles outlined in the Declaration of Helsinki for studies involving human subjects. It

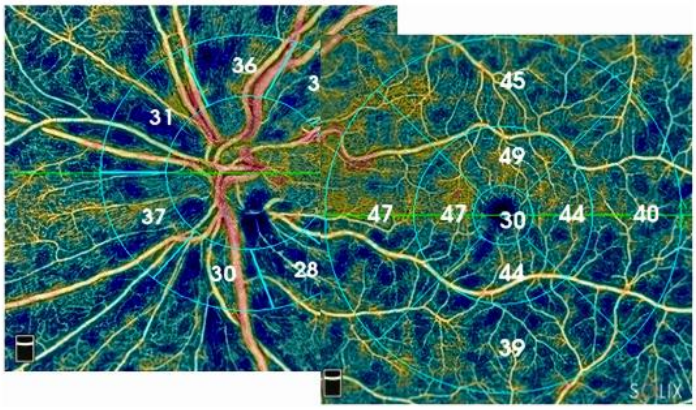


**Figure 1** OCTA imaging of the en-face superficial layer of a patient with glaucoma. Decreased vessel density on macular vulnerable zone stretching as an arciform defect inferiorly.

complies with all relevant national ethical guidelines, including the General Data Protection Regulation (GDPR) for data privacy and confidentiality within Europe. While HIPAA is specific to the United States, the GDPR ensures similar standards in the European context. Written informed consent was obtained from each participant before inclusion in the study.

All the participants were recruited from our clinic. An experienced glaucoma specialist (SP) determined the ground truth for glaucoma diagnosis.

Healthy subjects (non-glaucoma) had booked an appointment for an annual check-up or control of refractive error. They had a normal appearance of the optic disc on direct funduscopy with an intact neuroretinal rim and normal retina nerve fibre layer (RNFL) on OCT and an IOP $\leq$ 21 mmHg in both eyes. We did not perform standard visual field testing if it was not needed, for each healthy subject because of its inability to detect early glaucomatous damage, especially in the macula.[18]

All healthy subjects had a comprehensive ophthalmological examination, including auto-refractometry, BCVA, and tonometry. After obtaining their consent, we did an OCT/ OCTA examination in conjunction with our "standard of care". Thirteen residents of the Ophthalmology Department, five students, three secretaries, and one consultant took voluntary part in this study as well.

Glaucomatous participants were selected from our database of Glaucoma-OCTA study group, and from referred glaucomatous patients to one of the glaucoma consultants for surgery. They had an abnormal optic disc with thinning of the RNFL and the neuroretinal rim with or without visual field loss. The IOP levels were not considered as an inclusion criterion because most patients were already medically treated.

We did not exclude any participants with high refractive error if the quality of the images was acceptable.

## Methods

### OCTA and Acquisition of the Images

The AngioVue imaging system, Solix Optovue, Inc. in Fremont, CA, USA (Solix V1.1.100.20 FullRang AngioVue Expert 8/2020), was utilized to conduct OCTA and Spectral-domain OCT imaging of the nerve head (ONH) and macula. This system allows for the acquisition of OCTA and Spectral-domain OCT images from the same scans, ensuring precise alignment and automatic segmentation of the regions of interest being analyzed. AngioAnalytics™ OCT-A Metrics enables a non-invasive, dye-free OCT-based approach for visualization and quantification of retinal vasculature. It allows the 6.4 mm AngioVue® Retina scans to assess retinal vascular density, FAZ, flow area, non-flow area, and retinal layer thickness.

Additionally, it permits optic disc measurements for 6 mm AngioVue® disc scans as well as the determination of radial peripapillary capillary (RPC) density and RNFL thickness.

DualTrac™ Motion Correction Technology (MCT) with enhanced visualization combines real-time tracking and patented post-processing to enable true 3D motion correction. It uses the split-spectrum amplitude-decorrelation angiography (SSADA) algorithm to visualize the perfused retinal vasculature in high resolution in three dimensions at various user-defined layers of the retina, including the capillary level. This algorithm captures the dynamic motion of red blood cells from sequential cross-sectional B-scans. The percentage of the measured area filled by flowing blood vessels —defined as pixels with decorrelation values surpassing a predetermined threshold level—is automatically calculated by the AngioVue program. As such, the vessel density and thickness values that this software provides are from scans that have undergone accurate automatic registration.

The vessel density (VD) measurements are determined only with projection artefact removal (PAR) correction. PAR removes the shadow effect of the higher vascular beds in the visualization of deeper layers.

Comprehensive analysis combining structural and vascular pictures and data, including ONH, ganglion cell complex (GCC), focal loss of volume (FLV), global loss of volume (GLV), Bruch's membrane opening (BMO), and vessel density (VD) registration with Garway-Heath nerve fibre sectors, is provided by the Optovue Solix glaucoma package.

OCTA **macula** imaging 6.4×6.4 $mm^2$ was obtained, centred on the fovea, to ensure the examination of the eventual enlarged foveal avascular zone (FAZ) that can increase in diameter in glaucoma patients.[19]

The predefined en-face slabs used initially for this study were the superficial retinal capillary plexuses (en-face S) in a slab from the internal limiting membrane to the inner plexiform layer −10 µm and choroid slab (en-face C) extending from upper limit = BRM-10µm to lower limit = BRM+30µm. The whole image of 6.4×6.4 $mm^2$ of the macula was divided into 9 equal sectors grid and the vascular density was calculated by the machine (Figure 2).

The **disc** images were obtained from the optic disc cube area of 6×6 $mm^2$. The peripapillary region is defined by two rings of 2.5mm and 4.5mm centred on the disc centre and as determined by BMO fitted circle (Figure 3), divided into the middle, superior, and inferior hemi-sectors and 8 equal peripapillary sectors.

The radial peripapillary capillary (RPC) network was visualized with excellent detail as a distinctive pattern of parallel, long, uniform-diameter vessels around ONH, oriented parallel to the retinal nerve fibre layer.

The whole image of 6×6 $mm^2$ of disc scan was also divided into 9 equal sectors grid and the vascular density was calculated (Figure 4).

Based on the evidence of the publications of two groups, namely Lee et al[20] and Schottenhaml et al[21] we decided to use only the data of the en-face superficial layer for our CNN models.

In their work, Lee et al used OCTA and macula-centred OCT pictures from individuals with high myopia to compare CNN models. The evaluation of ImageNet over various layers with OCTA superficial layers had an AUC of 0.946, which was similar to OCT GCL+ IPL (ganglion cell layer + inner plexiform layer) at 0.982. With an AUC of 0.779, both models performed much better than OCTA deep-layer images. This implies that a more successful diagnostic approach

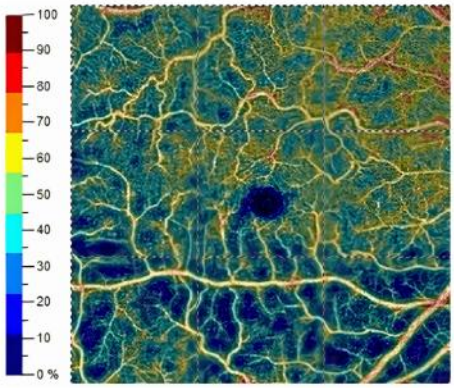


**Figure 2** Vessel density measurements in nine equally divided quadrants of the en-face superficial layer.

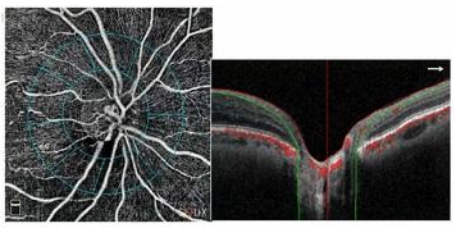

**Figure 3** Defining the peripapillary region by two rings of 2.5mm and 4.5mm centred on the disc centre and as determined by Bruch's membrane opening (BMO) fitted circle.

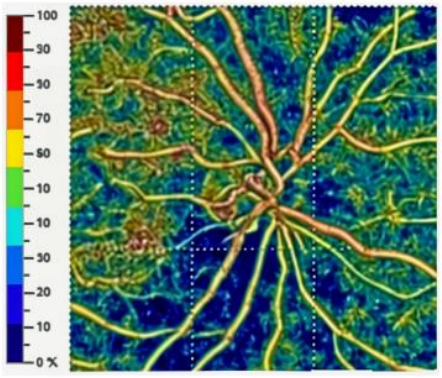


**Figure 4** Vessel density calculation in nine equal sectors grid on the en-face layer centred on the optic disc.

than using images from the deep layer is to use a CNN based on OCTA images from the superficial layer. The work by Schottenhamml et al, which contrasted a CNN based on 3×3 $mm^2$ images from various levels, comes to a similar conclusion.

All the scans with a quality score (SQ) lower than 6 and/or signal strength index (SSI) values lower than 48 were discarded as VD measurements are positively correlated with SSI.[22] All the en-face pictures were examined by the glaucoma specialist (SP) and the images with any other abnormality of the macula (drusen, membrane, etc) were rejected as well.

## Convolutional Neural Networks (CNN) with Deep Learning

### Image Pre-Processing

The OCTA images of en-face S of the macula and optic disc of glaucomatous patients and healthy subjects and the OCT images of the same anatomical locations were used for the dataset. The gathered images had a resolution of 512×512 pixels in black and white color which were scaled to 128×128 pixels and normalized from 0 − 255 to 0 − 1 for computational performance. Additionally, the dataset was divided into 48 eyes for testing and 190 eyes for training using a 5-fold stratified classification. The testing set included only images that had not been used for training purposes by the model. Twenty completely independent different runs were performed. Each time the performance metrics (accuracy, AUC, sensitivity, and specificity) of the testing were registered.

### AI-GlauOCTA Architecture

The CNN architecture consists of two main parts.[23] The first part is tailored to each image type and location (OCT-D, OCT-M, OCTA-D, OCTA-M), involving convolutional, pooling, and flattening layers. The second part involves concatenating these flattened vectors and passing them through four fully connected layers, resulting in a binary output that distinguishes between healthy and glaucomatous eyes. This approach allows for an effective classification process (Figure 5).

### IOP Measurements

Eye pressure was measured by calibrated Goldmann tonometry after OCT/OCTA measurements to prevent image distortion.

### Visual Field Testing

For the visual field test, we used Humphrey Field Analyzer, Carl Zeiss; 24–2C Sitafaster grid that incorporates 10 additional test points within the central 10° from fixation, 5 in each hemifield, to be able to identify the initial glaucoma damage in the central visual field which previously was less remarkable with Sita standard 24–2 algorithm.[24]

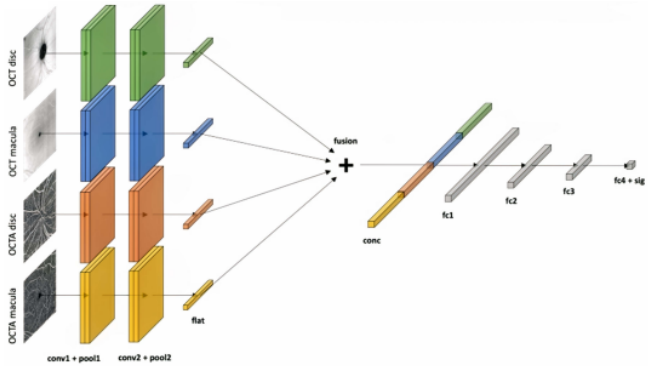


**Figure 5** AI-Glau-OCTA's intermediate fusion CNN architecture for glaucoma detection with four image types as input.

## Results

The baseline demographic characteristics are shown in Table 1. Patients with Glaucoma had significantly worse VFI, MD, lower RNFL and older age. The average mean deviation of the glaucoma patients was nearly −8 dB which according to the VF loss classification scoring system, proposed in the 5th Guidelines of the European Glaucoma Society refers to a moderate loss of function.

The range of values for the attained accuracy was from 82.35% to 92.44%, the AUC values were from 91.40% to 96.94%, the sensitivity was from 83.74% to 94.71%, and the specificity was from 77.7% to 89.34%.

Table 2 presents the comprehensive outcomes, which include the 95% confidence intervals derived from bootstrap resampling.

## Discussion

We reviewed peer-reviewed articles from 2018 to 2023, analyzing the use of OCT and OCTA in glaucoma diagnosis. Previous studies, like the comprehensive review by Van Melkebeke et al[25] in 2018, highlighted that OCTA demonstrates strong reliability in both normal and glaucomatous eyes. Glaucoma eyes typically show lower OCTA parameters compared to healthy eyes, suggesting its potential for diagnostic use. The discriminatory power of OCTA is similar to OCT, and combining the two enhances diagnostic accuracy, especially in early glaucoma. OCTA parameters, particularly

**Table 1** Patient Characteristics

| | Normal (Mean ± SD) (Min to Max) | GL (Mean ± SD) (Min to Max) |
|---|---|---|
| Nr. participant | 51 | 45 |
| Nr. Eyes | 103 | 135 |
| Age (yr) | 49.7± 17 (19 to 84) | 66.4 ±12 (31 to 86) |
| Sex: Women/Man% | 72.5/27.5 | 47.7/52.3 |
| RNFL (μm) | 93.22 ± 9.7 | 67.9 ± 15.5 |
| VF MD (dB) | −0.4 ± 1.6 (−4.7 to 1.9) | −7.9 ± 7.4 (−27.5 to 0.65) |

**Table 2** The 95% Confidence Interval and Bootstrap Metrics Averaged Across Nine Models

| | OCT | | | OCTA | | | OCT+OCTA | | |
|---|---|---|---|---|---|---|---|---|---|
| | **Disc** | **Macula** | ***Disc+Macula*** | **Disc** | **Macula** | ***Disc+Macula*** | **Disc** | **Macula** | ***Disc+Macula*** |
| ACC (95% CI) | 0.8235 (0.774–0.873) | 0.8445 (0.797–0.892) | 0.8782 (0.836–0.920) | 0.8950 (0.857–0.933) | 0.8697 (0.827–0.912) | ***0.9244*** (0.89–0.958) | 0.8697 (0.829–0.91) | 0.8866 (0.846–0.927) | *0.8992* (0.861–0.937) |
| AUC (95% CI) | 0.9140 (0.878–0.950) | 0.9262 (0.895–0.957) | 0.9549 (0.932–0.978) | 0.9501 (0.923–0.977) | 0.9380 (0.906–0.97) | ***0.9694*** (0.948–0.99) | 0.9534 (0.931–0.976) | 0.9604 (0.938–0.983) | *0.9692* (0.951–0.988) |
| SE (95% CI) | 0.8584 (0.801–0.916) | 0.8374 (0.775–0.899) | 0.8966 (0.844–0.949) | 0.9329 (0.892–0.974) | 0.9112 (0.863–0.959) | ***0.9471*** (0.91–0.984) | 0.9184 (0.874–0.963) | *0.9261* (0.882– 0.971) | *0.9261* (0.883–0.97) |
| SP (95% CI) | 0.777 (0.701–0.853) | 0.8552 (0.788–0.922) | 0.8546 (0.785–0.924) | 0.8446 (0.775–0.915) | 0.8166 (0.74–0.893) | ***0.8934*** (0.835–0.952) | 0.8057 (0.73–0.882) | 0.8377 (0.768–0.907) | *0.8651* (0.801–0.93) |

**Notes:** Table 2 provides the 95% confidence interval and bootstrap performance metrics (ACC, AUC, SE, SP) for Optical Coherence Tomography (OCT), Optical Coherence Tomography Angiography (OCTA), and combined OCT +OCTA averaged across nine predictive models. Each metric is presented separately for Disc, Macula, and Disc+Macula regions. The values in bold highlight the best overall model performance, while the best metrics for each subcategory (OCT, OCTA, and OCT+OCTA) are italicized.

in the peripapillary area, show promise for detecting early glaucoma and demonstrate less susceptibility to floor effects compared to OCT, making them valuable for monitoring disease progression.

While OCT excels in structural assessment, various studies emphasize the superiority of OCT for glaucoma diagnosis,[26] particularly when using parameters like circumpapillary vessel density (cpVD) and comparing it with RNFL thickness. However, limitations exist for OCTA, such as the smaller 3 mm scan area, which might miss lesions in the 3 to 6 mm range.

In our study, we addressed the integration of OCTA with deep learning for glaucoma diagnosis, noting that OCTA alone outperforms combined OCT+OCTA in sensitivity when assessing the macula and disc areas (OCTA M+D). This finding suggests that vascular information provided by OCTA plays a crucial role in early glaucoma detection, particularly in cases where OCT's structural data is less indicative of early-stage disease.

We observed that the integration of Optical Coherence Tomography Angiography (OCTA) as a diagnostic tool in glaucoma continues to face challenges due to its ongoing reliance on structural OCT data and in most of the studies the diagnosis of glaucoma is based solely on OCT results.

Additionally, the absence of comprehensive reports combining structural and functional data hinders the appreciation of OCTA's insights. To date, Solix Optovue stands out as one of the few OCT products offering such combined reports.

We did not base our diagnosis only on OCT results but on the whole clinical knowledge of each patient. We neither exclude any patients with higher refractive errors if the QS and SSI were acceptable We wanted to mimic the "real life" measurements.

We acknowledge the difference in average ages between normal and glaucoma patients as a potential limitation. While age is a risk factor for glaucoma, our primary focus was on the diagnostic capability of OCT and OCTA. Future studies may benefit from age-matching the control and glaucoma groups to minimize this bias. In "real life" most of the glaucoma patients are elderly. However, the significant structural and vascular differences detected by OCT and OCTA in our study support the conclusion that these methods are effective for glaucoma diagnosis, even with age as a variable.

It's essential to view OCTA as part of the broader OCT analysis, providing supplementary biomarkers to enhance diagnostic precision.

Deep learning analyses indicate that OCTA M+D exhibits heightened sensitivity compared to OCT alone, particularly promising for detecting anatomical and vascular abnormalities in pre-perimetric glaucoma.

The combined assessment of OCTA M+D demonstrates superior sensitivity in identifying early glaucomatous pathology, aligning with established structural damage patterns in glaucoma.

It emphasizes surprisingly that when we combine the values of OCT with OCTA, it may even reduce the sensitivity in distinguishing healthy individuals from those with glaucoma.

When OCT and OCTA are combined, the sensitivity for distinguishing between healthy and glaucoma patients may decrease.

This study marks an initial validation of deep learning techniques for distinguishing between healthy and glaucomatous states, paving the way for more sophisticated investigations into disease detection at earlier, sub-clinical stages.

Our hypothesis regarding the difference between findings in studies that do not employ deep learning (DL) and our results lies in the understanding that OCTA provides a limited and static perspective of "flow". Deep Learning enables the analysis of additional factors beyond what a single value can capture.

## Conclusion

AI-GlauOCTA's intermediate fusion architecture greatly enhances the comparison of various image types crucial for glaucoma detection such as OCT-D, OCT-M, OCTA-D, and OCTA-M images. In conclusion, this study demonstrates that OCTA alone showed superior sensitivity in detecting glaucomatous changes in disc and macula areas compared to combined OCT+OCTA. The integration of both disc and macula regions is pivotal for accurate glaucoma detection. While OCT+OCTA showed higher accuracy in certain metrics, our results emphasize the value of vascular information captured by OCTA for early glaucoma detection. This finding aligns with the study's objective to evaluate the diagnostic power of OCT, OCTA, and their combination. The use of deep learning models further enhances diagnostic performance, highlighting the potential for integrating these imaging modalities into clinical practice for more effective glaucoma diagnosis to assist non-glaucoma sub-specialist ophthalmologists as part of their clinical decision support system for patient management.

## Funding

A grant has been awarded from Fondation Saint Luc, Cliniques Universitaire Saint Luc, UCL Brusseels for the doctorate thesis of the first author of which this article is one of the publications. Glaucoma Centre Zaventem outpatient financially supported the publication of this article.

## Disclosure

No conflicting relationship exists for any author.

## References

1. GBD 2019 Blindness and Vision Impairment Collaborators; Vision Loss Expert Group of the Global Burden of Disease Study. Causes of blindness and vision impairment in 2020 and trends over 30 years and prevalence of avoidable blindness in relation to VISION 2020: the right to sight: an analysis for the global burden of disease study. *Lancet Glob Health*. 2021;9(2). doi:10.1016/S2214-109X(20)30489-7
2. Johansson LH, Kalaboukhova L, Erhag HF, Skoog I, Zetterberg M. The prevalence of glaucoma in a 70-year-old Swedish population in the city area of Gothenburg. *Acta Ophthalmol*. 2024;102(2):208–215. doi:10.1111/aos.15734
3. Tham Y-C, Li X, Wong TY, Quigley H, Aung T, Cheng C-Y. Global prevalence of glaucoma and projections of glaucoma burden through 2040: a systematic review and meta-analysis. *Ophthalmology*. 2014;121(6):2081–2090. doi:10.1016/j.ophtha.2014.05.013
4. Prum BE, Rosenberg LF, Gedde SJ, et al. Primary open-angle glaucoma preferred practice pattern® guidelines. *Ophthalmology*. 2016;123(1). doi:10.1016/j.ophtha.2015.10.053
5. Breusegem C, Fieuws S, Stalmans I, Zeyen T. Agreement and accuracy of non-expert ophthalmologists in assessing glaucomatous changes in serial stereo optic disc photographs. *Ophthalmology*. 2010;118(3):742–746. doi:10.1016/j.ophtha.2010.08.019
6. Jampel H, Friedman D, Quigley H, et al. Agreement among glaucoma specialists in assessing progressive disc changes from photographs in open-angle glaucoma patients. *Am J Ophthalmol*. 2008;147(1):39–44.e1. doi:10.1016/j.ajo.2008.07.023
7. Heijl A, Leske MC, Bengtsson B, et al. Reduction of intraocular pressure and glaucoma progression: results from the Early Manifest Glaucoma Trial. *Arch Ophthalmol*. 2002;120(10):1268–1279. doi:10.1001/archopht.120.10.1268
8. Latif K, Nishida T, Moghimi S, Weinreb RN. Quality of life in glaucoma. *Graefes Arch Clin Exp Ophthalmol*. 2023;261(10):3023–3030. doi:10.1007/s00417-023-06050-z
9. Nayyar S, Kumar S, Rehman O, Ichhpujani P, Singla E. Impact of moderate and severe primary open-angle glaucoma on quality of life due to activity limitation. *Indian J Ophthalmol*. 2022;70(2):552–557. doi:10.4103/ijo.IJO_1687_21
10. Pezzullo L, Streatfeild J, Simkiss P, Shickle D. The economic impact of sight loss and blindness in the UK adult population. *BMC Health Serv Res*. 2018;18(1):63. doi:10.1186/s12913-018-2856-0
11. Gardiner SK, Mansberger SL, Fortune B. Time lag between functional change and loss of retinal nerve fiber layer in glaucoma. *Invest Ophthalmol Vis Sci*. 2020;61(12):3314. doi:10.1167/iovs.61.13.5
12. Lim AB, Park J-H, Jung JH, Yoo CK, Kim YY. Characteristics of diffuse retinal nerve fiber layer defects in red-free photographs as observed in optical coherence tomography en face images. *BMC Ophthalmol*. 2020;20(1):1–7. doi:10.1186/s12886-020-01640-7
13. Zeppieri M, Marsili S, Enaholo ES, et al. Optical coherence tomography (OCT): a brief look at the uses and technological evolution in ophthalmology. *Medicina*. 2023;59(12):2114. doi:10.3390/medicina59122114
14. Spaide RF, Fujimoto JG, Waheed NK, Sadda SR, Staurenghi G. Optical coherence tomography angiography. *Prog Retin Eye Res*. 2018;64:1–55. doi:10.1016/j.preteyeres.2017.11.003
15. Zhang H, Qie Y. Applying deep learning to medical imaging: a review. *Appl Sci*. 2023;13(18):10521. doi:10.3390/app131810521
16. Chan H-P, Samala RK, Hadjiiski LM, Zhou C. Deep learning in medical image analysis: challenges and applications. *Deep Learn Med Image Anal*. 2020;3–21. doi:10.1016/B978-0-12-816554-3.00001-4
17. Ahmed S, Mahadevappa V. Advancing glaucoma detection with convolutional neural networks: a paradigm shift in ophthalmology. *Rom J Ophthalmol*. 2023;67(3):222. doi:10.22336/rjo.2023.222
18. Hood DC. Imaging glaucoma. *Annu Rev Vis Sci*. 2015;1:51–72. doi:10.1146/annurev-vision-082114-035347
19. Kwon J, Choi J, Shin JW, Lee J, Kook MS. Glaucoma diagnostic capabilities of Foveal avascular zone parameters using optical coherence tomography angiography according to visual field defect location. *J Glaucoma*. 2017;26(12):1120–1129. doi:10.1097/IJG.0000000000000800
20. Lee YJ, Sun SY, Kim SH, Jeoung JW, Park KH. Diagnostic ability of macular microvasculature with swept-source OCT angiography for highly myopic glaucoma using deep learning. *Sci Rep*. 2023;13(1):5209. doi:10.1038/s41598-023-32117-2
21. Schottenhamml J, Würfl T, Mardin SM, et al. Glaucoma classification in 3 x 3 mm en face macular scans using deep learning in different plexus. *Biomed Opt Express*. 2021;12(12):7434–7444. doi:10.1364/BOE.433054
22. Pradhan ZS, Sreenivasaiah S, Srinivasan T, et al. The importance of signal strength index in optical coherence tomography angiography: a study of eyes with pseudoexfoliation syndrome. *Clin Ophthalmol*. 2022;16:3481–3489. doi:10.2147/OPTH.S378722
23. Gouverneur F, Pourjavan S, Macq B. Abu-Dhabi 10/2024 International Conference on Image Processing Deep Convolutional Neural Network Prediction For Glaucoma Detection Using OCT and OCT-Angiography Disc-and Macula-Centered Images and Their Combined Power. 2088-2094. doi: 10.1109/ICIP51287.2024.10647463. 2024
24. Phu J, Kalloniatis M. Ability of 24-2C and 24-2 grids to identify central visual field defects and structure-function concordance in glaucoma and suspects. *Am J Ophthalmol*. 2020;219:317–331. doi:10.1016/j.ajo.2020.07.014
25. Van Melkebeke L, Barbosa-Breda J, Huygens M, Stalmans I. Optical coherence tomography angiography in glaucoma: a review. *Ophthalmic Res*. 2018;60(3):139–151. doi:10.1159/000488495
26. Khallouli A, Oueslati Y, Gouider D, et al. Diagnostic accuracy and relationship between optical coherence tomography angiography vessel density and structural/functional parameters in healthy, preperimetric, and manifest glaucoma eyes. *J Curr Ophthalmol*. 2022;34(2):173–179. doi:10.1016/j.joco.2021.12.006

**Clinical takeaway**

*This study confirms the added value of multimodal AI in binary classification and suggests that vascular biomarkers may outperform structural ones in the early detection of disease. It supports the hypothesis that vascular dysfunction may precede irreversible structural changes, marking a potential early instability phase in glaucoma progression.*

## 3.9 Advancing AI-Driven Glaucoma Diagnosis Through Multimodal Imaging.

Our third study reaffirmed the value of deep learning in integrating both structural and vascular imaging modalities for the classification of glaucoma. By leveraging CNN-based analysis of OCT and OCTA images, this study provided clinically relevant insights into the complementary nature of these imaging techniques.

Deep learning-enhanced OCTA analysis exhibited slightly superior performance to deep learning-enhanced structural OCT metrics. This suggests that vascular alterations may manifest earlier than structural loss, reinforcing the hypothesis that glaucoma is, at least partially, a microvascular disease. The ability of AI to detect complex vascular features beyond numerical vessel density values supports the notion that early microcirculatory changes might serve as the first detectable biomarker of glaucomatous neurodegeneration. This underscores the need for further research into the clinical applicability of AI-assisted vascular imaging for early glaucoma risk assessment and disease monitoring.

Moreover, these findings highlight an ongoing challenge in glaucoma diagnostics: how best to incorporate AI-driven multimodal biomarkers into clinical decision-making. While deep learning has shown potential in enhancing diagnostic precision, AI models must evolve beyond single-modality analysis to integrate multiple physiological parameters for a truly personalized approach.

While our research has demonstrated AI's potential in glaucoma diagnostics, its integration into clinical practice remains challenging. The next chapter explores how AI models can move from research to real-world implementation, addressing key hurdles such as validation, regulatory approval, and ethical considerations

## References


1. Tonti E, Tonti S, Mancini F, Bonini C, Spadea, D'Esposito, F, Gagliano C, Musa M, Zeppieri M. Artificial Intelligence and Advanced Technology in Glaucoma: A Review. J Pers Med. 2024 Oct 16;14(10):1062. doi: 10.3390/jpm14101062. PMID: 39452568; PMCID: PMC11508556.
2. Shi N.N., Li T., Cheng S., Wong T.Y. Quantifying the Performance of Artificial Intelligence (AI) in Detecting Glaucoma Using Spectral Domain Optical Coherence Tomography Images. Int. J. Ophthalmol. 2024;17:10-110.
3. Hemelings R, Elen B, Barbosa-Breda J, Lemmens S, Meire M, Pourjavan S, Vandewalle E, Van de Veire S, Blaschko MB, De Boever P, Stalmans I. Accurate prediction of glaucoma from colour fundus images with a convolutional neural network that relies on active and transfer learning. Acta Ophthalmol. 2020 Feb;98(1):e94-e100. doi: 10.1111/aos.14193. Epub 2019 Jul 25. PMID: 31344328.
4. Hemelings, R., Elen, B., Schuster, A.K. *et al.* A generalizable deep learning regression model for automated glaucoma screening from fundus images. *Npj Digit. Med.* 6, 112 (2023). https://doi.org/10.1038/s41746-023-00857-0
5. Heijl A, Leske MC, Bengtsson B, et al. Reduction of intraocular pressure and glaucoma progression: results from the Early Manifest Glaucoma Trial. *Arch Ophthalmol.* 2002;120(10):1268-1279. doi:10.1001/archopht.120.10.1268
6. Lim WS, Ho HY, Ho HC, Chen YW, Lee CK, Chen PJ, Lai F, Jang JR, Ko ML. Use of multimodal dataset in AI for detecting glaucoma based on fundus photographs assessed with OCT: focus group study on high prevalence of myopia. BMC Med Imaging. 2022 Nov 24;22(1):206. doi: 10.1186/s12880-022-00933-z. PMID: 36434508; PMCID: PMC9700928.
7. Muhammad H, Fuchs TJ, De Cuir N, De Moraes CG, Blumberg DM, Liebmann JM, Ritch R, Hood DC. Hybrid Deep Learning on Single Wide-field Optical Coherence tomography Scans Accurately Classifies Glaucoma Suspects. J Glaucoma. 2017 Dec;26(12):1086-1094. doi: 10.1097/IJG.0000000000000765. PMID: 29045329; PMCID: PMC5716847.
8. Pourjavan S, Bourguignon GH, Marinescu C, Otjacques L, Boschi A. Evaluating the Influence of Clinical Data on Inter-Observer Variability in Optic Disc Analysis for AI-Assisted Glaucoma Screening. Clin Ophthalmol. 2024 Dec 27;18:3999-4009. doi: 10.2147/OPTH.S492872. PMID: 39741794; PMCID: PMC11687089.
9. Robert D. Fechtner and Albert S. Khouri. Evolving global risk assessment of ocular hypertension to glaucoma. Curr Opin Ophthalmol 18:104–109. 2007 Lippincott Williams & Wilkins.
10. McMonnies CW. Glaucoma history and risk factors. J Optom. 2017 Apr-Jun;10(2) :71-78. doi: 10.1016/j.optom.2016.02.003. Epub 2016 Mar 23. PMID: 27025415; PMCID: PMC5383456.
11. Mohammadzadeh V, Liang Y, Moghimi S, Xie P, Nishida T, Mahmoudinezhad G, Eslani M, Walker E, Kamalipour A, Micheletti E, Wu JH, Christopher M, Zangwill LM, Javidi T, Weinreb RN. Detection of glaucoma progression on longitudinal series of en-face macular optical coherence tomography angiography images

with a deep learning model. Br J Ophthalmol. 2024 Nov 22;108(12):1688-1693. doi:10.1136/bjo-2023-324528. PMID: 39117359.
12. Ebrahimi B, Le D, Abtahi M, Dadzie AK, Lim JI, Chan RVP, Yao X. Optimizing the OCTA layer fusion option for deep learning classification of diabetic retinopathy. Biomed Opt Express. 2023 Aug 16;14(9):4713-4724. doi: 10.1364/BOE.495999. PMID: 37791267; PMCID: PMC10545199.
13. Guarrasi V, Aksu F, Caruso C, Di Feola F, Rofena A, Ruffini F, Soda P. Image and Vision Computing 158 (2025) 105509. doi/10.1016/j.imavis.2025.105509

# Chapter 4: Building the Foundation for AI-Based Glaucoma Risk Assessment: Defining Normative OCTA Values

## 4.1 Introduction: The Need for Normative OCTA Values

Although Optical Coherence Tomography Angiography (OCTA) has revolutionised our ability to visualise retinal microcirculation, establishing robust normative databases remains underdeveloped, particularly in glaucoma risk assessment and AI-based diagnostics.

Small sample sizes, insufficient age stratification or the inclusion of heterogeneous patient populations without detailed screening for systemic diseases limit most published OCTA normative studies [1]. In many cases, exclusion criteria are based solely on ocular abnormalities, while key systemic and neurological conditions, including hypertension, diabetes, or early cognitive decline, are overlooked. This introduces variability that undermines the clinical and computational utility of the data.

One example is the study by Xu et al [2]. (2024), which reported normative vessel density values across four macular plexuses in healthy elderly individuals using 6 × 6 mm OCTA scans. They included over 1,400 subjects and confirmed a strong negative correlation between age and vessel density. However, the data were not stratified by decade, and patients younger than 50 were excluded entirely. This limits its utility for clinical interpretation and AI models, which require age-adjusted baselines to distinguish physiological ageing from pathology.

Moreover, several studies report only statistical significance in VD changes without providing the absolute numeric values, which are essential for machine learning training and clinical interpretation. Others fail to extend their sampling across age decades or exclude critical regions, such as the peripapillary zone, which is fundamental for glaucoma research. While the inferior peripapillary region is widely recognised for its diagnostic sensitivity, the superior hemisphere, especially the superotemporal quadrant, is equally vulnerable to progression and late-stage disease. Hood and colleagues have demonstrated that glaucomatous damage in the superior retina often occurs just outside the central macula, affecting the parafoveal region while sparing the fovea in the early stages (Figure 1) [3,4]. Therefore, an ideal normative dataset must include macular and peripapillary vascular densities across stratified age groups.

**Figure1. Hood's Vulnerability zones with its location on the optic disc rim.**

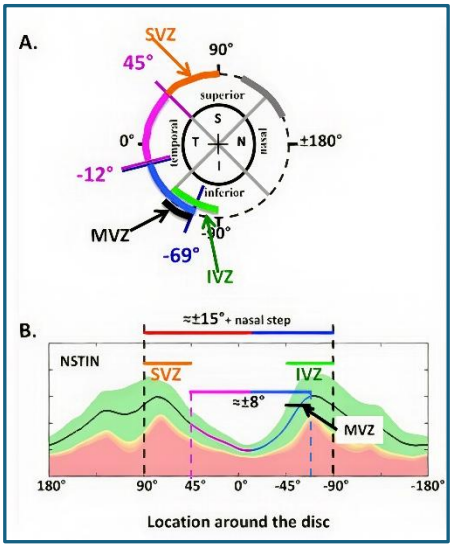


## 4.2 Challenges in defining normative data

Defining normative OCTA vascular density values is inherently challenging due to the multifactorial nature of retinal perfusion. Vascular density is not a static parameter; rather, it is influenced by a complex interplay of ocular, systemic, and demographic factors. These variations must be carefully considered when establishing a normative dataset, as they can introduce significant bias if not adequately accounted for.

- Demographic factors
    - Age: Various studies have shown a decline in VD in the retina with age [5-7].
    - Racial differences in vascular density have been observed. In a study published by Giocanti-Aurégan, she found that the SCP, DCP, and VD are lower in black Africans compared to Caucasians [8].
    - Sex: Females exhibited higher VD in the macula, characterised by a larger FAZ [9].

- Ocular factors
    - Refractive error: studies have shown that even in diabetic patients without DRP, there is a negative correlation between axial length and vascular density in the superficial and deep macula and the peripapillary area [10].

    - RNFL thickness. In healthy subjects, retinal perfusion in small vessels was closely correlated with the thickness of the inner retinal layers in both the macular and peripapillary areas [11].

- Systemic factors
    - Diabetes: Even in patients with DRP, the FAZ area and perimeter of the macular area for the superficial retina expanded, and the blood flow density decreased in the macular area and around the optic disc [12].
    - AHT causes retinal microvascular abnormalities [13]. A recent study showed that the superficial plexus VD, FAZ area, capillary density, and inner retinal thickness changed significantly in hypertensive patients without hypertensive retinopathy [14].
    - Vascular diseases cause alteration of the retinal vasculature.
    - Smoking decreases the VD of the Deep Capillary Plexus (DCP). The DCP is more vulnerable to oxidative damage and poor perfusion induced by cigarette smoking than SCP [15]. The optic nerve VD is also reduced in smokers [16].
    - Manifest kidney disease
    - Vasculitis,
    - Cardiac conditions (including heart failure and atrial fibrillation)
    - History of cancer involving chemotherapy

Beyond physiological variations, technical and methodological factors also pose challenges. Differences in OCTA imaging device type (SS-OCTA versus SD-OCTA), segmentation algorithms, and signal strength can introduce measurement discrepancies, making cross-study comparisons challenging. Notably, SD-OCTA systems, such as the Optovue Solix used in our study, remain more widely adopted in routine clinical practice, making them more applicable for widespread normative baselines than their SS-OCTA counterparts.

## 4.3 Diurnal Variability: Minimal but Not Negligible

Another key factor is vessel density stability across the day when establishing normative OCTA databases. Several studies have evaluated diurnal variation in retinal and optic nerve head (ONH) perfusion in healthy eyes. Wu et al. (2021) observed a small but statistically significant increase in circumpapillary VD toward the evening; however, the change remained within test-retest variability, suggesting it is not clinically relevant [17]. Similarly, Baek et al. (2019) found that diurnal fluctuations in VD were minimal in healthy individuals but more pronounced in patients with glaucoma [18]. These findings support the assumption that macular and peripapillary VD remains relatively stable throughout the day in healthy eyes, reinforcing the validity of OCTA-derived normative values independent of scan timing and allowing normative values to be used reliably throughout the day.

## 4.4 The Role of Normative Data in AI Development

With the implementation of DL and CNN in glaucoma diagnostics and treatment, one may wonder whether AI “explicitly needs normative values or can learn patterns and distinguish between normal and abnormal VD on its own.

However, normative values are still essential for several reasons:

### 4.4.1 Improved supervised learning needs labels (Ground Truth)

- If we train a CNN to distinguish between normal and glaucomatous OCTA scans, we need labelled data (healthy vs. diseased). Normative values provide a continuous spectrum, helping the CNN recognise subtle deviations from normal before glaucoma is fully established.
- Having a well-defined normative dataset reduces bias and improves accuracy, ensuring the model learns correct patterns rather than artefacts.

### 4.4.2 Better Clinical Interpretability

- AI predictions need to be clinically interpretable. If a CNN detects an anomaly in vascular density, we must compare it to *normal*.
- Without reference data, clinicians won’t know if the AI’s output is meaningful in real-world practice.

### 4.4.3 Transfer Learning & Generalisation

- Many AI models pre-train on general datasets before being fine-tuned for a specific task.
- If normative data is available, we can pre-train the CNN on healthy eyes before exposing it to pathology, leading to better generalisation. A well-documented case of Transfer Learning benefiting from pre-training on normative data is found in AI models for diabetic retinopathy (DR). In a study by Gulshan et al. (2016), Google’s DeepMind initially trained a CNN only on diseased retinal images, without exposure to healthy eyes. When tested on unseen populations, the model struggled with false positives and false negatives, misinterpreting normal anatomical variations as pathology [19]. To improve performance, researchers pre-trained the AI on a large dataset of healthy retinal images (ImageNet) before fine-tuning it on disease cases. This approach enabled the AI to learn normal structural variations, thereby improving its ability to detect true pathology and increasing generalisation across diverse populations, thereby reducing bias. The publication became a benchmark for medical AI models, influencing glaucoma AI research.
- The study by Lee et al. (2017) highlights the importance of large, well-defined datasets in training deep learning models for automated OCT

classification. Their CNN model, trained on a normal and AMD OCT image dataset, achieved an AUROC of 97.45% at the patient level, demonstrating its potential for real-world clinical applications [20]. However, the model's performance was influenced by the quality and diversity of training data, emphasising the need for normative datasets to improve AI generalisability.

- A key takeaway is that pretraining AI models on healthy OCT images before fine-tuning on pathological cases allows the network to learn normal structural variations, reducing overfitting and improving classification accuracy across diverse populations. This reinforces the importance of establishing normative OCTA datasets for glaucoma AI models, ensuring robust disease detection without bias.

### 4.4.4 AI Validation Against Population-Based Norms

- Even if a CNN can differentiate between normal and glaucomatous eyes without explicit normative values, regulatory agencies and clinicians still need validation data.

- Having normative OCTA values ensures that AI is not overfitting to a specific dataset but aligns with real-world clinical expectations. An example is the study by Lee et al., where a well-documented case of AI overfitting was observed in diabetic retinopathy screening models [21]. The study evaluating seven commercially available AI systems found that their sensitivities ranged from 50.98% to 85.90% and their specificities from 60.42% to 83.69% when tested on real-world datasets. These AI systems were trained on highly curated, high-quality images, but their performance dropped significantly when tested on diverse, lower-quality real-world fundus images. Instead of recognising actual pathological features, the AI had overfitted to image quality differences, assuming that more explicit images belonged to healthy patients and lower-quality images indicated disease.

### 4.4.5 Outlier Detection & Early Diagnosis

- Some early glaucoma cases may fall into a grey zone, where they are not yet classified as glaucoma but deviate from normal.

- By having normative values, AI can identify patients who are statistical outliers or borderline and may be at high risk before functional damage occurs.

Establishing a normative OCTA study is not just for the AI, it's for better AI training, validation, and clinical application. CNN will learn patterns, but our dataset will provide it with structure and medical relevance.

## 4.5 Bridging the gap

To address these limitations, we designed a study that carefully stratifies subjects based on both ocular and systemic health factors, aiming to construct a robust and clinically relevant normative dataset. Specifically, we excluded all smokers, individuals with diagnosed or visible arterial hypertension or antihypertensive medication use, patients with diabetes, and any recent use of systemic vasodilators such as Sildenafil citrate [22]. Patients with ocular comorbidities were also excluded. However, to better reflect real-world variability, we included healthy subjects with high myopia or hyperopia, as well as normal anatomical outliers that are often underrepresented in normative studies.

The study by Fernández-Vigo et al. represents one of the most comprehensive efforts to date in defining normative peripapillary vessel density using swept-source optical coherence tomography angiography (SS-OCTA) in a healthy Caucasian population [23]. Their decade-wise age stratification and regional analysis of the superficial capillary plexus (SCP), deep capillary plexus (DCP), and choriocapillaris offer valuable insights into age- and axial length-related vascular changes. However, their focus was confined to the peripapillary region, without assessment of macular microvasculature or key biomarkers such as the foveal avascular zone (FAZ).

By integrating macular and optic disc microcirculation and including FAZ-derived metrics, our study extends this work toward a more comprehensive model of retinal vascular ageing. In addition to peripapillary analysis, we included detailed measurements of FAZ area, perimeter, and the foveal density in the 300 µm ring surrounding the FAZ (FD-300), a robust and reproducible biomarker increasingly recognised for its sensitivity to early perfusion changes. Furthermore, while Fernández-Vigo et al. used SS-OCTA, our use of SD-OCTA is more prevalent in everyday clinical practice, enhancing the applicability and transferability of our findings to real-world settings, particularly in institutions without access to high-cost imaging platforms.

## 4.6 Our Pilot Study: Submitted and Under Review

### Normative Ocular Coherence Tomography Angiography (OCTA) Vascular Metrics and AI-Based Ageing Models in Healthy Eyes: Pilot Study

**Normative Ocular Coherence Tomography Angiography (OCTA) Vascular Metrics and AI-Based Ageing Models in Healthy Eyes: Pilot Study**

Sayeh Pourjavan, Niki Nazaran, Tom Vaucourt, Nasim Abdouli, Adil El Maftouhi, Benoit Macq

**Abstract**

**Purpose:**

This study aims to define decade-stratified normative values for OCTA-derived vascular parameters in healthy eyes and evaluate their accuracy in predicting biological ocular age.

**Methods:**

This cross-sectional study included 132 healthy subjects. Structural and vascular parameters were extracted from OCT and OCTA scans. Vessel density was measured in the superficial capillary plexus using the ETDRS grid (macula) and the Garway-Heath map (peripapillary region). FAZ area, FD-300 density, and FAZ circularity were also analysed. Disc and RNFL metrics were included. Subjects were stratified by age decade. Support Vector Regression was applied to develop vascular, structural, and combined ageing models. Model performance was evaluated using root mean squared error (RMSE) and $R^2$ under subject-level grouped cross-validation.

**Results:**

Both macular and peripapillary vessel density (VD) demonstrated a progressive, decade-wise decline with age, particularly after the fifth decade of life. FAZ area increased, and the circularity decreased with age, while FD-300 remained relatively stable. An SVR model trained exclusively on structural OCT or vascular OCTA data alone showed poor to modest performance ($R^2$ = -0.111 and 0.295, respectively). In contrast, combining OCT and OCTA inputs improved predictive accuracy significantly ($R^2$ = 0.99; RMSE = 0.299 years), supporting the integration of structural and vascular features for estimating biological ocular age.

**Conclusion:**

Our study establishes decade-stratified normative OCTA values and demonstrates the utility of combining structural and vascular imaging for AI-based ocular ageing estimation. The resulting AI model offers a promising foundation for early glaucoma risk stratification through biologically meaningful ocular age prediction.

**Keywords:** Glaucoma, OCTA, optic disc, macula, vessel density, OCTA normative values, GlauOCTA, GlauOCTA-AI, Neurovascular degeneration

**Conflict of interest statement:** No conflicts of interest exist for any author.

**Introduction:**

Glaucoma is a neurodegenerative disease of the optic disc characterised by a gradual loss of visual field. It is often asymptomatic in the early stages and has an insidious onset, which makes a timely diagnosis challenging, as it relies heavily on the clinical expertise of the ophthalmologist. Even among trained glaucoma specialists, interobserver variability remains high when distinguishing early glaucomatous changes from normal optic disc anatomy [1-3]. Early and accurate diagnosis is critical, as timely intervention has been shown to significantly improve patient outcomes and reduce long-term healthcare costs associated with glaucoma progression and visual incapacity [4].

The current diagnostic paradigm involves structural and functional assessments, including optic disc evaluation, retinal nerve fibre layer (RNFL) analysis with optical coherence tomography (OCT), visual field (VF) testing, vascular imaging via optical coherence tomography angiography (OCTA), and intraocular pressure (IOP) measurement. While effective, this multimodal approach is not immune to subjective interpretation and delayed detection.

Recent developments in artificial intelligence (AI) and machine learning (ML) have shown promise in supporting glaucoma diagnosis and risk stratification by identifying subtle patterns across high-dimensional imaging data.

Robust normative databases are essential for such systems to perform reliably in real-world clinical settings and to ensure generalisability. These serve as ground-truth references, enabling the model to differentiate between pathological changes and normal anatomical variability.

Despite growing interest in OCTA-based vascular ageing models, existing normative studies remain limited by small sample sizes, lack of age stratification, heterogeneous inclusion criteria, and insufficient screening for systemic confounders. Most studies do not exclude patients with hypertension, diabetes, or cognitive decline, nor do they account for smoking status. Additionally, many report only statistical trends in vessel density (VD) without providing actual raw numeric values required for ML training and validation.

This study aims to establish a high-quality, decade-stratified normative OCTA dataset in a rigorously screened healthy population using spectral-domain OCTA. Furthermore, we assess the predictive value of vascular biomarkers for estimating biological ocular age using a supervised machine learning model (support vector regression, SVR). Finally, we evaluate whether combining structural OCT and vascular OCTA features enhances model performance in an AI-based ageing framework.

**Participants:**

The Institutional Ethical Committee of the Cliniques Universitaires Saint-Luc in Brussels approved the study protocols (GlauOCTA and GlauOCTA-AI). The research adhered to the principles of the Declaration of Helsinki and complied with all relevant national and European ethical guidelines, including the General Data Protection Regulation (GDPR) for data privacy and confidentiality. Although HIPAA applies specifically to the United States, the GDPR ensures comparable protection in the European context. Written informed consent was obtained from all participants prior to inclusion.

Participants were recruited from the outpatient clinic during routine ophthalmological consultations or refractive error assessments. Eligible subjects had intraocular pressure (IOP) $\leq$ 21 mmHg in both eyes and a clinically normal optic disc, as assessed by indirect ophthalmoscopy using a 60D lens and spectral-domain OCT. The neuroretinal rim was intact, and the retinal nerve fibre layer (RNFL) appeared within normal limits. A glaucoma specialist (SP) confirmed the ground truth classification of 'healthy' based on a comprehensive ophthalmological examination, which included auto-refractometry, best-corrected visual acuity (BCVA), Goldmann applanation tonometry, and indirect funduscopy. After obtaining consent, each participant underwent OCT and OCTA imaging.

The study population also included hospital and outpatient staff volunteers: thirteen ophthalmology residents, five medical students, seven administrative personnel, and one consultant.

Participants were excluded if they met any of the following criteria: An abnormal optic disc or neuroretinal rim on direct funduscopy or on OCT, IOP > 21 mmHg, any retinal pathology (e.g., drusen, age-related macular degeneration), history of intraocular surgery other than uncomplicated phacoemulsification, systemic conditions such as diabetes or arterial hypertension, central neurodegenerative diseases, recent use of systemic vasodilators (e.g., Sildenafil citrate), cardiac disease, chronic kidney disease, history of cancer with chemotherapy treatment and smoking habits. We did not exclude participants with high refractive errors if the image quality was sufficient for analysis. Standard visual field testing was not systematically performed unless clinically indicated.

Participants were stratified by age decades. Table 1 provides the demographic characteristics of the study population.

**Table 1. Patients' Characteristics.**

| | ≤19 | 20-29 | 30-39 | 40-49 | 50-59 | 60-69 | 70+ | Total |
|---|---|---|---|---|---|---|---|---|
| Nr screened | 14 | 24 | 25 | 18 | 24 | 17 | 15 | 137 |
| Nr included | 14 | 23 | 21 | 18 | 19 | 13 | 12 | 120 |
| Eyes | 27 | 44 | 38 | 33 | 36 | 24 | 19 | 221 |
| Sex M/F | 6/8 | 8/15 | 11/10 | 16/12 | 3/16 | 2/12 | 3/9 | 39/81 |

**Methods:**

**Study Design and Feature Extraction**

This cross-sectional study included 132 healthy subjects. All participants underwent spectral-domain OCT and OCTA imaging using the Optovue Solix platform. From the structural OCT scans, 478 features were extracted, including disc and rim area measurements and retinal nerve fibre layer (RNFL) thickness globally and across the temporal, superior, nasal, and inferior quadrants.

OCTA scans provided 156 vascular features. All vascular measurements were performed in the superficial capillary plexus (SCP). Macular vessel density (VD) was quantified using the ETDRS grid, while peripapillary VD was measured using the Garway-Heath sectoral map applied to the radial peripapillary capillary (RPC) network. Additional macular vascular metrics included foveal avascular zone (FAZ) area, FD-300 density, and FAZ circularity (calculated as $4\pi \times \text{Area} / \text{Perimeter}^2$).

OCT and OCTA images were reviewed for segmentation accuracy and image quality. Scans with a quality score (SQ) below 6 and/or signal strength index (SSI) below 48 were excluded, as VD measurements positively correlate with signal strength. Participants were stratified by age into decades for comparative analysis.

**OCTA and OCT acquisition of the images**

OCTA and spectral-domain OCT imaging were performed using the AngioVue imaging system (Optovue Solix, V1.1.100.20, Fremont, CA, USA). This platform enables simultaneous acquisition and automatic registration of structural and vascular data from the same scan, ensuring precise alignment and segmentation. The AngioAnalytics™ software quantitatively analysed vessel density (VD), flow area, non-flow area, FAZ parameters and retinal layer thickness. Macular OCTA scans (6.4 × 6.4 mm²) were centred on the fovea. VD was calculated across nine en-face ETDRS grid sectors. FAZ metrics, FD-300 and FAZ circuity were extracted from the Superficial capillary plexus (SCP) layer, which contains the internal limiting membrane (ILM) to 10 µm below the inner plexiform layer (IPL).

OCTA can also visualise the VD in the choroid and show, in some cases [5], a complete choriocapillaris loss in areas of localised peripapillary atrophy, the so-called deep microvascular dropout [6].

Optic disc scans (6 × 6 mm²) included a peripapillary annulus (2.5 mm to 4.5 mm diameter) centred on the BMO-fitted disc circle. VD was calculated in a 9-sector grid and across the 8 Garway-Heath regions. The RPC network was visualised as a distinctive pattern of parallel, long, uniform-diameter vessels surrounding the optic nerve head (ONH), oriented parallel to the retinal nerve fibre layer (RNFL).

The Solix glaucoma package enabled integrated structural and vascular assessment, including ONH, GCC, FLV, GLV, BMO, and VD analysis aligned with Garway-Heath sectors.

Motion artefacts were reduced using DualTrac Motion Correction Technology (MCT), which combines real-time tracking with post-processing algorithms. OCTA signal generation was based on the split-spectrum amplitude-decorrelation angiography (SSADA) algorithm, which detects erythrocyte motion across sequential B-scans. Vessel density was calculated as the percentage of pixels surpassing a decorrelation threshold, after projection artefact removal (PAR) to reduce shadowing from superficial vasculature.

Given the potential for residual ghost signals even after projection artefact removal (PAR), vessel density quantification was limited to the superficial capillary plexus (SCP), where projection interference is minimal.

The author, an experienced glaucoma specialist, reviewed all en-face images. Scans were excluded if they exhibited artefacts, segmentation errors, or macular abnormalities (e.g., drusen, epiretinal membranes). High refractive error was not an exclusion criterion if image quality was sufficient.

**IOP measurements**
To prevent image distortion, eye pressure was measured by calibrated Goldmann tonometry after OCT/OCTA measurements.

**Supervised Machine Learning with Support Vector Regression**
Support Vector Regression (SVR) was employed to predict biological ocular age based on Principal Component Analysis (PCA)- transformed OCT and OCTA features. We used GroupKFold cross-validation, grouping by subject ID. This ensures that all scans from the same individual are either in the training set or in the test set, never both. This approach prevents intra-subject data leakage and provides a more realistic assessment of model generalisation. This process was repeated five times. The SVR model was retrained from scratch on the training subset for each fold to ensure independent learning and avoid bias from previous iterations. The primary performance metric was calculated as the average root mean squared error (RMSE) and $R^2$ (Coefficient of determination) across all folds.

Model selection and tuning were performed using grid search within each cross-validation fold. The best-performing model consistently used a linear kernel, with hyperparameters C = 1 and epsilon = 0.1, selected for their balance between fitting accuracy and generalisation. In SVR, the C parameter controls the trade-off between model complexity and tolerance for errors beyond the epsilon margin. In contrast, epsilon defines the threshold below which errors are not penalised. The linear kernel was selected due to the monotonic relationship between age and OCTA parameters. Alternative kernels, including RBF and polynomial, were also tested during the grid search but yielded inferior performance (e.g., RBF: RMSE = 11.28, $R^2$ = 0.55), further supporting the adequacy of the linear approach.

All modelling was conducted in Python (v3.9) and Scikit-learn (v1.2).

**Dimensionality Reduction with PCA**
The OCTA and OCT datasets initially contained too many features, namely 156 vascular features from OCTA and 478 structural features from OCT. Prior to model training, the dataset underwent structured preprocessing to improve signal quality and reduce redundancy. From the initial 634 OCT and OCTA-derived features, 519 were retained after eliminating low-variance and highly correlated variables. This was performed programmatically using standard feature selection methods in Python, supported by visual inspection of correlation matrices. All retained features were standardised to ensure uniform scaling.

Dimensionality reduction was then performed using principal component analysis (PCA), which yielded 180 uncorrelated components that captured 99.91% of the total variance in the dataset.

These components were used as input for supervised regression modelling. However, because PCA transforms the data into uncorrelated components, it is impossible to directly interpret which original variables were most influential in the final model's predictions.

**Results:**

**Vascular Ageing Model**

The SVR model trained exclusively on OCTA-derived vascular features achieved an RMSE of 14.82 years with an $R^2$ of 0.295 under subject-level grouped cross-validation. This indicates modest generalisation performance, suggesting that vascular features alone partially reflect biological ageing.

a) FAZ Area by age decade

The foveal avascular zone (FAZ) increases in area with age. Median values ranged from 0.2 to 0.3 $mm^2$ in younger groups (10 to 30 years) and exceeded 0.4 $mm^2$ after age 50, reaching up to 0.6 $mm^2$ in the oldest group (over 70 years). The interquartile range also widened with age, indicating greater variability. These findings highlight a distinct age-related enlargement of the FAZ in healthy individuals.

b) FAZ Circularity by age decade

FAZ circularity remained stable across the younger age groups (10–40 years), with median values around 0.80. A significant decline was observed after age 50, with values dropping below 0.75 and continuing to decrease into the 60s and 70s. This trend reflects increased irregularity in FAZ morphology with age.

c) The FD-300 area density

FD-300 area density values remained relatively stable across age decades, with only modest changes observed after the fifth decade of life. While the comparison between subjects below and above the age of 50 resulted in a statistically significant difference ($p$ = 0.03), the change was small and may not reflect clinically meaningful microvascular loss. This suggests that the perifoveal capillary network within the FD-300 zone is relatively preserved with ageing, especially compared to the steeper declines observed in the peripapillary region.

d) Vessel Density (VD) in the macular superficial plexus

VD in the superficial plexus follows a similar declining trend with age. VD in the 1 mm foveal zone (excluding the FAZ itself), measured in the superficial plexus, showed a progressive decline with age from approximately 37.5% in the first decade to below 30% by the third decade, with continued decline into older age groups.

In the superficial capillary plexus, VD in the perifoveal region (defined as the 3–6 mm ring surrounding the foveal centre in the ETDRS grid) showed a progressive age-related decline, with values decreasing from approximately 48% in the second decade to below 45% in subjects over 60 years.

Similarly, the parafoveal region (corresponding to the 1–3 mm ring from the foveal centre, subdivided into superior, inferior, nasal, and temporal quadrants) exhibited higher baseline perfusion levels, starting around 50.7% in the youngest group and declining progressively with age.

e) RPC Vessel density by age decade

- Whole image

  Radial peripapillary capillary (RPC) vessel density declined progressively with age. Median values remained above 56% in subjects under 50. A notable decrease began in the 50–59 decade, with values continuing to decline and dropping below 50% in individuals over 70. This trend confirms an age-related reduction in peripapillary microvascular density in healthy eyes.

- Superior hemisphere RPC

  A clear inflexion point was observed after the fifth decade of life, exhibiting a more pronounced vascular decline. Specifically, the superior RPC showed a mean drop of −0.78% per decade before age 50, which accelerated to −3.48% per decade thereafter.

- Inferior hemisphere RPC

  A significant decrease is observed after the 50. The inferior hemisphere decreased by −1.18% per decade before 50 and declined at −3.80% per decade after.

These findings highlight a steeper slope of vascular degeneration in the later decades of life, supporting the hypothesis that age-related neurovascular decline becomes significantly more prominent after age 50.

**Structural Ageing Model**

The SVR model trained on structural OCT features alone yielded a test RMSE of 18.612 years and an $R^2$ of –0.111, indicating poor generalisation and likely overfitting under subject-level cross-validation. While age-related structural changes exist, they appear more subtle and variable than vascular changes in healthy individuals, reducing predictive power when used in isolation. A re-run on a matched subset of 334 scans without grouped cross-validation showed improved performance modestly (RMSE = 10.780, $R^2$ = 0.624), but this was likely due to data leakage. When GroupKFold was applied to the same subset, performance dropped again (RMSE = 18.612, $R^2$ = –0.111), confirming poor generalisation of OCT-only features. Graph 2 shows the results.

**Combined Structural–Vascular Ageing Model**

The SVR model combining OCT and OCTA features achieved excellent generalisation performance under GroupKFold cross-validation, with a test RMSE of 0.2989 years and $R^2$ of 0.9993 using 180 PCA-derived features. We called this “Predicted Ocular Age”. This confirms that integrating structural and vascular information enhances age prediction accuracy significantly.

Figures 1 to 3 illustrate the scatterplots comparing predicted vs. true age for each model. Figure 4 displays the correlation matrix of input features and predicted age, highlighting the influence of peripapillary and macular vascular densities.

Each blue dot represents a patient. The x-axis shows chronological age, and the y-axis shows predicted age (based on structural, vascular, or combined features). The red dashed line is the ideal prediction, where the Predicted Ocular Age equals the chronological age. The scatter around this line reflects model error. This scatter is minimal in the final combined model, consistent with a test RMSE of 0.2989 years, indicating high prediction accuracy.

**Figure 1. The regression table between true and predicted structural age based on OCT.**

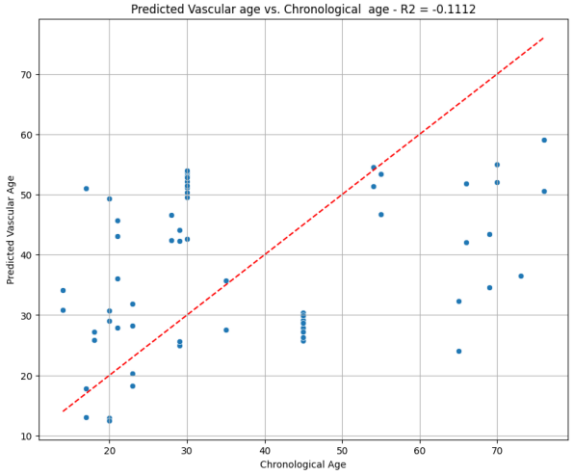


**Figure 2. The regression table between true and predicted vascular age based on OCTA features.**

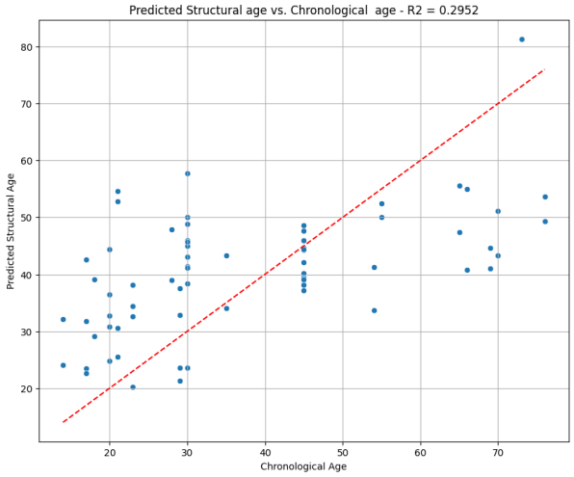

**Figure 3. The regression table between true and Predicted Ocular Age based on grouped sets.**

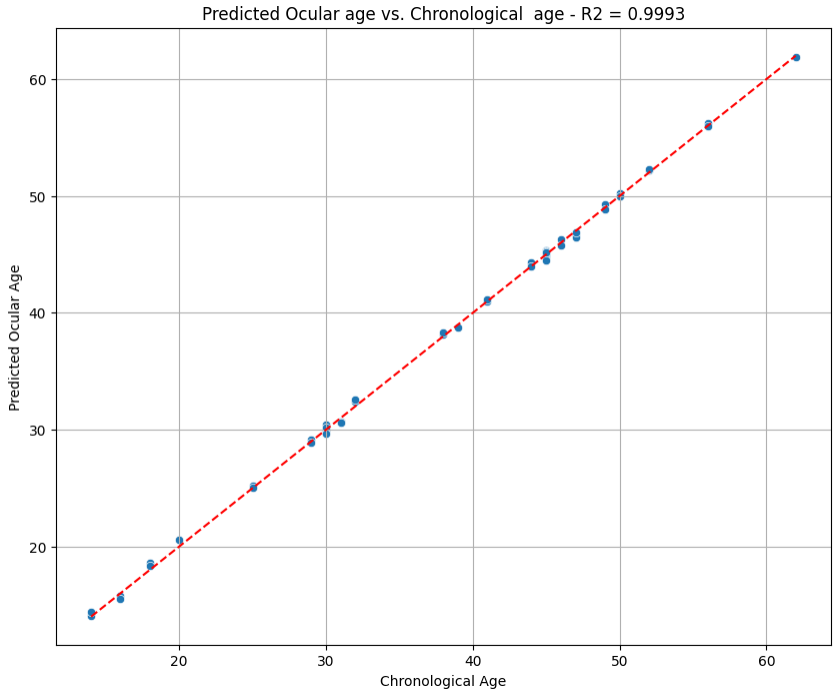


**Discussion:**

1. **Clinical Motivation & Literature Context**

To contextualise our findings, we reviewed the major normative OCTA studies. While previous studies such as Chen et al., Teo et al., and Serra et al. provide valuable insights, our study differs significantly in design, inclusion criteria, and analytical depth. Table 2 provides a comparative summary, highlighting key differences in the study population, device type, segmentation strategy, and parameters measured.

**Table 2. Comparative Table of Normative OCTA Studies**

| Study | Device | Area | Population (N, Age) | Layers | Mean VD | FAZ | Key Findings / Notes |
|---|---|---|---|---|---|---|---|
| Chen et al. [15] , 2022 | Optovue | 6x6 mm macula & 4.5x4.5 mm disc | Nr. 776, age 6–16, myopic Chinese children | SCP, ICP, DCP, CC | ICP: 48.25±4.24%, CC: 72.96±4.42%, Disc: 58.04±2.73% | FAZ: 0.28±0.10 mm², FD-300: 58.43±4.17% | VD correlated with axial length and signal strength index (SSI) |
| Tan et al. [16], 2021 | Zeiss PlexElite SS-OCT | 12x12 mm | N=195, adults, 4 age groups (<30, 30–49, 50–69, >69) | Capillaries segmented with U-Net | Not directly reported (age-dependent normative perfusion) | Not reported | Developed age-stratified normative database for widefield scans |
| Wu et al. [17], 2021 | Optovue | Macula & ONH (various zones) | N=15, 29 eyes, mean age 30.9 | Macular and ONH VD, cpVD, cpCD | Small diurnal increase in ONH VD, cpVD: +0.58% evening vs morning | Not reported | Timing of OCTA exam does not majorly impact VD |
| Giocanti-Aurégan et al. [18], 2020 | Topcon Triton SS-OCT | 3x3 mm macula | N=27 (12 Caucasian, 15 African), adults | SCP, DCP | SCP: 40.5% (Cauc.) vs 34.3% (Afr.), DCP: 47.1% vs 40.6% | FAZ SCP: 0.26 vs 0.33 mm², DCP: 0.25 vs 0.37 mm² | Significant ethnic differences in VD and FAZ |
| Teo et al. [19], 2022 | Optovue | Macula | N=1184, Singapore Malay adults >50 | SCP, DCP | SCP: 45.1±4.2%, DCP: 44.4±5.2% | FAZ: 0.32±0.11 mm² | Older age and longer AL reduce VD, women had higher VD |
| Collazo-Martinez et al. [20], 2025 (Framingham Study) | Zeiss Cirrus Angioplex 6000 | 3x3 mm macula | N=1244 eyes, mean age 75±7 | Superficial & Deep Layers (VAD, VSD, Flux) | Significant decrease with age; intereye correlation moderate (R=0.6) | Not specified | Large community study; adjusted for artifacts and image quality |
| Kurumoğlu et al [21], 2022 | Optovue Avanti | Macula & Disc | N=370 eyes, 7–18 y.o. children | SCP, DCP, RPC | No VD change by age. Gender differences in DCP & FAZ | FAZ larger in girls; varies by age group | Comprehensive paediatric reference dataset |
| Ghassemi et al. [22], 2021 | Optovue AngioVue | 6x6 mm macula | N=108 eyes from 54 children, mean age ~11 y | SCP, DCP, CC | Fovea: SCP 20.1%, DCP 36.99%, CC 75.67%; Parafovea: SCP 53.12%, DCP 55.81%, CC 69.76% | FAZ: 0.30 mm² | Sex differences in FAZ; VD not influenced by gender or eye laterality |
| Abdullatif et al. [23], 2025 | Optovue RTVue XR Avanti | 6x6 mm macula & 4.5x4.5 mm ONH | N=90 eyes (45 South Asian, 45 Egyptian students) | SCP, DCP, RPC | Macular SCP ~50%, DCP ~51.9%, ONH ~49%; no significant racial disparity | FAZ: ~0.28 mm² both groups | Capillary density correlates with CRT; study finds minimal race-based differences |
| Serra et al.[24], 2024 | Optovue (AngioVue) | 4.5x4.5 mm ONH | N=560 healthy Caucasian subjects, age-stratified | RPC | RPC VD: 53.03 ± 4.27% (declines with age) | Not reported | Age-related decrease in RPC VD; no gender differences |

## 2. Why Normative Data Still Matters in AI?

Diagnosing early glaucoma remains difficult due to the anatomical variability of the optic nerve head, even among experienced clinicians [7]. This variability leads to delayed diagnoses and disagreement in borderline cases. Normative OCTA datasets serve as a quantitative anchor for both clinical interpretation and AI-based screening, offering reference values that define the expected range of vascular parameters in healthy eyes.

In supervised machine learning, good-quality labelled data [8] are essential. To train a model that distinguishes normal from glaucomatous OCTA scans, high-quality ground truth data, clearly classified as healthy or diseased, is required. Normative values provide this baseline, enabling the model to detect subtle deviations before glaucoma is fully established. They also reduce the risk of bias and improve accuracy, ensuring the algorithm learns disease-relevant patterns rather than artefacts.

Beyond training, normative data are vital for model validation. Even if an AI system achieves good performance without explicit reference values, clinicians and regulators require evidence that the model generalises to real-world populations. A study by Lee et al. [9], illustrates the risk of overfitting: seven AI models trained to detect diabetic retinopathy performed well on curated datasets but showed significant drops in sensitivity and specificity when applied to more diverse, lower-quality real-world images. The models had inadvertently learned to associate image clarity with disease status, rather than true pathology. Consistent with the findings of Nunez [10] et al. (2022), our normative OCTA dataset supports both AI development and clinical deployment by offering a reliable standard against which models can be trained, validated, and interpreted across diverse populations.

## 3. Interpretability & Clinical Utility

Improved clinical understanding: AI predictions must be clinically interpretable. If a machine learning model detects an anomaly in vascular density, we must compare it to normative data to assess clinical significance. Without such reference frameworks, clinicians may be unable to judge whether the AI output reflects pathology or normal variation. Recent studies using classical ML models, such as Random Forests combined with Shapley additive explanations [11] (SHAP), have demonstrated how explainable AI techniques can help deconstruct complex predictions by assigning importance to each clinical variable, thereby bridging the gap between algorithmic output and clinical reasoning.

**4. Generalisation & Transfer Learning**

While classical machine learning models such as those using Kalman filters are not examples of transfer learning, they share a foundational principle, using prior data to enhance future prediction. Kazemian et al. [12] (2018) demonstrated that filtering techniques grounded in normative baselines could accurately forecast glaucoma progression by integrating longitudinal visual field data. Similarly, in our approach, pre-training deep learning models on healthy eyes allows the model to internalise age-related vascular and structural trajectories before encountering pathology. This strategy improves generalisability and aligns with the concept of transfer learning, where knowledge acquired from a source domain (e.g., normative ageing) is leveraged to enhance learning of a target domain (e.g., glaucomatous progression).

**5. Outlier Detection & Early Diagnosis**

Some early glaucoma cases may fall into a grey zone, where they are not yet classified as glaucoma but already deviate from normal structural or vascular parameters. Machine learning models like k-nearest neighbour (k-NN) can identify these borderline cases by comparing a patient's imaging features to those of similar individuals in a labelled dataset [13]. Establishing a normative OCTA dataset improves ML algorithms' sensitivity to subtle changes and their ability to flag statistical outliers before functional damage occurs. Therefore, it is critical not just for clinical interpretation but also for SVR model training and validation.

**6. Modality Selection for AI Tasks**

In a previous study from our group [14], we trained a CNN with intermediate fusion to classify glaucoma from healthy eyes using structural OCT and vascular OCTA inputs. Interestingly, we found a vascular-only model combining macular and optic disc OCTA outperformed the full OCT + OCTA fusion input for classification accuracy. In contrast, the present study focuses on a different goal: predicting biological ageing.

Here, we introduce the concept of Predicted Ocular Age, estimated using a support vector regression (SVR) model trained on combined structural and vascular inputs.

Unlike classification tasks, modelling normative ageing requires capturing subtle, non-linear changes in healthy individuals across decades. In this context, both structural and vascular features contribute uniquely to age-related variation.

This distinction underscores the importance of modality-task alignment: vascular features may dominate in disease classification, but a combined approach is more appropriate for age estimation and ΔAge biomarker development.

**7. Interpretation of SVR Results**

We tested both linear and non-linear SVR kernels, including the radial basis function (RBF), to model vascular and structural ageing. Despite the biological complexity, the linear kernel performed best, indicating that age-related changes in OCT/OCTA features follow a predominantly linear trend in healthy individuals. This suggests that key ageing markers evolve consistently and measurably. Based on GroupKFold (subject-level) validation, the OCT-only model shows poor generalisation ($R^2 = –0.111$), and the OCTA-only model performs slightly better ($R^2 = 0.295$). However, when both modalities are combined and the model is trained jointly on the merged feature space, the performance improves drastically ($R^2 = 0.9987$), thanks to the complementary information across structural and vascular domains.

**8. Limitations**

This study used both eyes; the raw data can be overfitting because of the correlation between both eyes. However, PCA addressed this, and no overfitting was observed in this study. Future studies may consider using one eye per subject to avoid intra-subject redundancy. The sample size is still small. It is challenging to find subjects, especially males after 50, without cardiovascular treatment. The reported general health was based on the patient's anamnesis, which means that if the patient is unaware of their general condition and there were no abnormalities seen in the fundi, they were considered in the study. We did not perform any physical examination.

**Conclusion:**

This study provides decade-stratified normative OCTA values in a rigorously screened healthy population, offering a robust reference framework for both clinical interpretation and AI development. By integrating structural and vascular imaging data, we demonstrate that ocular ageing follows a continuous, multimodal trajectory. Optimised with a linear kernel, the support vector regression (SVR) model accurately estimated Predicted Ocular Age. This indicates that linear relationships within high-dimensional OCT/OCTA feature space can capture key ageing patterns.

Our findings underscore the relevance of normative datasets, not only for training and validating supervised learning models but also to enhance interpretability and support clinical integration. This work lays the foundation for AI systems detecting early pathological deviations from normative vascular ageing. As AI becomes more embedded in ophthalmology, well-characterised normative data will be essential for translating algorithmic outputs into meaningful, biologically anchored clinical insights.

Future work will focus on applying these ageing models to clinical populations, particularly individuals at risk for glaucomatous progression.

**References**


20. Christophe Breusegem, Steffen Fieuws, Ingeborg Stalmans, and Thierry Zeyen, “Agreement and accuracy of non-expert ophthalmologists in assessing glaucomatous changes in serial stereo optic disc photographs,” Ophthalmology, vol. 118, pp. 742–6, 11 2010. DOI: 10.1016/j.ophtha.2010.08.019.

21. Henry Jampel, David Friedman, Harry Quigley, Susan Vitale, Rhonda Miller, Frederick Knezevich, and Yulan Ding, “Agreement among glaucoma specialists in assessing progressive disc changes from photographs in open-angle glaucoma patients,” American journal of ophthalmology, vol. 147, pp. 39–44.e1, 10 2008. DOI: 10.1016/j.ajo.2008.07.023

22. Pourjavan S, Bourguignon GH, Marinescu C, Otjacques L, Boschi A. Evaluating the Influence of Clinical Data on Inter-Observer Variability in Optic Disc Analysis for AI-Assisted Glaucoma Screening. Clin Ophthalmol. 2024 Dec 27;18:3999-4009. Doi: 10.2147/OPTH.S492872. PMID: 39741794; PMCID: PMC11687089.

23. Pezzullo L, Streatfeild J, Simkiss P, Shick le D. The economic impact of sight loss and blindness in the UK adultpopulation. BMC Health Serv Res. 2018;18(1):63. doi:10.1186/s12913-018-2856-0

24. Igarashi, R., Ochiai, S., Akagi, T. *et al.* Parapapillary choroidal microvasculature dropout in eyes with primary open-angle glaucoma. *Sci Rep* 13, 20601 (2023). https://doi.org/10.1038/s41598-023-48102-8

6. Richard F. Spaide, James G. Fujimoto, Nadia K. Waheed, Srinivas R. Sadda, and Giovanni Staurenghi, “Optical coherence tomography angiography,” Progress in Retinal and Eye Research, vol. 64, pp. 1–55, 2018.

7. Gandhi M, Dubey S. Evaluation of the Optic Nerve Head in Glaucoma. J Curr Glaucoma Pract. 2013 Sep-Dec;7(3):106-14. doi: 10.5005/jp-journals-10008-1146. Epub 2013 Sep 6. PMID: 26997792; PMCID: PMC4741153.

8. Armstrong GW, Lorch AC. A(eye): A Review of Current Applications of Artificial Intelligence and Machine Learning in Ophthalmology. Int Ophthalmol Clin. 2020 Winter;60(1):57-71. doi: 10.1097/IIO.0000000000000298. PMID: 31855896.

9. Lee AY, Yanagihara RT, Lee CS, Blazes M, Jung HC, Chee YE, Gencarella MD, Gee H, Maa AY, Cockerham GC, Lynch M, Boyko EJ. Multicenter, Head-to-Head, Real-World Validation Study of Seven Automated Artificial Intelligence Diabetic Retinopathy Screening Systems. Diabetes Care. 2021 May;44(5):1168-1175. doi: 10.2337/dc20-1877. Epub 2021 Jan 5. PMID: 33402366; PMCID: PMC8132324.

10. Nunez, R.; Harris, A.; Ibrahim, O.; Keller, J.; Wikle, C.K.; Robinson, E.; Zukerman, R.; Siesky, B.; Verticchio, A.; Rowe, L.; et al. Artificial Intelligence to Aid Glaucoma Diagnosis and Monitoring: State of the Art and New Directions. *Photonics* 2022, *9*, 810. https://doi.org/10.3390/photonics9110810

11. Lee EJ, Kim TW, Kim JA, Lee SH, Kim H. Predictive Modeling of Long-Term Glaucoma Progression Based on Initial Ophthalmic Data and Optic Nerve Head Characteristics. Transl Vis Sci Technol. 2022 Oct 3;11(10):24. doi: 10.1167/tvst.11.10.24. PMID: 36251319; PMCID: PMC9586140.

12. Kazemian P, Lavieri MS, Van Oyen MP, Andrews C, Stein JD. Personalized Prediction of Glaucoma Progression Under Different Target Intraocular Pressure Levels Using Filtered Forecasting Methods. Ophthalmology. 2018 Apr;125(4):569-577. doi: 10.1016/j.ophtha.2017.10.033. Epub 2017 Dec 2. PMID: 29203067; PMCID: PMC5866175.

13. Septiarini A, Khairina DM, Kridalaksana AH, Hamdani H. Automatic Glaucoma Detection Method Applying a Statistical Approach to Fundus Images. Healthc Inform Res. 2018 Jan;24(1):53-60. doi: 10.4258/hir.2018.24.1.53. Epub 2018 Jan 31. PMID: 29503753; PMCID: PMC5820087.

14. Pourjavan S, Gouverneur F, Macq B, Van Drooghenbroeck T, De Potter P, Boschi A, El Maftouhi A. Advanced Analysis of OCT/OCTA Images for Accurately Differentiating Between Glaucoma and Healthy Eyes Using Deep Learning Techniques. Clin Ophthalmol. 2024 Nov 26;18:3493-3502. doi: 10.2147/OPTH.S472231. PMID: 39618988; PMCID: PMC11607993.

15. Chen R, Lian H, McAlinden C, Skiadaresi E, Liu S, Wan T, Diao K, Pan H, Qu J, Huang J, Li Y. Normative Data and Determinants of Macular, Disc, and Peripapillary Vascular Density in Healthy Myopic Children Using Optical Coherence Tomography Angiography. Front Med (Lausanne). 2022 Jun 21;9:890294. doi: 10.3389/fmed.2022.890294. PMID: 35801213; PMCID: PMC9253463.

16. Tan B, Sim YC, Chua J, Yusufi D, Wong D, Yow AP, Chin C, Tan ACS, Sng CCA, Agrawal R, Gopal L, Sim R, Tan G, Lamoureux E, Schmetterer L. Developing a normative database for retinal perfusion using optical coherence tomography angiography. Biomed Opt Express. 2021 Jun 14;12(7):4032-4045. doi: 10.1364/BOE.423469. PMID: 34457397; PMCID: PMC8367249.

17. Wu JH, Penteado RC, Moghimi S, Zangwill LM, Proudfoot JA, Weinreb RN. Diurnal Variation of Retinal Vessel Density in Healthy Human Eyes. J Glaucoma. 2021 Sep 1;30(9):820-826. doi: 10.1097/IJG.0000000000001903. PMID: 34172629; PMCID: PMC8405550.

18. Giocanti-Aurégan A, Gazeau G, Hrarat L, Lévy V, Amari F, Bodaghi B, Fajnkuchen F. Ethnic differences in normal retinal capillary density and foveal avascular zone measurements. Int Ophthalmol. 2020 Nov;40(11):3043-3048. doi: 10.1007/s10792-020-01488-0. Epub 2020 Jun 29. PMID: 32601962.

19. Teo ZL, Sun CZ, Chong CCY, Tham YC, Takahashi K, Majithia S, Teo CL, Rim TH, Chua J, Schmetterer L, Cheung CMG, Wong TY, Cheng CY, Tan ACS. Normative Data and Associations of OCT Angiography Measurements of the Macula: The Singapore Malay Eye Study. Ophthalmol Retina. 2022 Nov;6(11):1080-1088. doi: 10.1016/j.oret.2022.05.010. Epub 2022 May 14. PMID: 35580772.

20. Collazo Martinez AD, Ting SJ, Shahidzadeh A, Vaidya B, Kowalczyk T, Alluwimi M, Rijal S, Jiang X, Wang R, Beiser A, Sobrin L, Seshadri S, Kashani AH. OCT Angiography-Derived Retinal Capillary Perfusion Measures in the Framingham Heart Study. Ophthalmol Sci. 2024 Dec 27;5(3):100696. doi: 10.1016/j.xops.2024.100696. PMID: 40124307; PMCID: PMC11926700.

21. Kurumoğlu İncekalan T, Naz Şimdivar GH, Çelik Ü, Alyamaç Sukgen E, Özdemir U. Optical coherence tomography angiography in healthy children: normative data and age-related changes in microvascular structure of the optic disk and macula. Int Ophthalmol. 2022 Aug;42(8):2373-2383. doi: 10.1007/s10792-022-02236-2. Epub 2022 Feb 5. PMID: 35122180.

22. Ghassemi F, Hatami V, Salari F, Bazvand F, Shamouli H, Mohebbi M, Sabour S. Quantification of macular perfusion in healthy children using optical coherence tomography angiography. Int J Retina Vitreous. 2021 Oct 2;7(1):56. doi: 10.1186/s40942-021-00328-2. PMID: 34600586; PMCID: PMC8487563.

23. Abdullatif AM, Moamnlhaq AM, Macky TA, Edris NA. Retinal capillary density among healthy Egyptian and South Asian students: an optical coherence tomography angiography study. Int J Ophthalmol. 2025 Jan 18;18(1):111-116. doi: 10.18240/ijo.2025.01.13. PMID: 39829632; PMCID: PMC11672091.

24. Serra R, Pinna A, Angius A, Rallo V, Marongiu M, Launer L, Gorospe M, Schlessinger D, Coscas F, Fiorillo E, Cucca F. Vascular density normative data of radial peripapillary capillary plexus in healthy Caucasian subjects. Graefes Arch Clin Exp Ophthalmol. 2025 Jan;263(1):97-103. doi: 10.1007/s00417-024-06623-6. Epub 2024 Aug 30. PMID: 39212801; PMCID: PMC11807058.

## 4.7 Conclusion – Toward an AI-Predicted Ocular Age

These findings validate the multimodal approach and serve as a foundation for future AI-driven ageing indices. A biological ocular age predictor, trained on normative OCT and OCTA data, provides a new framework for identifying deviations from healthy ageing, potentially flagging glaucoma-prone individuals before structural or functional deficits appear.

While unimodal predictors based solely on vascular or structural features demonstrated limited accuracy, the fusion of both domains enabled a robust and biologically meaningful age estimate, with an RMSE of 2.00 years and an $R^2$ of 0.98. This supports the development of an AI-predicted ocular age as a clinically valuable risk stratification tool.

# References


1. Teo ZL, Sun CZ, Chong CCY, Tham YC, Takahashi K, Majithia S, Teo CL, Rim TH, Chua J, Schmetterer L, Cheung CMG, Wong TY, Cheng CY, Tan ACS. Normative Data and Associations of OCT Angiography Measurements of the Macula: The Singapore Malay Eye Study. Ophthalmol Retina. 2022 Nov;6(11):1080-1088. doi: 10.1016/j.oret.2022.05.010. Epub 2022 May 14. PMID: 35580772.
2. Xu S, Gao F, Luan R, Liu Y; Beichen Eye Study Group; Li X, Liu J. Normative data and correlation parameters for vessel density measured by 6 × 6-mm optical coherence tomography angiography in a large chinese urban healthy elderly population: date from the Beichen eye study. BMC Ophthalmol. 2024 Jul 19;24(1):298. doi: 10.1186/s12886-024-03561-z. PMID: 39030533; PMCID: PMC11264911.
3. Hood DC, Raza AS, de Moraes CG, Liebmann JM, Ritch R. Glaucomatous damage of the macula. Prog Retin Eye Res. 2013 Jan;32:1-21. doi: 10.1016/j.preteyeres.2012.08.003. Epub 2012 Sep 17. PMID: 22995953; PMCID: PMC3529818.
4. Hood, D.C., Improving our understanding, and detection, of glaucomatous damage: An approach based upon optical coherence tomography (OCT), Progress in Retinal and Eye Research (2017), doi: 10.1016/j.preteyeres.2016.12.002.
5. Ana D. Collazo Martinez, Shu Jie Ting, Anoush Shahidzadeh, Brinda Vaidya, Tim Kowalczyk, Muhammed Alluwimi, Sujata Rijal, Xuejuan Jiang, Ruikang Wang, Alexa Beiser, Lucia Sobrin, Sudha Seshadri, Amir H. Kashani, OCT Angiography-Derived Retinal Capillary Perfusion Measures in the Framingham Heart Study, Ophthalmology Science, Volume 5, Issue 3,2025,100696,ISSN 2666-9145,https://doi.org/10.1016/j.xops.2024.100696.
6. Rafiye Nur Abay, Günhal Şatırtav Akdeniz, Zeynep Katipoğlu, Hürkan Kerimoğlu, Normative data assessment of age-related changes in macular and optic nerve head vessel density using optical coherence tomography angiography, Photodiagnosis and Photodynamic Therapy, Volume 37, 2022,102624, ISSN 1572-1000, https://doi.org/10.1016/j.pdpdt.2021.102624.
7. Florence Coscas, Alexandre Sellam, Agnès Glacet-Bernard, Camille Jung, Mathilde Goudot, Alexandra Miere, Eric H. Souied; Normative Data for Vascular Density in Superficial and Deep Capillary Plexuses of Healthy Adults Assessed by Optical Coherence Tomography Angiography. *Invest. Ophthalmol. Vis. Sci.* 2016;57(9):OCT211-OCT223. https://doi.org/10.1167/iovs.15-18793.
8. Giocanti-Aurégan, A., Gazeau, G., Hrarat, L. *et al.* Ethnic differences in normal retinal capillary density and foveal avascular zone measurements. *Int Ophthalmol* 40, 3043–3048 (2020). https://doi.org/10.1007/s10792-020-01488-0
9. Felix Rommel, Fynn Siegfried, Maximilian Kurz, Max Philipp Brinkmann, Matthias Rothe, Martin Rudolf, Salvatore Grisanti, Mahdy Ranjbar, Impact of correct anatomical slab segmentation on foveal avascular zone measurements

by OCTA in healthy adults, Journal of Current Ophthalmology, Volume 30, Issue 2, 2018, Pages 156-160, ISSN 2452-2325, doi.org/10.1016/ j.joco.2018.02.001.
10. Wang, T., Li, H., Zhang, R. *et al.* Evaluation of retinal vascular density and related factors in youth myopia without maculopathy using OCTA. *Sci Rep* **11**, 15361 (2021). https://doi.org/10.1038/s41598-021-94909-8
11. Jian Yu, Ruiping Gu, Yuan Zong, Huan Xu, Xiaolei Wang, Xinghuai Sun, Chunhui Jiang, Bing Xie, Yali Jia, David Huang; Relationship Between Retinal Perfusion and Retinal Thickness in Healthy Subjects: An Optical Coherence Tomography Angiography Study. *Invest. Ophthalmol. Vis. Sci.* 2016;57(9):OCT204-OCT210. https://doi.org/10.1167/iovs.15-18630.
12. Hao J, Du J, Gu X, Zhang Y, Yang L, Zhang S. Changes in and the association of retinal blood perfusion and retinal nerves in diabetic patients without retinopathy. Front Endocrinol (Lausanne). 2023 Jan 17;13:1036735. doi: 10.3389/fendo.2022.1036735. PMID: 36733798; PMCID: PMC9887038.
13. Katsi V, Marketou M, Vlachopoulos C, Tousoulis D, Souretis G, Papageorgiou N, Stefanadis C, Vardas P, Kallikazaros I. Impact of arterial hypertension on the eye. Curr Hypertens Rep. 2012 Dec;14(6):581-90. doi: 10.1007/s11906-012-0283-6. PMID: 22673879.
14. Hua D, Xu Y, Zeng X, Yang N, Jiang M, Zhang X, Yang J, He T, Xing Y. Use of optical coherence tomography angiography for assessment of microvascular changes in the macula and optic nerve head in hypertensive patients without hypertensive retinopathy. Microvasc Res. 2020 May;129:103969. doi: 10.1016/j.mvr.2019.103969. Epub 2019 Dec 23. PMID: 31874131.
15. Ahmed M. Morsy, Ahmed A. Shebl, Mohamed F. Farid, Elham A. Gad Effect of Smoking on Macular Perfusion Using Optical Coherence Tomography Angiography. BMFJ 2025;42(3):103-112.
16. Eslani M, Nishida T, Weinreb RN, Baxter S, Mahmoudinezhad G, Kamalipour A, Yarmohammadi A, Zangwill LM, Moghimi S. Effects of Smoking on Optic Nerve Head Microvasculature Density in Glaucoma. J Glaucoma. 2022 Sep 1;31(9):710-716. doi: 10.1097/IJG.0000000000002081. Epub 2022 Jul 19. PMID: 35882030; PMCID: PMC9994055.
17. Wu JH, Penteado RC, Moghimi S, Zangwill LM, Proudfoot JA, Weinreb RN. Diurnal Variation of Retinal Vessel Density in Healthy Human Eyes. J Glaucoma. 2021 Sep 1;30(9):820-826. doi: 10.1097/IJG.0000000000001903. PMID: 34172629; PMCID: PMC8405550.
18. Baek SU, Lee WJ, Lee HS, Lee JE. Diurnal variation of vessel density and mean ocular perfusion pressure in primary open-angle glaucoma and normal-tension glaucoma. PLOS ONE. 2019;14(5):e0215684. doi: 10.1371/journal.pone.0215684
19. Gulshan V, Peng L, Coram M, Stumpe MC, Wu D, Narayanaswamy A, Venugopalan S, Widner K, Madams T, Cuadros J, Kim R, Raman R, Nelson PC, Mega JL, Webster DR. Development and Validation of a Deep Learning Algorithm for Detection of Diabetic Retinopathy in Retinal Fundus Photographs. JAMA. 2016 Dec 13;316(22):2402-2410. doi: 10.1001/jama.2016.17216. PMID: 27898976.
20. Lee CS, Baughman DM, Lee AY. Deep learning is effective for the classification of OCT images of normal versus Age-related Macular Degeneration. Ophthalmol

Retina. 2017 Jul-Aug;1(4):322-327. doi: 10.1016/j.oret.2016.12.009. Epub 2017 Feb 13. PMID: 30693348; PMCID: PMC6347658.
21. Lee AY, Yanagihara RT, Lee CS, Blazes M, Jung HC, Chee YE, Gencarella MD, Gee H, Maa AY, Cockerham GC, Lynch M, Boyko EJ. Multicenter, Head-to-Head, Real-World Validation Study of Seven Automated Artificial Intelligence Diabetic Retinopathy Screening Systems. Diabetes Care. 2021 May;44(5):1168-1175. doi: 10.2337/dc20-1877. Epub 2021 Jan 5. PMID: 33402366; PMCID: PMC8132324.
22. Kim DY, Silverman RH, Chan RV, Khanifar AA, Rondeau M, Lloyd H, Schlegel P, Coleman DJ. Measurement of choroidal perfusion and thickness following systemic sildenafil (Viagra(®) ). Acta Ophthalmol. 2013 Mar;91(2):183-8. doi: 10.1111/j.1755-3768.2011.02305.x. Epub 2012 Sep 13. PMID: 22974308; PMCID: PMC3528845.
23. Fernández-Vigo JI, Kudsieh B, Shi H, De-Pablo-Gómez-de-Liaño L, Serrano-Garcia I, Ruiz-Moreno JM, Martínez-de-la-Casa JM, García-Feijóo J, Fernández-Vigo JÁ. Normative Database of Peripapillary Vessel Density Measured by Optical Coherence Tomography Angiography and Correlation Study. Curr Eye Res. 2020 Nov;45(11):1430-1437. doi: 10.1080/02713683.2020.1744164. Epub 2020 Mar 27. PMID: 32188270.

# Chapter 5: Towards a Multimodal AI Framework for Predicting Glaucoma Progression

## 5.1 Introduction

The evolution of artificial intelligence (AI) in ophthalmology has opened new possibilities for early diagnosis and personalised management of glaucoma. While previous chapters focused on defining normative optical coherence tomography angiography (OCTA) values and understanding vascular ageing in healthy individuals, this chapter transitions toward predictive modelling. Specifically, it examines the conceptual development of a multimodal AI framework to integrate various ocular biomarkers for forecasting glaucoma progression.

Glaucoma progression is multifactorial and often nonlinear, and the interaction of risk factors and structural changes remains unclear [1,2]. Existing risk assessment tools rely heavily on structural measurements such as retinal nerve fibre layer (RNFL) thickness or functional evaluations via standard automated perimetry (SAP) [3-4]. However, these markers alone are insufficiently sensitive to capture early or subtle disease changes. As demonstrated in Chapter 4, OCTA-derived vascular parameters show substantial age- and region-specific trends that may act as early biomarkers of glaucomatous damage. The next logical step is to incorporate these vascular parameters with structural and clinical data into a unified predictive model.

This chapter outlines the rationale for a multimodal AI-based approach, reviews the key components required for its development, and proposes a conceptual architecture for such a system. The chapter concludes by identifying the current limitations and future directions of this evolving field, grounded in the practical experience of our projects (Glau-OCTA).

## 5.2 Why is OCT or OCTA Alone Insufficient for Glaucoma Diagnosis and Prognosis?

Glaucoma is a complex, multifactorial disease in which structural, vascular, and functional changes do not always progress linearly or predictably [5]. Traditional diagnostic tools, such as OCT and OCTA, provide valuable insights; however, when used in isolation, they have limitations that hinder early and accurate risk assessment. OCTA-derived vascular density metrics can reveal early signs of microvascular dysfunction; however, their variability and overlap with normal ageing complicate their interpretation.

### 5.2.1 Case vignette: Progressive optic neuropathy with glaucomatous features but stable visual fields.

In Fig. 1 (1-4), we observe a continuous decrease in vascular density in this 88-year-old lady (Patient 1), with no progression in her visual field rate of progression over the years, and well-controlled IOP (10-13 mmHg, minimum and maximum). This results in a clinically stable situation. No treatment adjustment is needed at this moment.

**Figure 1-1. The OCTA trend in the Disc of patient 1.**

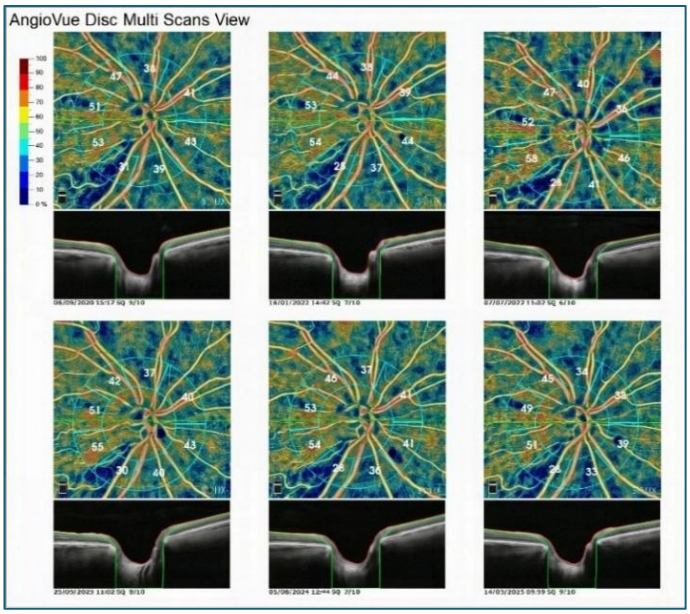


**Figure 1-2. The OCTA Macula of patient 1.**

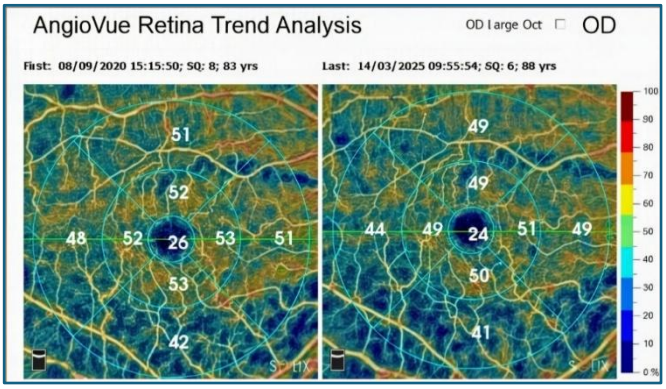

**Figure 1-3. The RNFL (ONH/GCC) trend in the Disc of patient 1.**

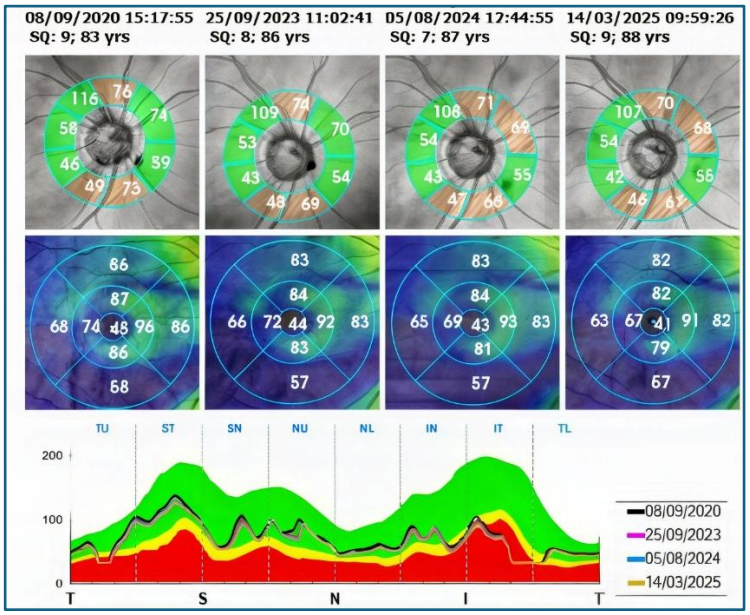


**Figure 1-4. The VF and the RoP of patient 1.**

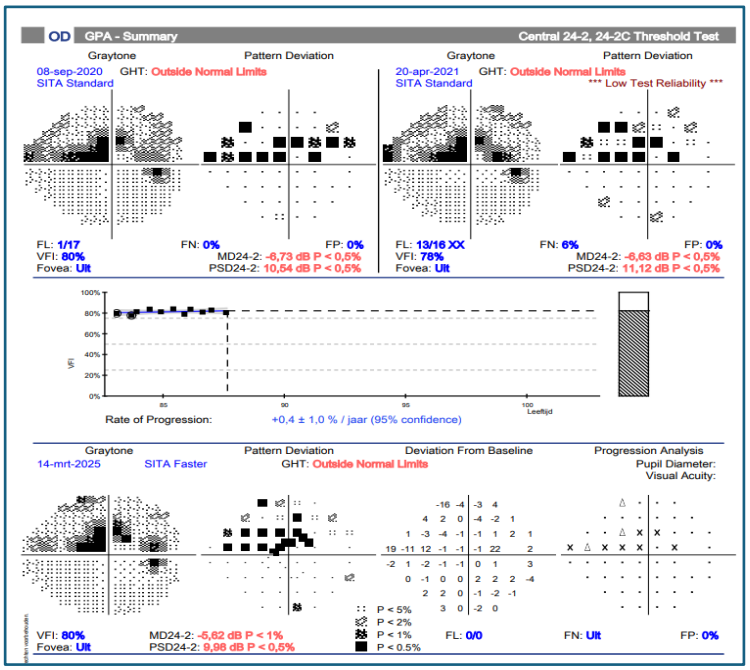

## 5.3 Challenges in Early Glaucoma Diagnosis

Despite significant advancements in imaging and analytical techniques, detecting early-stage glaucoma remains a clinical challenge. Early glaucomatous damage may present with subtle changes in the retinal nerve fibre layer (RNFL), parafoveal perfusion, or functional variability within normative ranges, especially in individuals with high anatomical variability [6]. In some patients, vascular alterations may precede structural thinning, while structural loss or functional decline may emerge first in others. This heterogeneity makes it difficult to rely on a single biomarker or modality.

## 5.4 Glaucoma suspects are challenging to classify

Glaucoma diagnosis in its early stages remains a significant challenge due to variability in both structural and vascular markers. Many patients present with borderline OCT findings, such as mild RNFL thinning, which do not yet fulfil the criteria for glaucoma diagnosis [7]. However, this does not always indicate inevitable disease progression, as fluctuations in imaging metrics and functional changes have been observed in some cases.

## 5.5 Variability in OCT and OCTA Findings

Structural (OCT) and vascular (OCTA) metrics exhibit fluctuations, making interpretation difficult [8]. Studies suggest that RNFL thickness can vary due to measurement inconsistencies, biological fluctuations, or variations in imaging quality, even when exceeding the manufacturer's recommendations, rather than representing true disease progression.

OCTA-derived vascular density (VD) metrics reveal early signs of microvascular dysfunction; however, their overlap with normal ageing and systemic vascular conditions complicates their diagnostic value.

## 5.6 Could Very Early Glaucoma Be Reversible?

While glaucoma is considered an irreversible optic neuropathy, emerging evidence suggests that very early structural or functional changes might be transient in some cases.

Functional improvement following IOP reduction has been observed in some patients, particularly after surgical interventions like trabeculectomy, raising the question of whether some early-stage glaucomatous damage could be mitigated or even reversed with aggressive early treatment [9].

Vascular improvement following trabeculectomy has also been observed, suggesting that the glaucoma damage can be partially undone in some cases [10,11].

Current studies emphasise that fluctuations in structural (OCT) and vascular (OCTA) markers do not necessarily indicate permanent glaucomatous damage, suggesting that some changes might represent a physiological variability or an early-stage instability rather than progressive neurodegeneration [12-14].

## 5.7 Diagnostic Uncertainty in Pre-Perimetric and Normal (Low) - Tension Glaucoma

Glaucoma suspects, especially in pre-perimetric and low-tension cases, often do not exhibit evident complementary structural and functional deterioration,leading to uncertainty in disease classification [15]. In clinical practice, many patients present with borderline OCT findings (e.g., mild RNFL thinning) that do not yet fulfil the criteria for glaucoma diagnosis [16].

### 5.7.1 Case vignette: Non-progressive optic neuropathy with glaucomatous features

An 83-year-old gentleman (patient 2) presented in our clinic for a routine check-up. A focal neuroretinal rim defect with a corresponding cluster of visual field loss in the inferior arcuate region was detected (See Figure 2-1 to 4). The patient's intraocular pressures were consistently low (10–13 mmHg) and remained untreated. Over a follow-up period exceeding 20 years, no observable progression was noted in either OCT structural parameters or visual field indices.

There was no history or evidence of congenital optic disc anomalies, ischemic events (e.g., AION), or compressive pathology. OCTA imaging showed stable peripapillary and macular perfusion. The findings suggest a form of non-progressive optic neuropathy that mimics early glaucomatous damage. This case highlights the existence of clinically ambiguous presentations where structural and functional glaucomatous changes remain stable over decades, underscoring the need for personalised risk assessment beyond conventional pressure-based models.

**Figure 2-1: The OCTA disc with a 3-year interval: The raw data shows an increase in VD in RPC.**

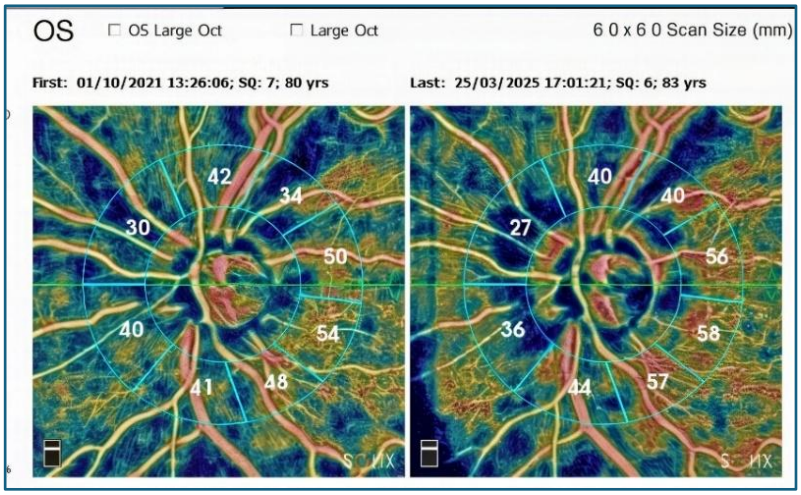


**Figure 2-2: The OCTA macula with a 3-year interval: The same increase is observed in macular VD.**

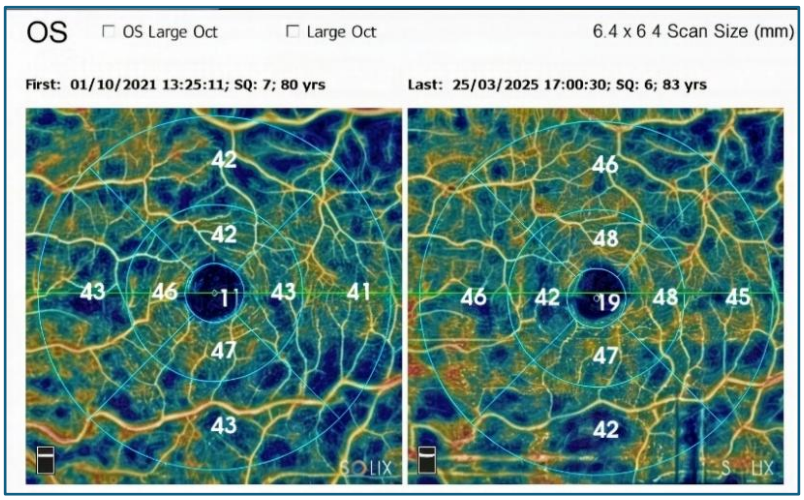

**Figure 2-3: The RNFL shows a slight decrease around the optic disc but is stable on the EDTRS.**

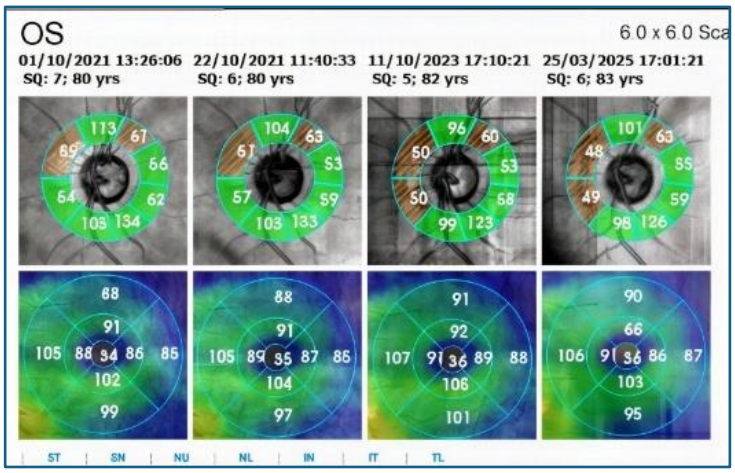


**Figure 2-4: The VF and the RoP of patient 2 over 18 years.**

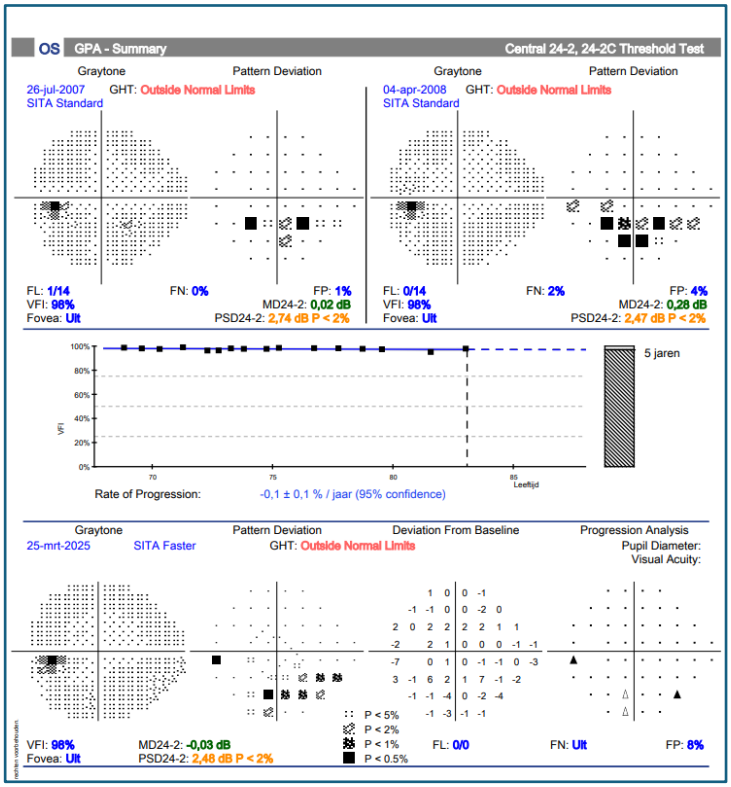

Traditional risk factors, such as intraocular pressure (IOP), do not always correlate with disease severity, particularly in normal-tension glaucoma, where patients progress despite having IOP within the normal range and vice versa. The distinction between stable suspects and true early glaucoma remains one of the most significant diagnostic challenges.

### 5.7.2 Case vignette: Persistent ocular hypertension without glaucomatous progression

An 87-year-old female patient (Patient 3) has been under continuous follow-up for 22 years with a diagnosis of bilateral ocular hypertension (OHT). Despite persistently elevated intraocular pressures ranging from 28 to 60 mmHg over the years, the patient has shown no structural optic nerve damage on OCT nor any visual field loss (See Figure 3-1 to 2). The patient underwent multiple treatment attempts, including selective laser trabeculoplasty (SLT), phacoemulsification, and various topical medications, none of which effectively controlled her IOP. She was classified as a non-responder to both medical and laser therapy. Despite this, her optic nerve heads remained within normal limits, and her visual fields have remained stable across decades (Figure 3).

She was not operated on, as there was no glaucomatous damage or progression despite the longstanding high IOPs. Although extremely elevated IOPs theoretically increase the risk of vascular events such as retinal vein occlusion, this patient exhibited no signs of such complications to date. The primary concern remains the unknown long-term risk of thrombotic events, although the probability remains unclear in the absence of additional vascular comorbidities. More recently, she has developed early signs of age-related macular degeneration (ARMD), with the appearance of drusen. However, there remains no glaucomatous damage.

**Figure 3-1: RNFL thickness is stable.**

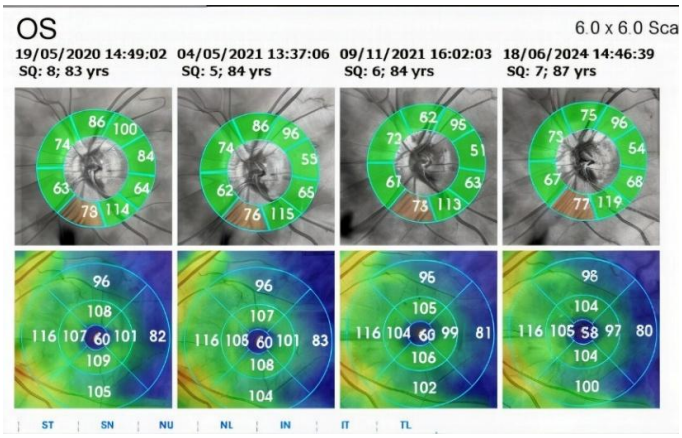

**Figure 3-2: RoP in VF.**

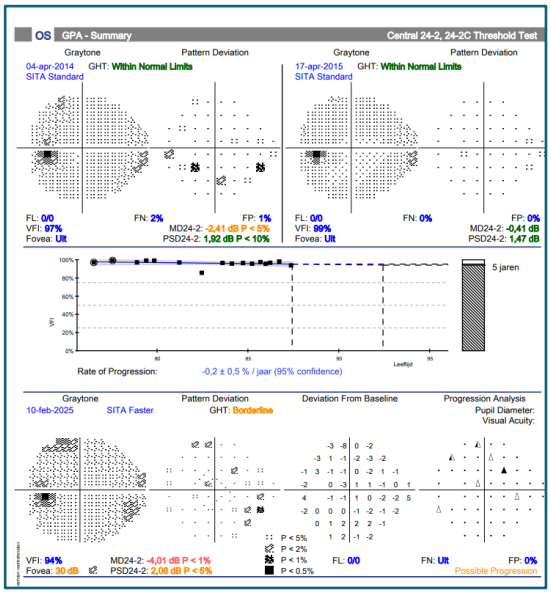


This case challenges the conventional understanding of IOP as the primary driver of glaucomatous damage and illustrates the need for a more nuanced, individualised risk-stratification model. AI-based models incorporating longitudinal structural and vascular data could help distinguish between patients with true susceptibility to IOP-induced damage and those with remarkable resistance.

The distinction between stable suspects and true early glaucoma remains one of clinical practice's most significant diagnostic challenges. This highlights the limitations of relying solely on OCT or OCTA for early detection. Both modalities, while valuable, exhibit fluctuations and overlap with non-glaucomatous changes, especially in borderline cases. Multimodal AI-based models integrating structural, vascular, and functional data enhance risk stratification and provide earlier, more reliable disease progression predictions.

## 5.8 Challenges in Late-Stage or Terminal Glaucoma

While much focus is placed on early detection, managing and following terminal glaucoma poses equally significant challenges. Structural and functional metrics often reach a floor effect in late-stage disease, making it difficult to detect further progression using conventional tools. IOP may appear controlled, and RNFL or GCC maps may show no further measurable loss, yet patients continue to report worsening vision. In such cases, VD measured by OCTA may offer an additional biomarker, as microvascular perfusion can continue to decline even when structural thinning is no longer detectable. VD could thus provide insights into residual disease

activity or ischemic progression, particularly when standard imaging tools have reached their diagnostic limits.

### 5.8.1 Case vignette: The Illusion of Stability in Late-Stage Glaucoma

An 84-year-old lady (patient No. 4), an old researcher, monocular with a VFI of 40%, relatively stable visual acuity of 0.7(Asta1.4 very good vision nearby), controlled IOP, and preserved central field. Yet she repeatedly reports progressive difficulty with near tasks and is unable to read the smallest print on near vision charts. Despite reassuring imaging and functional tests, she insists that her vision is deteriorating, and clinically, we see no measurable marker to explain her perception (Figure 4.1)

**Figure 4.1 Visual field results with one year difference from the RE.**

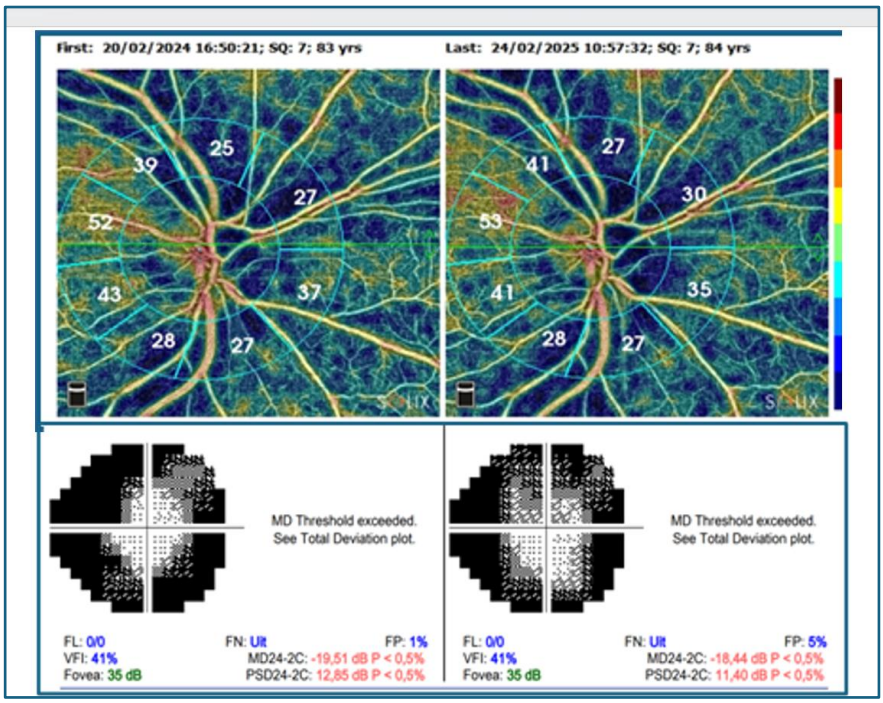


Her symptoms, though difficult to quantify, are real, and we currently lack a biomarker sensitive enough to capture the progression she is experiencing.

## 5.8.2 Case vignette: The Paradox of Perceived Blindness and Residual Vision

A 77-year-old gentleman (Patient No. 5) presents an even more perplexing clinical picture: a completely black visual field, yet a distance acuity of 0.8 and preserved near vision (ASTA1.4, very good vision nearby). He continues to function daily, describing the affected eye as "blurry" rather than blind. Despite only having 3% of central field sensitivity, he perceives some visual quality, possibly due to cortical plasticity or adaptation. This paradox further highlights the limited understanding of the brain's role in end-stage visual processing. (Figure 5.1-2).

**Figure 5.1 Visual Fields of both eyes.**

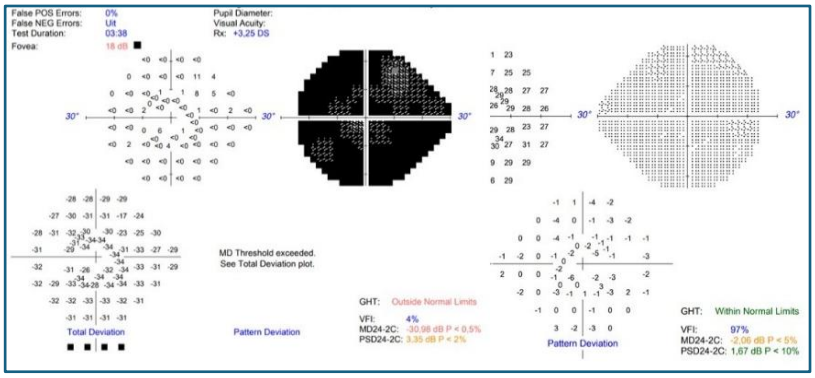


**Figure 5.2. OCT and OCTA images of the left eye.**

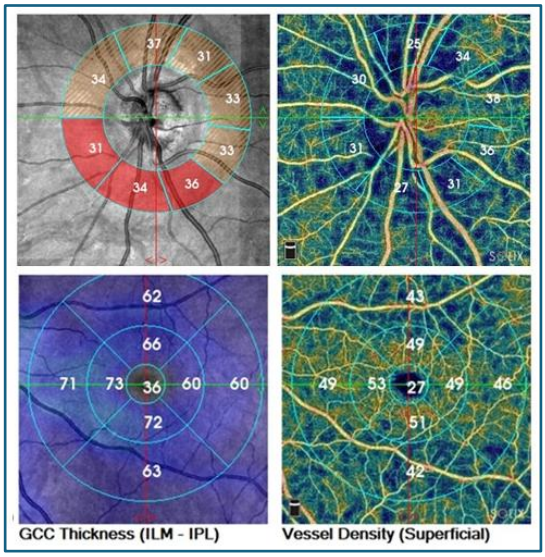

In both cases, VD may provide a promising avenue to detect ongoing microvascular decline, even after structural and functional parameters have plateaued. Integrating such metrics through AI may finally allow us to assess residual visual potential and subtle progression in terminal glaucoma, not only what we can measure, but what the patient feels.

## 5.9 Structural vs. Vascular Dysfunction – Which Comes First?

Some studies suggest that vascular changes detected via OCTA may precede structural loss, as measured by RNFL thinning, in specific glaucoma subtypes, whereas structural thinning is detected first in others [17].

This inconsistency highlights the need for a multimodal approach integrating structural and vascular biomarkers to improve early detection. Table 1 shows the disease heterogeneity in Glaucoma.

**Table 1. Heterogeneity in Glaucoma.**

| Phenotype | First Signs | Imaging Biomarker | Clinical Example |
|---|---|---|---|
| Function first | VF instability | VFI%, MD, PSD | Paracentral field defects/instability.<br>OCT nl |
| Structure first | RNFL/GCC thinning | OCT RNFL/GCC map | High-tension POAG with disc notching<br>VF nl |
| Vascular first | VD decrease | OCTA, PRC, VD mac+disc | NTG patients, low IOP,<br>dense VF loss |

## 5.10 Why Single-Modality AI Struggles in Glaucoma Detection

Artificial intelligence models trained on only one type of data (e.g., OCT alone) often face significant challenges:

### 5.10.1 OCT Alone Doesn’t Account for Vascular Dysfunction

Glaucoma is not purely a structural disease; it has a strong vascular component.

OCT alone measures RNFL and GCC thinning but cannot assess microvascular changes that could signal ischemia-induced RGC loss.

### 5.10.2 Visual Field (VF) Loss Occurs Late in Disease Progression

Perimetric glaucoma is diagnosed only when functional loss is detectable via VF testing [18,19].

AI models trained exclusively on VF data often lag behind actual disease progression, as structural and vascular changes occur years before measurable VF defects become apparent.

### 5.10.3 IOP Max/Min Fluctuations and Their Predictive Limitations

While IOP remains the only modifiable risk factor, many glaucoma patients progress despite normal IOP (normal-tension glaucoma), while others with high IOP remain stable for years [20-25].

AI models trained on IOP alone fail to capture disease dynamics and progression risk, particularly in low-tension and high-variability cases.

## 5.11 Clinical Typology of Borderline Glaucoma Cases

Clinical experience reveals a spectrum of challenging glaucoma presentations that do not fit clearly into classic diagnostic categories. These borderline or ambiguous cases highlight the limitations of single-modality imaging and are often where AI can provide the most assistance. The table below outlines four typical case profiles encountered in practice and the potential contribution of multimodal AI.

| Case Type | Typical Features | Multimodal AI function |
|---|---|---|
| Stable suspect | Suspicious optic disc, borderline RNFL/OCTA, stable VF & IOP | Confirms stability across inputs to reduce false alarms |
| Unstable suspect | Disc/RNFL borderline, OCTA VD, fluctuating VF or IOP | Detects early vascular changes before irreversible damage |
| False positive | AI or human red or greenflags for myopic disc or artifact | Cross-validates across modalities to reduce misclassification |

| | | |
|---|---|---|
| False negative | Normal OCT and VF, but vascular loss on OCTA or a suspicious disc overlooked | Adds vascular analysis to reveal hidden early progression |

## 5.12 Why Multimodal AI Improves Glaucoma Risk Assessment?

A single-modality approach is often insufficient for accurately capturing the complexity of glaucoma. Multimodal AI integrates structural (OCT), vascular (OCTA), functional (VF), and pressure-based (IOP) data, alongside clinical variables, to build a more comprehensive and personalised risk profile.

- This integration enhances early detection, particularly in pre-perimetric stages where changes may be subtle or isolated in one modality.
- Studies show that combining functional and structural inputs (e.g., VF + fundus photos) improves early diagnostic performance [26].
- A multimodal approach supports timely risk stratification, helping clinicians prioritise early, aggressive treatment in high-risk patients.

## 5.13 Fusion Strategies in Multimodal AI

Effective glaucoma prediction often relies on combining diverse data types such as OCT, OCTA, and clinical metrics. The fusion strategy determines how these modalities are integrated:

- Early fusion merges pre-processed features (e.g., RNFL, VD, IOP) before model training. While it enables joint feature learning, it may be sensitive to noise or modality imbalance.
- Late fusion processes each modality separately and combines their outputs at the decision level. This offers robustness to missing data and clinical flexibility, but may overlook subtle intermodal interactions and reduce transparency in decision-making.
- Intermediate fusion balances the two approaches by combining features midway through the network after separate extraction. It enables deeper intermodal learning and better captures synergistic patterns across modalities, particularly in high-dimensional tasks such as glaucoma detection.
- We plan to use intermediate fusion for imaging (CNN) and late fusion for clinical data (MLP) to optimise integration and handle missing values. Unlike traditional models that require long-term follow-up, our multimodal AI might be able to estimate glaucoma risk and vascular ageing from the first visit, enabling earlier, personalised intervention.

## 5.14 Differentiation between Glaucoma and Central Nervous System

Differentiating glaucomatous damage from retinal changes secondary to central nervous system (CNS) neurodegeneration remains a major clinical challenge.

**Table 1: Distinguishing Features of Glaucoma vs CNS Neurodegeneration**

| | Glaucoma | CNS Neurodegeneration |
|---|---|---|
| **Optic disc** | Cupping, Rim, notch | Palor |
| **RNFL thinning** | Localized, MVZ, SVZ | Diffuse |
| **OCTA VD** | Focal PP dropout, CC dropout | Diffuse |
| **VF defect** | Nasale step, paracentral, arcuate | Generalized, Unrelated |
| **OCT** | Focal wedge-shaped thinning | General reduction |
| **History** | IOP, familial Glaucoma | Cognitive decline, neurologic symptoms |
| **Response to IOP therapy** | Stabilization, decrease of progression or reversal | None |
| **Combined representation** | Yes: Careful interpretation | Yes: Diagnostic complexity |

Both glaucoma and CNS-related conditions exhibit RNFL thinning and reduced OCTA vascular density but differ in their patterns. Glaucoma typically shows localised arcuate RNFL loss with optic disc cupping and peripapillary dropout, while CNS diseases cause diffuse or temporal thinning without disc changes. Differentiation remains a challenge, underscoring the need for AI models that integrate structural, vascular, and systemic data. Our study supports this by providing normative OCTA baselines that are essential for distinguishing between glaucomatous and CNS-related neurodegeneration.OCT/OCTA values can be modified during the early stages of CNS degeneration as well as in glaucoma.

Recognising these subtle differences is already challenging for expert clinicians who establish the ground truth. The concomitant existence of both in a patient poses a challenge for both specialists and AI.

## 5.15 Next Steps: From Multimodal to Self-Supervised Learning

The limitations of single-modality diagnostics in glaucoma highlight the value of multimodal AI frameworks for individualised risk assessment. This approach shifts glaucoma management from static thresholds to dynamic, patient-specific disease trajectories.

However, a key barrier to robust AI development is the scarcity of well-annotated datasets, particularly for early progression stages where clinical labelling is subjective and inconsistent. Self-supervised learning (SSL) addresses this challenge by enabling models to learn from unlabelled data through auxiliary tasks, such as predicting transformations or reconstructing masked inputs, thereby capturing meaningful representations without manual annotation.

In our future study, Phase 1 leverages SSL on healthy OCTA scans to model predicted ocular ageing patterns. This will not only improve generalisability but also enhance sensitivity to subtle, preclinical changes, laying the foundation for early glaucoma risk prediction without relying on extensive labelled datasets.

## 5.16 Postdoc Study: Forecasting the Future: Multimodal AI and Vascular Ageing as New Frontiers in Glaucoma Risk Stratification

**Purpose:** To determine whether vascular age estimated from a single OCTA image can serve as a biomarker of glaucoma risk and disease stability. The secondary goal was to evaluate whether this vascular age prediction could reflect underlying IOP dynamics and be used as a personalised predictor of progression at first consultation.

**Method:** This retrospective-prospective study included 200 patients with glaucoma who had been followed at our tertiary glaucoma clinic for up to 20 years. Longitudinal data were meticulously compiled, including intraocular pressure (IOP) measurements and standard automated perimetry (SAP) visual fields. Since 2020, patients have also undergone multimodal retinal imaging using optical coherence tomography (OCT) and OCT angiography (OCTA) on the Optovue Solix SD-OCT platform.

**Longitudinal Clinical Data Collection**

- IOP History: For each patient, all recorded IOP values from the initial diagnosis to the present were collected. Key derived variables included mean IOP, maximum IOP (IOPmax), minimum IOP, and IOP fluctuation (ΔIOP).
- Visual Field Data: All available SAP exams (24-2) were analysed for mean deviation (MD) and visual field index (VFI or % preservation). These were used to assess both disease stage and progression rate.

**Imaging Acquisition and Parameters**

- OCT and OCTA: In 2020, high-resolution scans of the macula and optic nerve head were acquired. OCTA parameters included VD in the superficial and deep capillary plexuses, radial peripapillary capillaries (RPC), and foveal avascular zone (FAZ) characteristics. Structural OCT parameters included RNFL and ganglion cell complex (GCC) thicknesses.
- All images were reviewed to ensure a sufficient quality score (greater than 6) and a sufficient signal strength index (SSI) according to Optovue quality criteria (SSI greater than 48).

### 5.16.1 Workflow Box: Conceptual Development of GlauOCTA-AI (Fig 6)

**Phase 1 – AI Model Development and Training on Healthy Eyes**

- Train AI using OCTA scans from healthy subjects aged 10–80 years.
- Learn normative vascular ageing patterns from macular and peripapillary OCTA maps.

**Phase 2 – Model Inference and Predicted Ocular Age Estimation in Glaucoma Patients**

- Apply trained model to OCTA scans from glaucoma patients
- Predict vascular age based on microvascular OCTA features

**Phase 3 – Clinical Correlation**

- Compare predicted ocular age to chronological age
- Correlate mismatch with:
    - IOP history (mean, max, ΔIOP)
    - VF parameters (MD, progression)
    - OCT structure (RNFL, GCC)

**Phase 4 – Predictive Refinement (Postdoc Phase)**

- Fine-tune model using real outcomes (progression vs. stability)
- Integrate additional clinical data such as treatment response, glaucoma subtype, and systemic risk factors
- Retrain or expand the model to improve individualised risk prediction using multimodal data inputs.
- Validate the refined model in external datasets for generalisability

This AI framework enables a shift from reactive to predictive glaucoma care, capturing risk early through vascular ageing. “Personalised treatment in glaucoma will not come from a target IOP, and it will come from understanding how each eye

behaves in the vascular and structural space. AI will not replace us. It will enable us to treat smarter, earlier, and more confidently.

**Fig 6. GlauOCT-AI possible model representation**

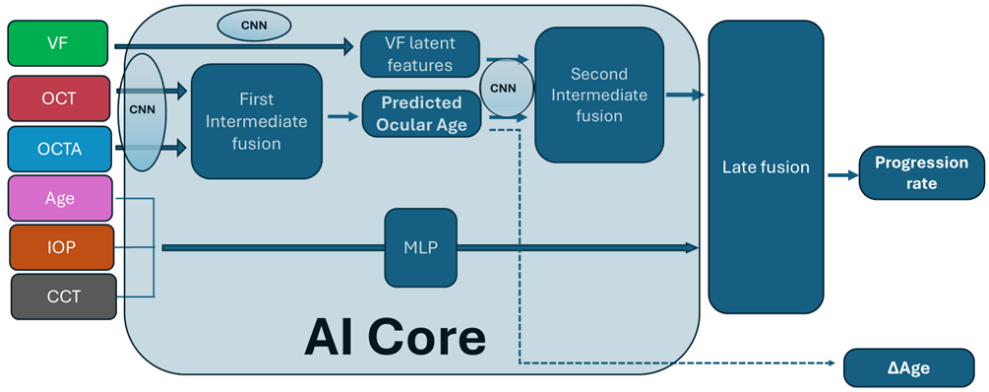


Justification for this model:

- Interpretability: It provides separate estimates of vascular and structural age, allowing clearer clinical insight into the nature and pace of disease progression.
- Modular design: OCT, OCTA, and VF data are processed independently by separate CNNs, allowing future model refinement or replacement without affecting the full pipeline.
- Late fusion with clinical features: Tabular data (e.g. age, IOP, sex) is integrated at the decision level, improving prediction without diluting modality-specific learning.
- Ethical and explainable AI: By isolating and explicitly combining sub-decisions, the model promotes transparency and aligns with responsible AI practices in healthcare.

Race and ethnicity were not included in the predictive model due to their limited biological precision and potential to introduce confounding. Future models may consider ancestry-informative genetic markers rather than sociocultural race labels.

### 5.16.2 Note on Clinical Variability and Treatment History

Patients included in this study represent a broad spectrum of glaucoma phenotypes, reflecting real-world clinical practice. Some were only observed and never treated due to consistently stable visual function over more than a decade. Others were treated medically or surgically and remained stable for years, while a subset exhibited continuous, delayed or stepwise progression despite stable IOP levels under treatment. These cases highlight glaucoma's complex and often unpredictable nature, where structural or functional changes may occur independently of IOP thresholds. The dataset preserved this variability to ensure the AI model could learn from all the progression patterns and apparent stability. The heterogeneity reinforces the need for data-driven approaches that integrate longitudinal trends rather than relying on static cut-off values.

## 5.17 Collaborative AI and Federated Learning in Glaucoma

Multicentred data integration is essential for training AI models that generalise across populations. However, legal, ethical, and privacy regulations restrict sharing medical imaging data across institutions.

Federated learning (FL) enables the development of collaborative AI models without requiring the transfer of patient data. Each participating centre trains the model locally in FL on its own data. The models' parameters, not the data, are aggregated centrally to form a global model.

This approach ensures data privacy (compliant with the GDPR), reduces the risk of bias toward a single institution's population, and facilitates the inclusion of underrepresented groups (e.g., young glaucoma patients, high myopia patients, or those with rare subtypes).

In the context of glaucoma, federated learning enables the training of models on diverse imaging devices, ethnicities, and clinical protocols, thereby enhancing their robustness in real-world applications. As GlauOCTA-AI evolves, FL could offer a future pathway for validation and scale-up without compromising patient confidentiality.

## 5.18 Current Architectures in Glaucoma AI: CNNs, LSTM Hybrids, and Emerging Transformers

Most convolutional neural networks (CNNs) currently used in glaucoma research are designed for static imaging tasks such as classification, segmentation, or regression. These models operate on individual OCT or OCTA scans and do not retain memory across time. As a result, they are limited in their capacity to model disease progression or temporal dynamics. To address this, CNNs can be combined with long short-term memory (LSTM) layers, enabling the network to learn temporal

patterns from sequential data such as visual field series or intraocular pressure trends.

This CNN+LSTM hybrid approach holds significant promise for longitudinal glaucoma monitoring. More recently, transformer-based architectures, particularly vision transformers (ViTs) and multimodal transformers, have emerged, offering advanced capabilities for integrating diverse data types and handling time-aware predictions [27]. While still experimental in ophthalmology, such models are expected to become more applicable as datasets grow in size and complexity.

The human brain doesn't work like a CNN or LSTM, it works like all of them, all the time, in ways we still don't fully understand.

As discussed in Chapter 2, transformer-based models may become relevant for glaucoma imaging in the future, though their integration remains limited by current dataset size and modality complexity.

## 5.19 Future directions

"Personalised treatment in glaucoma will not come from a target IOP, it will come from understanding how each eye behaves in the vascular and structural space. Multimodal AI will enable us to treat smarter, earlier, and more confidently."

Not "target IOP for all," but target perfusion recovery for each.

## References


1. Almarzouki N. Impact of Environmental Factors on Glaucoma Progression: A Systematic Review. Clin Ophthalmol. 2024 Sep 30;18:2705-2720. doi: 10.2147/OPTH.S484855. PMID: 39372224; PMCID: PMC11451402.
2. Omodaka, K., Kikawa, T., Kabakura, S. et al. Clinical characteristics of glaucoma patients with various risk factors. BMC Ophthalmol 22, 373 (2022). https://doi.org/10.1186/s12886-022-02587-5
3. Mohammadzadeh V, Wu S, Besharati S, Davis T, Vepa A, Morales E, Edalati K, Rafiee M, Martinyan A, Zhang D, Scalzo F, Caprioli J, Nouri-Mahdavi K. Prediction of Visual Field Progression with Baseline and Longitudinal Structural Measurements Using Deep Learning. Am J Ophthalmol. 2024 Jun;262:141-152. doi: 10.1016/j.ajo.2024.02.007. Epub 2024 Feb 12. PMID: 38354971; PMCID: PMC11226195.
4. Daneshvar R, Yarmohammadi A, Alizadeh R, Henry S, Law SK, Caprioli J, Nouri-Mahdavi K. Prediction of Glaucoma Progression with Structural Parameters: Comparison of Optical Coherence Tomography and Clinical Disc Parameters. Am J Ophthalmol. 2019 Dec;208:19-29. doi: 10.1016/j.ajo.2019.06.020. Epub 2019 Jun 25. PMID: 31247169.
5. Samaneh Sabouri, Saeedeh Pourahmad, Koenraad A. Vermeer, Hans G. Lemij, Siamak Yousefi; Pointwise and Region-Wise Course of Visual Field Loss in Patients With Glaucoma. Trans. Vis. Sci. Tech. 2022;11(7):20.
6. Weinreb RN, Aung T, Medeiros FA. The pathophysiology and treatment of glaucoma: a review. JAMA. 2014 May 14;311(18):1901-11. doi: 10.1001/jama.2014.3192. PMID: 24825645; PMCID: PMC4523637.
7. Hood DC, Raza AS, de Moraes CG, Liebmann JM, Ritch R. Glaucomatous damage of the macula. Prog Retin Eye Res. 2013 Jan;32:1-21. doi: 10.1016/j.preteyeres.2012.08.003. Epub 2012 Sep 17. PMID: 22995953; PMCID: PMC3529818.
8. Yang, H., Lee, H.S., Bae, H.W. et al. Effect of image quality fluctuations on the repeatability of thickness measurements in swept-source optical coherence tomography. Sci Rep 10, 13897 (2020). https://doi.org/10.1038/s41598-020-70852-y
9. Caprioli J, de Leon JM, Azarbod P, Chen A, Morales E, Nouri-Mahdavi K, Coleman A, Yu F, Afifi A. Trabeculectomy Can Improve Long-Term Visual Function in Glaucoma. Ophthalmology. 2016 Jan;123(1):117-28. doi: 10.1016/j.ophtha.2015.09.027. Epub 2015 Oct 24. PMID: 26602970.
10. Hong JW, Sung KR, Shin JW. Optical Coherence Tomography Angiography of the Retinal Circulation Following Trabeculectomy for Glaucoma. J Glaucoma. 2023 Apr 1;32(4):293-300. doi: 10.1097/IJG.0000000000002148. Epub 2022 Nov 28. PMID: 36730185.

11. Williams PJ, Gregory A, Komro J, You Q, Ross B, Colón C, Juzych MS, Hughes BA, Ridha F. The impact of intraocular pressure on optical coherence tomography angiography: A review of current evidence. Saudi J Ophthalmol. 2024 Jan 3;38(2):144-151. doi: 10.4103/sjopt.sjopt_112_23. PMID: 38988792; PMCID: PMC11232753.
12. Lisanne J. Balk, Judith M. Sonder, Eva M. M. Strijbis, Jos W. R. Twisk, Joep Killestein, Bernard M. J. Uitdehaag, Chris H. Polman, Axel Petzold; The Physiological Variation of the Retinal Nerve Fiber Layer Thickness and Macular Volume in Humans as Assessed by Spectral Domain–Optical Coherence Tomography. Invest. Ophthalmol. Vis. Sci. 2012;53(3):1251-1257. https://doi.org/10.1167/iovs.11-8209.
13. Lisanne J. Balk, Timm Oberwahrenbrock, Bernard M.J. Uitdehaag, Axel Petzold, Physiological variation of retinal layer thickness is not caused by hydration: A randomised trial, Journal of the Neurological Sciences,Volume 344, Issues 1–2,2014, Pages 88-93, ISSN 0022-510X, https://doi.org/10.1016/j.jns.2014.06.031.
14. Musch DC, Gillespie BW, Palmberg PF, Spaeth G, Niziol LM, Lichter PR. Visual field improvement in the collaborative initial glaucoma treatment study. Am J Ophthalmol. 2014 Jul;158(1):96-104.e2. doi: 10.1016/j.ajo.2014.04.003. Epub 2014 Apr 12. PMID: 24727262; PMCID: PMC4190842.
15. Jae Hoon Jeong, Ki Ho Park, Jin Wook Jeoung, Dong Myung Kim. Preperimetric normal tension glaucoma study: long-term clinical course and effect of therapeutic lowering of intraocular pressure. Acta Ophthalmol. 2014: 92: e185–e193. https://doi.org/10.1111/aos.12277
16. Kamalipour A, Moghimi S. Macular Optical Coherence Tomography Imaging in Glaucoma. J Ophthalmic Vis Res. 2021 Jul 29;16(3):478-489. doi: 10.18502/jovr.v16i3.9442. PMID: 34394875; PMCID: PMC8358749.
17. Pourjavan S, Gouverneur F, Macq B, Van Drooghenbroeck T, De Potter P, Boschi A, El Maftouhi A. Advanced Analysis of OCT/OCTA Images for Accurately Differentiating Between Glaucoma and Healthy Eyes Using Deep Learning Techniques. Clin Ophthalmol. 2024 Nov 26;18:3493-3502. doi: 10.2147/OPTH.S472231. PMID: 39618988; PMCID: PMC11607993.
18. Yousefi S, Kiwaki T, Zheng Y, et al. Detection of longitudinal visual field progression in glaucoma using machine learning. Am J Ophthalmol. 2018;193:71-79.
19. Jampel HD, Singh K, Lin SC, Chen TC, Francis BA, Hodapp E, Samples JR, Smith SD. Assessment of visual function in glaucoma: a report by the American Academy of Ophthalmology. Ophthalmology. 2011 May;118(5):986-1002. doi: 10.1016/j.ophtha.2011.03.019. PMID: 21539982.
20. Coleman AL, Kodjebacheva G. Risk factors for glaucoma needing more attention. Open Ophthalmol J. 2009 Sep 17;3:38-42. doi: 10.2174/1874364100903020038. PMID: 19816585; PMCID: PMC2759104.

21. Soltau JB, Zimmerman TJ. Changing paradigms in the medical treatment of glaucoma. Surv Ophthalmol. 2002 Aug;47 Suppl 1:S2-5. doi: 10.1016/s0039-6257(02)00291-6. PMID: 12204696.
22. Esporcatte BL, Tavares IM. Normal-tension glaucoma: an update. Arq Bras Oftalmol. 2016 Jul-Aug;79(4):270-6. doi: 10.5935/0004-2749.20160077. PMID: 27626157.
23. Gosling D, Meyer JJ. Normal Tension Glaucoma. 2022 Dec 12. In: StatPearls [Internet]. Treasure Island (FL): StatPearls Publishing; 2025 Jan–. PMID: 35015402.
24. Gordon MO, Kass MA. What We Have Learned From the Ocular Hypertension Treatment Study. Am J Ophthalmol. 2018 May;189:xxiv-xxvii. doi: 10.1016/j.ajo.2018.02.016. Epub 2018 Mar 1. PMID: 29501371; PMCID: PMC5915899.
25. Miglior S, Zeyen T, Pfeiffer N, Cunha-Vaz J, Torri V, Adamsons I; European Glaucoma Prevention Study (EGPS) Group. Results of the European Glaucoma Prevention Study. Ophthalmology. 2005 Mar;112(3):366-75. doi: 10.1016/j.ophtha.2004.11.030. PMID: 15745761.
26. Huang X, Sun J, Gupta K, Montesano G, Crabb DP, Garway-Heath DF, Brusini P, Lanzetta P, Oddone F, Turpin A, McKendrick AM, Johnson CA, Yousefi S. Detecting glaucoma from multi-modal data using probabilistic deep learning. Front Med (Lausanne). 2022 Sep 29;9:923096. doi: 10.3389/fmed.2022.923096. PMID: 36250081; PMCID: PMC9556968.
27. Ashish Vaswani, Noam Shazeer, Niki Parmar, Jakob Uszkoreit, Llion Jones, Aidan N. Gomez, Lukasz Kaiser, Illia Polosukhin. Computation and Language. arXiv:1706.03762.

# Chapter 6: Clinical Integration,

# Human–AI Collaboration, and Future Perspectives

## 6.1 How it began: My turning point

My PhD journey began in the aftermath of a legal conflict that dates to 2014. I received a notification during the COVID-19 pandemic in 2020, a case that remains unresolved to this day.

It involved a 53-year-old who had undergone surgery for a congenital cataract in both eyes, aphakic, highly myopic, with secondary glaucoma. I chose to implant a drainage tube in the better-seeing eye, having observed occasional pressure peaks up to 24 mmHg despite maximal tolerated topical and oral medication. The optic disc was small and dysversic, making clinical examination and interpretation especially challenging. OCT imaging was compromised by axial elongation, and visual fields with intermittent paracentral clusters, suggested instability on the verge of decompensation. Figure 1 shows the patient's OCT a copy of an old, black-and-white scanned file with limited diagnostic value due to incorrect segmentation of the optic disc. The patient's history included several retinal detachment surgeries, leaving the conjunctiva severely altered.

Guided by the TVT Study (Tube versus Trabeculectomy), which supports the tube implantation in such cases, I considered the surgical choice appropriate and timely. Yet a rare complication reduced his vision from 0.6 to 0.2. An insurance ophthalmologist, specialised in refractive surgery, questioned the indication for the operation, labelling the eye as "stable." Legal action followed [1].

Looking back one thought persists:

*If only I had had a objective tool, data-driven, capable of demonstrating the subtle progression, perhaps others would have better understood the rationale behind my decision. Perhaps my expertise and clinical judgement would not have been put into question.*

Because what I saw was not captured in a single test, or snapshot, or number. It was the result of pattern recognition, a holistic integration of subtle structural changes, fluctuating functional signs, pressure and the knowledge built from experience, that instability often precedes irreversible loss.

That moment marked the beginning of this PhD journey.

Beyond defending my decision, I wanted to prove to myself that I could transform this experience into something meaningful and purposeful. One colleague was

surprised I pursued a PhD “à fin de carrière” hinting it should have been done earlier. But I believe in “never stop learning”.

I wanted to build something, a model, that could help other clinicians quantify the risk of progression in complex, borderline cases. This tool aims to amplify clinicians’ vision, ensuring no patient’s sight id lost to diagnostic uncertainty.

A multimodal AI to amplify the clinician’s vision, before the vision is lost**.**

**Figure 1. OCT printout results of the patient in 2015.**

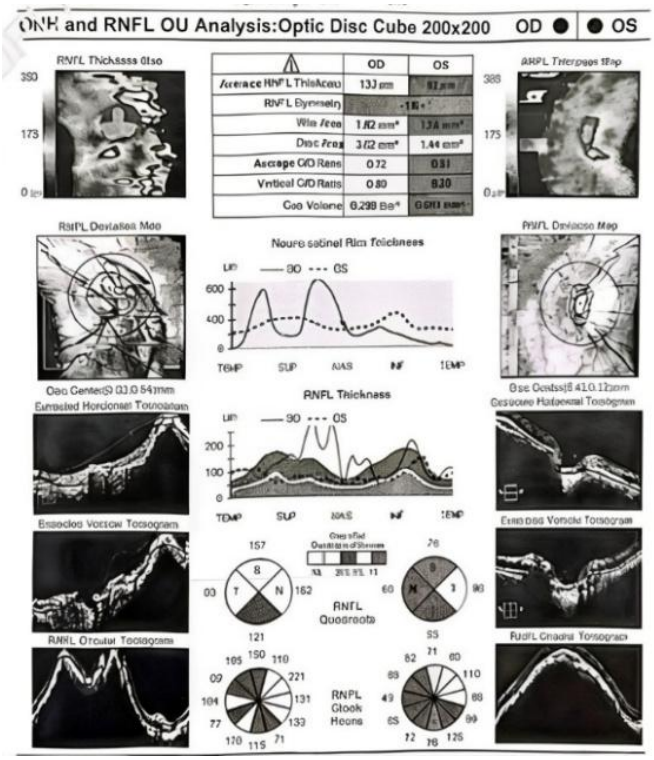


## 6.2 Integration into Clinical Practice

GlauOCTA-AI enhances diagnostic accuracy, personalises risk stratification, and supports proactive glaucoma management. The practical integration of this multimodal model has already been addressed in earlier chapters, particularly regarding its ability to enhance diagnostic accuracy, personalise risk stratification, and enable more proactive glaucoma management. It integrates seamlessly into existing OCT/OCTA workflows, providing real-time risk scores during patient

consultations. While the clinical potential is significant, real-world implementation will require addressing key challenges, including clinician acceptance, standardisation of data inputs, generalisation, external validation, and regulatory compliance. Standardized imaging protocols and compatibility with devices like the Optovue Solix ensure minimal disruption, while the model's adaptability to missing inputs supports its use in varied settings. Nonetheless, the model is designed to integrate seamlessly into existing OCT/OCTA-based workflows, providing support without disrupting clinical routine.

External validation across diverse populations and regulatory approval are critical next steps, aligning with European Medicines Agency guidelines for AI in medical devices [2]. This ensures GlauOCTA-AI meets clinical and ethical standards before widespread adoption.

## 6.3 The Reality: AI Will Transform, Not Simply Assist

The era when AI was limited to automating repetitive, low-level tasks is rapidly fading. AI is reshaping clinical medicine, particularly in imaging-intensive fields like ophthalmology. Modern AI, particularly through deep learning (DL) and convolutional neural networks (CNNs), has significantly expanded its role in clinical medicine. Deep learning models excel at pattern recognition in OCT and OCTA images, enabling precise risk stratification. These models can learn from complex, high-dimensional data such as OCT and OCTA images, enabling advanced pattern recognition, predictive modelling, and disease risk stratification. 2022, Oxipit AI, became the first autonomous system approved in Europe to analyse chest X-rays , clearing normal scans without human intervention [3]. In ophthalmology, AI has already enhanced visual field testing and OCT/OCTA interpretation, detecting subtle progressions that are often missed by human eyes.

The next frontier lies in multimodal AI, which integrates data from various sources, such as imaging, clinical records, and biomarkers, to make more holistic and accurate decisions [4-5]. These systems are expected to eventually match or exceed the performance of human experts in specific diagnostic tasks. Moreover, generalised multimodal models have the potential to bring high-quality diagnostic capabilities to underserved regions, where access to ophthalmologists or imaging experts is limited, ultimately saving lives and preserving vision.

Additionally, generative AI is emerging as a powerful tool for simulation, training, and quality assurance. It can help pre-train clinicians and even other AI systems by generating synthetic yet realistic clinical scenarios. Foundation AI models, such as large-scale pre-trained systems, offer a more comprehensive approach to diagnostics, akin to having multiple subspecialists review a patient with coexisting conditions, such as glaucoma and a retinal melanoma [6].

Beyond diagnosis, AI also plays an expanding role in drug discovery and therapeutic innovation [7]. This includes identifying new molecular targets, repurposing existing compounds, and simulating disease pathways to accelerate pharmacological development. Additionally, AI can support the design of novel drug delivery systems, helping to optimise bioavailability, minimise side effects, and personalise treatment strategies.

While generative AI models such as Modela offer exciting opportunities for interpretability and educational support, particularly in image-based specialities like histopathology, their integration into real-time ophthalmology consultations requires caution [8]. In glaucoma care, the patient is physically present. Our role is not limited to interpretation; it involves listening, guiding, and holding the trust of someone navigating a potentially blinding disease. Even if well-intentioned, engaging in dialogue with a language model during the consultation risks conveying uncertainty, distraction, or reliance on an impersonal system. It may unintentionally undermine the human bond that is essential to therapeutic trust. Therefore, the use of generative models in ophthalmology must be deliberately confined to contexts that preserve clinical authority and empathy, such as pre-visit preparation, educational review, or post-hoc analysis, rather than replacing direct clinician–patient dialogue. The clinician's presence must remain central in this field, where reassurance, subtle communication, and clinical judgement are inseparable.

## 6.4 AI as Complementary, Not Replacement for Ophthalmologists

The notion that AI will never replace clinicians is comforting, yet real-world developments increasingly challenge it. AI is already embedded in our daily lives, from GPS algorithms that determine our optimal route to social media platforms that curate the information we see. A similar shift is occurring in ophthalmology, as its imaging-intensive speciality provides fertile ground for AI implementation, thanks to its structured data and potential for pattern recognition. In radiology, AI is projected to perform the full spectrum of current diagnostic tasks eventually.

Implementing AI has already helped clinicians perform twice as many breast cancer readings as before [9]. In ophthalmology, AI is already embedded in visual field testing and OCT/OCTA devices, recognising patterns, detecting progression, and suggesting interpretation. The real question is not *if* AI will be used, but *how*. Clinicians can either use AI as a tool to enhance insight and precision or rely on it passively.

Despite its growing capabilities, human expertise remains irreplaceable in clinical practice, where decisions must be made in context, considering patient history, subtle clinical signs, and often emotions. AI can process vast amounts of data quickly and consistently, helping to reduce the cognitive load associated with demanding

workloads, especially in high-volume settings. By handling time-consuming tasks such as image analysis or early-stage triage, AI enables clinicians to focus more on complex decision-making and meaningful patient interactions.

Moreover, in conditions such as glaucoma, where progression is often subtle and multifactorial, the judgment of an experienced ophthalmologist cannot currently be replicated by algorithms alone. As illustrated in the case vignettes in Chapter 4, patients with extreme IOPs or complex treatment histories often present interpretive challenges that AI would currently struggle to manage autonomously.

AI can support early detection and risk modelling, but interpretation within the clinical picture remains a human responsibility. As such, the future of ophthalmology lies in a synergy between human insight and machine precision, a partnership, not a replacement. AI will likely resolve many of the diagnostic bottlenecks we currently face. However, clinicians who ignore its evolution risk being replaced, not by AI itself, but by colleagues who have adopted it to enhance accuracy, efficiency, and personalisation of care.

## 6.5 Human Reasoning as Multimodal, Multi-axonal Activation

Human clinical reasoning does not operate in the linear, rule-based fashion typical of deep learning architectures such as CNNs or memory-dependent models like LSTMs. Instead, it emerges from a flexible and highly individualised network of neuronal activations, shaped by prior experience, emotion, and associative learning. This complexity is highlighted in neuroscience research showing that certain neurons, such as the so-called “Jennifer Aniston neurons”, fire selectively in response to specific concepts, regardless of modality. While anecdotal, such findings underscore the sparsity and individuality of neural coding.

In clinical settings, even well-trained ophthalmologists may interpret the same patient data differently, influenced by context, personal experience, and subconscious priors. This variability does not necessarily reflect diagnostic error, but rather the multidimensional, often non-linear nature of expert judgement. It also poses a challenge for AI development, where a single “ground truth” is frequently imposed despite the real-world heterogeneity of human interpretation.

## 6.6 Risks of De-experting and How to Mitigate Them

Although multimodal AI significantly enhances diagnostic precision and clinical efficiency, it also introduces a deeper risk: the potential de-experting of clinicians [10]. Automation may unintentionally promote complacency, diminishing diagnostic intuition, analytical reasoning, and the clinical acumen essential for managing complex cases. The real danger of human replacement arises not because AI is inherently superior, but because clinicians may gradually surrender their intellectual responsibilities, relying too heavily on automated interpretations.

A particularly concerning trend is the decline in clinical intuition and diagnostic proficiency among the latest generations of ophthalmologists, many of whom train in environments where AI-driven protocols increasingly dominate diagnostic workflows. This phenomenon is already visible in practice: many younger ophthalmologists no longer interpret visual fields or OCT scans independently, instead relying entirely on protocol-generated outputs [11]. Over-trusting these without clinical oversight can result in diagnostic pitfalls, such as “Red or Green Disease” in OCT interpretation [12].

This mirrors my own experience while interpreting ECG: I often accept the automated report without reading the trace myself. That may be acceptable for me, but not for a cardiologist whose diagnostic decisions depend on such interpretation. This does not mean we should reject AI outputs; rather, we must strive to understand how algorithms reach their conclusions and whether these apply meaningfully to each unique clinical context.

Several studies have shown that AI models trained on pre-pandemic data underperformed during COVID-19 due to shifts in clinical practice, such as reduced laboratory testing or modified patient triage [13,14]. These examples underscore the importance of continuous model validation and the risks of over-relying on AI systems that were never designed to operate in crisis-mode environments.

The solution must be proactive: safeguarding the clinician’s role through continuous education, maintaining active clinical engagement, and cultivating critical appraisal skills. AI should remain a complementary tool, not an excuse to disengage. Ultimately, the greatest threat is not that AI will surpass human intelligence, but that humans may become too passive to fully leverage their potential. Unlocking the AI “black box" and ensuring explainability is another way to mitigate de-expertization and maintain clinician involvement in decision-making.

The challenge of black-box AI models can be partially overcome by tools like SHAP, which have been successfully applied in glaucoma diagnosis to demonstrate feature contributions and support clinicians' interpretability. However, explainability tools must also reflect clinical relevance, particularly in early glaucoma, high myopia, or mixed pathologies, where model assumptions may break down.

## 6.7 Ethics & Clinical Implications

AI in medicine raises complex questions of responsibility. Clinicians remain legally accountable as end-users, but liability frameworks are evolving [15]. The “Moral Machine Dilemma” or “Autonomous Vehicle Trolley Problem” illustrates ethical challenges [16]. In healthcare, the challenge is similar: the ethical framework of AI must extend beyond accuracy to encompass human values, contextual sensitivity, and the broader consequences of clinical decisions.

Until these questions are resolved in regulatory and legal frameworks, AI will continue to serve as a decision-support tool, rather than an autonomous actor.

At the same time, patients continue to trust human interaction, especially in high-stakes or emotionally complex situations. Unlike binary decision paths that AI systems often produce, clinical reality is frequently nuanced, requiring empathy, dialogue, and moral judgment, traits that remain uniquely human.

## 6.8 Humanising the Machine: The Definition of Anthropomorphism

Another subtle yet important phenomenon is anthropomorphism, the tendency to attribute human-like traits or intentions to non-human entities, including AI systems. Clinicians and patients may perceive these models as capable of reasoning, especially with conversational interfaces. While AI systems may mimic aspects of human cognition, but they are a statistical tool, not a sentient entity, requiring clear prompts to avoid misinterpretations. This psychological projection shapes trust bur can lead to overconfidence.

## 6.9 The Ethical Imperative of AI Explainability

As artificial intelligence becomes more integrated into glaucoma diagnostics and risk prediction, a critical ethical question emerges: Can we trust models we do not fully understand?

Unlike traditional statistical tools, many AI models, particularly deep learning systems, operate as “black boxes,” producing outputs without transparent reasoning pathways. This cataract-like opacity presents a major challenge in medicine, especially in ophthalmology. Clinicians are trained to justify decisions, correlate anatomical and functional findings, and communicate risk clearly to patients. An AI system that offers no rationale undermines clinical autonomy and the trust inherent in the physician–patient relationship.

Explainable AI (XAI) aims to address this by making machine decisions more interpretable. For example, saliency maps or heatmaps can highlight which parts of an OCT scan contributed to a model’s prediction in glaucoma. This allows clinicians to validate whether the model’s “attention” aligns with known glaucomatous damage, for example localised RNFL thinning or peripapillary VD dropout. When properly implemented, explainability bridges the gap between human expertise and machine assistance, enabling clinicians to remain at the centre of diagnostic reasoning. Oh et al. demonstrated the use of SHAP, radar, and gauge charts to visualise and explain individual glaucoma predictions made by an XGBoost model, providing a valuable step toward making AI decisions clinically interpretable in ophthalmology [17].

However, as multimodal AI models become more complex, integrating OCT, OCTA, visual field data, IOP profiles, and systemic information, achieving explainability

becomes increasingly difficult. Which modality drove the risk score? Which feature within that modality mattered most? Sometimes, the answer may not be accessible, even to the developers. This raises concerns about accountability, bias detection, and informed consent in AI-driven glaucoma care. Transparency is not optional, it's a requirement for ethical AI, ensuring clinicians and patients trust the diagnostic process.

We acknowledge that outcome matters, and in medicine, we sometimes accept a degree of opacity when efficacy and safety are proven, as with certain drugs approved without a fully known mechanism of action. However, AI plays a different role: it enters not after the diagnosis, but during the act of reasoning itself. Unlike drugs, which patients ingest without full understanding but with implicit trust in a regulatory system, AI enters the space between observation and interpretation, the sacred space of clinical judgement. There, blind faith is harder to sustain. In this context, explainability is not a luxury but a safeguard. It enables accountability, fosters clinician learning, and preserves trust in the human–machine partnership.

## 6.10 Limitations and Future Perspectives (Postdoc and Beyond)

While this thesis thoroughly explores vascular and structural ageing models for glaucoma risk assessment, several limitations should be acknowledged. The datasets were retrospective and monocentric, potentially limiting generalisability. However, using a single OCT/OCTA device ensured imaging consistency, a strength mitigating heterogeneity.

A second limitation lies in the longitudinal design: while follow-up data were available, imaging intervals and visit timing were not strictly uniform. More importantly, each patient received treatment according to their clinical needs, per European Glaucoma Society (EGS) guidelines. Some underwent selective laser trabeculoplasty (SLT), others required tube implantation, and treatment regimens varied in intensity and timing depending on the individual's disease dynamics. However, this also introduces confounding effects, as changes in vascular parameters may partly reflect therapeutic response rather than natural disease trajectory. This mirrors real-world practice, where withholding treatment solely for study purposes would be unethical.

Third, although deep learning models showed strong performance, explainability remains an area of ongoing development. From a clinician's perspective, explainability is critical for trust and communication, but the technical development and full integration of explainable AI pipelines fall within the engineering domain. My role in this PhD was to define clinical needs and design a robust vascular ageing model that reflects real-world decision-making; my postdoctoral work will focus on evaluating these models in real-time to accelerate intervention and better support patient care, not on designing interpretability frameworks from scratch.

Future directions include expanding validation across multiple centres and integrating functional and clinical data for even more personalised predictions. Ultimately, the aim is not to build an idealised AI in silico but a pragmatic tool embedded in clinical reality capable of supporting ophthalmologists and benefiting patients sooner rather than later.

While genomic data holds potential for many diseases, glaucoma's gene–phenotype link is too variable to support clinical use or AI training. Its clinical application remains limited due to genetic heterogeneity and the lack of validated predictive markers.

My focus remains on clinically validated multimodal inputs, structural, vascular, functional, and pressure-related, with the goal of accelerating risk stratification and supporting decision-making in real-world ophthalmology.

## 6.11 Final Conclusions

The integration of multimodal AI into glaucoma management represents not merely a technological advancement but a fundamental shift toward personalised, predictive care. Yet paradoxically, literature on healthcare management emphasises that systemic pressures, such as budget constraints, increased regulatory burdens, and managerial priorities, often undermine efforts to preserve clinical excellence, education, and expertise. Healthcare systems must prioritize clinical education and mentorship to sustain expertise alongside AI advancements [18]. Studies highlight how institutional cultures driven predominantly by financial and administrative targets inadvertently undervalue clinical teaching, mentorship, and professional development, risking the erosion of crucial clinical competencies [19]. To fully realise AI’s promise without compromising clinician expertise, healthcare organisations must actively foster environments that value and sustain clinical education, mentoring, and human judgment [20]. The future of glaucoma care lies in a synergy of human insight and intelligent technology, each empowering the other.

## 6.12 Epilogue: Personal Reflection, A Call to a Culture

What follows is a personal perspective, shaped by decades of clinical practice within an increasingly fragile system.

This chapter concludes with a personal reflection, not because it is outside the science, but because the science cannot live outside the system in which it exists.

Beyond clinical complacency and “de-experting,” the integration of AI in ophthalmology unfolds within a system strained by budget cuts, overregulation, and chronic underinvestment. Even university hospitals are pressured to prioritise financial performance over clinical excellence, compromising care quality and professional fulfilment.

For young doctors, medicine is becoming a paradox: highly competitive and high-risk, yet unrewarding, marked by burnout fear of litigation, and the emotional trauma of becoming a “second victim” in the aftermath of medical errors or lawsuits [21-25].

In this landscape, the allure of AI as a fast, “cheap” and convenient solution grows stronger, potentially driving clinicians towards overreliance on automated systems, reducing clinicians to passive users, and further eroding clinical expertise and connection.

Worse still, institutions often purposely fail to retain those best suited to guide change. Favouritism, nepotism, administrative overload, and undervaluing clinical mentorship are driving away the very individuals who should be leading the next generation and safeguarding human knowledge.

This underscores the urgency of reorienting institutional culture to genuinely value meritocracy and retain expert clinicians before the irreversible loss of irreplaceable human expertise occurs.

Ultimately, the future of glaucoma care depends not solely on AI. Still, on creating a culture where human insight and intelligent technology thrive in balanced partnership, each continually empowering the other.

## References

1. Gedde SJ, Schiffman JC, Feuer WJ, Herndon LW, Brandt JD, Budenz DL; Tube versus Trabeculectomy Study Group. Treatment outcomes in the Tube

Versus Trabeculectomy (TVT) study after five years of follow-up. Am J Ophthalmol. 2012 May;153(5):789-803.e2. doi: 10.1016/j.ajo.2011.10.026. Epub 2012 Jan 15. PMID: 22245458; PMCID: PMC4460598.
2. European Medicines Agency. Guideline on computerised systems and electronic data in clinical trials. 2023. www.ema.europa.eu.
3. Miró Catalina Q, Fuster-Casanovas A, Solé-Casals J, Vidal-Alaball J. Developing an Artificial Intelligence Model for Reading Chest X-rays: Protocol for a Prospective Validation Study. JMIR Res Protoc. 2022 Nov 16;11(11):e39536. doi: 10.2196/39536. PMID: 36383419; PMCID: PMC9713620.
4. Felix Krones, Umar Marikkar, Guy Parsons, Adam Szmul, Adam Mahdi, Review of multimodal machine learning approaches in healthcare, Information Fusion, Volume 114, 2025, 102690, ISSN 1566-2535, https://doi.org/10.1016/j.inffus.2024.102690.
5. Kaczmarczyk, R., Wilhelm, T.I., Martin, R. et al. Evaluating multimodal AI in medical diagnostics. npj Digit. Med. 7, 205 (2024). doi.org/10.1038/s41746-024-01208-3
6. Paul D, Sanap G, Shenoy S, Kalyane D, Kalia K, Tekade RK. Artificial intelligence in drug discovery and development. Drug Discov Today. 2021 Jan;26(1):80-93. doi: 10.1016/j.drudis.2020.10.010. Epub 2020 Oct 21. PMID: 33099022; PMCID: PMC7577280.
7. Luis R. Soenksen, Yu Ma, Cynthia Zeng, Leonard D.J. Boussioux, Kimberly Villalobos Carballo, Liangyuan Na, Holly M. Wiberg, Michael L. Li, Ignacio Fuentes, Dimitris Bertsimas. Integrated multimodal artificial intelligence framework for healthcare applications. arXiv:2202.12998v4.
8. Lu, M.Y., Chen, B., Williamson, D.F.K. et al. A multimodal generative AI copilot for human pathology. Nature 634, 466–473 (2024). https://doi.org/10.1038/s41586-024-07618-3
9. Elías-Cabot E, Romero-Martín S, Raya-Povedano JL, Brehl AK, Álvarez-Benito M. Impact of real-life use of artificial intelligence as support for human reading in a population-based breast cancer screening program with mammography and tomosynthesis. Eur Radiol. 2024 Jun;34(6):3958-3966. doi: 10.1007/s00330-023-10426-4. Epub 2023 Nov 17. PMID: 37975920; PMCID: PMC11166767
10. Avishek Choudhury, Zaria Chaudhry. Large Language Models and User Trust: Consequence of Self-Referential Learning Loop and the Deskilling of Healthcare Professionals.arXiv:2403.14691v2.
11. Valikodath NG, Cole E, Ting DSW, Campbell JP, Pasquale LR, Chiang MF, Chan RVP; American Academy of Ophthalmology Task Force on Artificial Intelligence. Impact of Artificial Intelligence on Medical Education in Ophthalmology. Transl Vis Sci Technol. 2021 Jun 1;10(7):14. doi: 10.1167/tvst.10.7.14. PMID: 34125146; PMCID: PMC8212436.
12. Donald C Hood, Sol La Bruna, Anvit Rai, Ari Leshno, Carlos G DeMoraes, Emmanouil Tsamis; Identifying and understanding OCT artifacts (“red disease")

that resemble arcuate damage due to glaucoma.. Invest. Ophthalmol. Vis. Sci. 2022;63(7):3316 – F0125.
13. Finlayson SG, Subbaswamy A, Singh K, Bowers J, Kupke A, Zittrain J, Kohane IS, Saria S. The Clinician and Dataset Shift in Artificial Intelligence. N Engl J Med. 2021 Jul 15;385(3):283-286. doi: 10.1056/NEJMc2104626. PMID: 34260843; PMCID: PMC8665481.
14. Bates DW, Syrowatka A, Rhee K, Jackson GP, Alfayez A, Kunz H. Call for better systems and data to support artificial intelligence for pandemic response. BMJ Health Care Inform. 2022 Jan;29(1):e100506. doi: 10.1136/bmjhci-2021-100506. PMID: 35074790; PMCID: PMC8787826.
15. Price WN, Gerke S, Cohen IG. Potential liability for physicians using artificial intelligence. JAMA. 2019;322(18):1765-1766. doi:10.1001/jama.2019.15064
16. Bonnefon, J-F., Shariff, A., & Rahwan, I. (2016). The social dilemma of autonomous vehicles. Science, 352(6293), 1573–1576. https://doi.org/10.1126/science.aaf2654
17. Oh, S.; Park, Y.; Cho, K.J.; Kim, S.J. Explainable Machine Learning Model for Glaucoma Diagnosis and Its Interpretation. Diagnostics 2021, 11, 510. https://doi.org/10.3390/diagnostics11030510
18. Faustinella F, Jacobs RJ. The decline of clinical skills: a challenge for medical schools. Int J Med Educ. 2018 Jul 13;9:195-197. doi: 10.5116/ijme.5b3f.9fb3. PMID: 30007951; PMCID: PMC6129153.
19. Sascha K.R. Spencer, Patrick A. Ireland, Jorja Braden, Jenny L. Hepschke, Michael Lin, Helen Zhang, Jessie Channell, Hessom Razavi, Angus W. Turner, Minas T. Coroneo, Boaz Shulruf, Ashish Agar, A Systematic Review of Ophthalmology Education in Medical Schools: The Global Decline, Ophthalmology, Volume 131, Issue 7, 2024, Pages 855-863, ISSN 0161-6420, doi.org/10.1016/j.ophtha.2024.01.005.
20. Christie B. Lack of leadership was at heart of hospitals' failings, report says. BMJ. 2015 Jul 10;351:h3799. doi: 10.1136/bmj.h3799. PMID: 26162915.
21. Van Gerven, E., Vander Elst, T., Vandenbroeck, S., Dierickx, S., Euwema, M., Sermeus, W., De Witte, H., Godderis, L., Vanhaecht, K. (2016) Increased Risk of Burnout for Physicians and Nurses Involved in a Patient Safety Incident. Medical Care, 54 (10) , 937-943.
22. Vandenbroeck, S., Lambreghts, L., De Witte, H., Vanhaecht, K., Godderis, L. (2017) Burn-out en bevlogenheid bij artsen in opleiding en specialisten. Tijdschrift voor Geneeskunde, 73 (1), 9-16.
23. Seys D., Wu A., Van Gerven E., Vleugels A., Euwema M., Panella M., Scott S., Conway J., Sermeus W., Vanhaecht K. (2013) Health care professionals as second victims after adverse events: a systematic review. Evaluation & the Health Professions, 36 (2), 135-162
24. Vanhaecht, K., Van Gerven, E., Seys, D., Coeckelberghs, E., Godderis, L., Euwema, M., Sermeus, W. (2016) De impact op de zorgverlener na betrokkenheid bij een patiëntveiligheidsincident wordt onderschat. Tijdschrift voor Geneeskunde, 72 (23) , 1371-1373.

25. Vanhaecht, K, Schouten, L., Coeckelberghs, E., Zeeman, G. (2017). Onbedoelde schade treft ook de arts: impact van patiëntveiligheidsincident op zorgverlener wordt onderschat (in Dutch). Medisch Contact, 37, September, 14-16.

## Autobiography

Sayeh Pourjavan was born on July 18, 1969, in Tehran, Iran. In March 1985, following the political changes in her home country, she moved with her family to Belgium.

She pursued her medical studies at KULeuven, where she also completed her residency in ophthalmology. She then completed a one-year glaucoma fellowship under the mentorship of Professor P. Zeyen.

During her studies, she was awarded an Erasmus scholarship and spent one year at the University Hospitals Federico II in Naples, Italy. She also expanded her international experience by working during her ophthalmology residency at NHS Torbay Hospital in the United Kingdom.

Since 2004, she has been actively engaged in clinical practice at Cliniques Universitaires Saint-Luc, first as a fellow under the mentorship of Dr. Michèle Detry, and subsequently as a consultant ophthalmologist and head of the Glaucoma Clinic till May 2025.

She is the vice-president of the Belgian Glaucoma Society.

Beyond her clinical responsibilities, she has participated in humanitarian missions, operating in Africa and other underprivileged regions through the private organisation See & Smile.

Parallel to her clinical career, she developed a strong interest in healthcare management and earned a master's in hospital management. Her leadership abilities were recognised when she won third prize in the INAMI/RIZIV interuniversity programme for Management and Leadership in Medicine for her innovative project, "Virtual Glaucoma Clinic."

Her academic and professional interests extend to neuroscience, artificial intelligence, and their intersections with medical imaging. She is deeply fascinated by the parallels between AI models and the human brain and actively explores how technological innovations can enhance patient care.

Multilingual and culturally versatile, she combines her passion for ophthalmology, innovation, and education. Her ongoing mission is to transform residents into the best versions of themselves; scientifically, professionally, and humanly.